THE MEASUREMENT OF MAGNETIC MOMENTS OF EXCITED STATES IN PALLADIUM, TUNGSTEN, AND THULIUM NUCLEI

Thesis by

Elton Neil Kaufmann

In Partial Fulfillment of the Requirements

For the Degree of

Doctor of Philosophy

California Institute of Technology

Pasadena, California

1969

(Submitted August 30, 1968)

ACKNOWLEDGMENTS

The experiments reported here were carried out in collaboration with Dr. S.K. Bhattacherjee and Dr. J.D. Bowman. The author wishes to express his appreciation for their contributions to this work.

The author would also like to thank Mr. Herbert Henrikson, who designed much of the experimental apparatus, and the following co-workers who contributed to the completion of this work; Dr. E.C. Seltzer, Dr. J. Trischuk, Mr. L. Varnell, Mr. M. Levanoni and Mr. C. Moeller.

The author takes pleasure in expressing his gratitude to Dr. Egbert Kankeleit and especially Professor Felix Boehm for their guidance and encouragement during the course of the author's graduate study.

By no means least among those who helped bring this work to completion is the author's wife Diane. For her continued patience and cooperation, the author's gratitude has been earned many times over.

This work was supported in part by the United States Atomic Energy Commission and the National Science Foundation.

Abstract

The perturbed gamma-gamma angular correlation technique has been used to measure the magnetic moments of several nuclear excited states. The magnetic moment of the second excited 2^+ state in ^{106}Pd has been measured to be $\mu = 0.74 \pm 0.14$ nm, in good agreement with the interpretation of that state as a two-phonon quadrupole vibration about spherical equilibrium. The magnetic moment of the two-quasiparticle 2^- state at 1289 keV in ^{182}W has been measured to be $\mu = 1.04 \pm 0.24$ nm, in poor agreement with the predictions of the "strong-coupling" approximation. The probable origin of the discrepancy is discussed. The following magnetic moments in odd-mass thulium nuclei have been measured: the $5/2^+$ level at 118.2 keV in ^{169}Tm with $\mu = 0.79 \pm 0.08$ nm; the $7/2^+$ level at 138.9 keV in ^{169}Tm with $\mu = 1.33 \pm 0.07$ nm; the $5/2^+$ level at 116.7 keV in ^{171}Tm with $\mu = 0.81 \pm 0.37$ nm; and the $7/2^+$ level at 129.1 keV in ^{171}Tm with $\mu = 1.44 \pm 0.14$ nm. In addition, the multipole mixing amplitude for the 109.8 keV transition in ^{169}Tm has been measured to be $\delta(E2/M1) = -0.15 \pm 0.02$, and the crossover-to-cascade transition intensity ratios for the $5/2^+$(116.7 keV) and $7/2^+$(129.1 keV) states in ^{171}Tm have been measured to be $I_\gamma(5/2 \rightarrow 1/2)/I_\gamma(5/2 \rightarrow 3/2) = 0.115 \pm 0.005$ and $I_{tot}(7/2 \rightarrow 3/2)/I_{tot}(7/2 \rightarrow 5/2) = 3.22 \pm 0.58$, respectively. The results of the measurement in the thulium nuclei have been used in conjunction with other data to determine the parameters in the rotational model description of the nuclei. The magnetic parameters are interpreted in terms of transverse and

longitudinal spin polarization effects, where only qualitative agreement with theory is found. A correction to the rotational model predictions of electric quadrupole transition rates is also discussed.

TABLE OF CONTENTS

I. INTRODUCTION

Nuclear ground state spins and magnetic moments determined from nuclear magnetic resonance, atomic and molecular beam, and optical spectroscopy experiments have played a large part in the development of the nuclear shell model. The use of Mössbauer effect and perturbed angular correlation methods has permitted the measurement of spins and moments of nuclear excited states. Based on these and other spectroscopic properties of excited states in nuclei, theoretical descriptions of nuclear structure have been developed which account for many of the observed nuclear properties. In Chapter II, the perturbed angular correlation technique is discussed, and in following chapters, measurements of several magnetic moments of nuclear excited states using that technique are described. The measurements provide a test of the applicability and limitations of the theories pertaining to three different classes of excited states.

The concept of two basic modes of excitation in nuclei has been utilized, rather successfully, to explain observed spectroscopic properties of nuclear excited states. They are the collective excitations, in which a large number of nucleons participate, and the particle excitations, in which only one or a few nucleons are involved. Any given nuclear state may consist of one or a combination of both excitation modes. In Chapter III, the theoretical models describing some collective vibrational states in spherically shaped nuclei are discussed, and the measurement of the magnetic moment of a state to which the models apply is presented. The state under consideration is in the medium weight even-even nucleus ^{106}Pd and may tentatively be

classified as a two phonon[+] collective vibrational level. As yet, no other moment measurement on such a state in the medium weight region of spherical nuclei has been reported. The measurement is intended to discover whether that state is truly collective or includes single particle excitations. The instrumentation developed to perform the measurement with high data collection rates and minimal systematic errors is also described.

In addition, several measurements have been performed on nuclei possessing a stable spheroidally deformed shape. Besides single particle and collective vibrational states, these nuclei display collective rotational excitations. In fact, it has been found that rotational bands, analogous to those found in molecular spectra, are built on all particle and vibrational excitations. The rotational model, which accounts for the properties of these bands, contains at least one, and in one case considered, two parameters related to the magnetic structure of the intrinsic state upon which the bands are built. The values of these parameters are in turn predicted by the model applicable to the intrinsic excitations, which, in the cases studied, is the Nilsson model for the shell structure of deformed nuclei.

In Chapter IV, the measurement of the magnetic moment of a state, formed by the excitation of two protons, in the even-even nucleus ^{182}W is described. The result of the measurement, along with other known

---

+ The term "phonon" is borrowed from the solid state nomenclature where it refers to one quantum of lattice vibrational energy.

properties of the rotational band built on this intrinsic state, is used to deduce the magnetic parameter characteristic of the structure of the state. In this way, the validity of the strong-coupling rule, which suggests the two protons are coupled independently to the deformed nuclear core without interacting with each other, is tested.

The last two chapters are devoted to the description of measurements performed in the odd-mass deformed nuclei ^{169}Tm and ^{171}Tm and of least-squares fits of the rotational model to all currently known electromagnetic properties of the ground state rotational bands in these nuclei. The measurement of the magnetic moments of two levels in the ground state rotational bands of each nucleus is presented in Chapter V. The determination of the multipole mixing amplitude of an intraband transition in ^{169}Tm and the crossover-to-cascade branching intensity ratios from two states in the ^{171}Tm band is also described there. In Chapter VI, the results of Chapter V and of other investigators are compiled and fit to the rotational model description of the nuclei. The electric and magnetic parameters of the model, determined in this way, are then used to investigate the intrinsic structure of the ^{169}Tm and ^{171}Tm ground states. Specifically, the renormalization of some single particle Nilsson model matrix elements due to a spin-spin interaction of the odd proton in thulium with the remaining nucleons is accurately determined, and a correction to the rotational model description of electric quadrupole transition rates is discussed.

All of the measurements to be presented here may be found reported in less detail in refs. (1), (2), and (3).

II. DESCRIPTION OF THE PERTURBED ANGULAR CORRELATION TECHNIQUE

II.1 Introduction

In 1950, Brady and Deutsch[4] recognized the possibility of measuring the g-factors of nuclear excited states using an anisotropic angular correlation between gamma rays emitted in cascade. Aeppli et al.[5] performed the first such measurement in 1951. Since that time the technique has been used extensively, and improvements in electronics and radiation detectors in recent years have allowed the measurement of moments previously inaccessible. The complete mathematical treatment of the theory of angular correlations is to be found in several comprehensive articles[6]. A short outline of the theoretical results needed to analyze data collected in our experiments is presented below.

II.2 The Directional Angular Correlation between Gamma Rays Emitted in Cascade

The probability of emission of a gamma ray from a nucleus depends on the angle between the emission direction and the nuclear spin axis. Generally, in a radioactive sample the nuclear spins are randomly oriented leading to an isotropic emission pattern for gamma rays. However, the observation of the direction of emission of the first gamma ray of a gamma-gamma cascade selects an ensemble of nuclei whose spins have a preferred orientation in space relative to the observed propagation direction. If one then measures the emission direction of the second member of the cascade, it will in general show an anisotropic distribution about the direction of emission of the first.

An idealized gamma-gamma cascade is depicted in Fig. 1, where

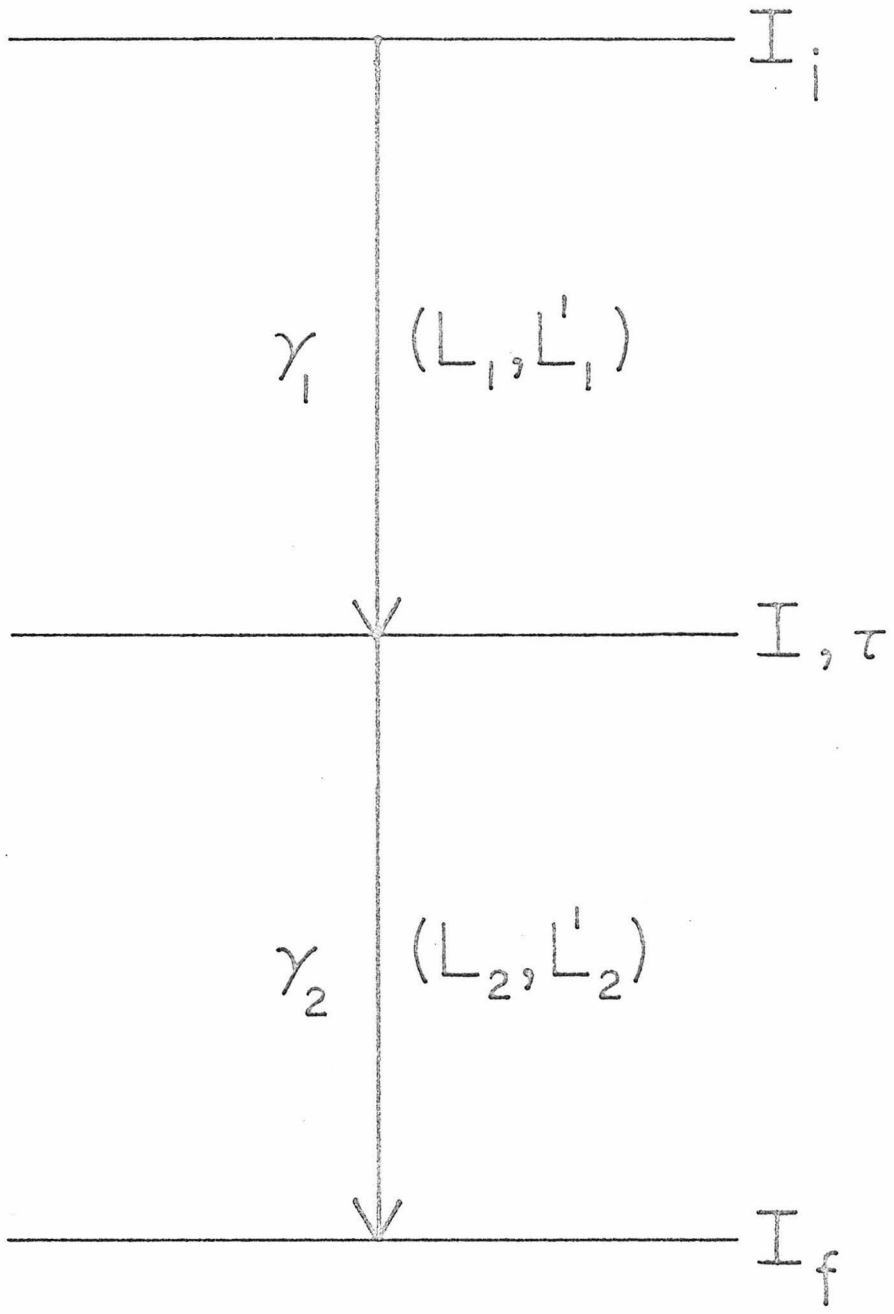

Figure 1

Ideal gamma-gamma cascade. The symbols are defined in the text.

I_i, I, and I_f are the spins of the initial, intermediate, and final state, respectively. The two gamma rays, γ_1 and γ_2, have multipolarities (L_1, L_1') and (L_2, L_2'). The notation (L,L') indicates a possibly mixed multipole transition: for instance, for a mixed M1 + E2 (or E1 + M2) transition, L and L' would be equal to 1 and 2, respectively. If γ_1 and γ_2 are detected by counters separated by the angle θ in the geometry shown in Fig. 2, then the probability distribution for the observation of γ_2 at the angle θ relative to γ_1 is given by

$$W(\theta) \propto 1 + \sum_{\substack{k=2 \\ (\text{even})}}^{k_{max}} A_{kk} P_k(\cos\theta) \quad . \tag{1}$$

The $P_k(\cos\theta)$ are Legendre polynomials and the coefficients A_{kk} depend on the spins of the nuclear states, I_i, I, and I_f, and the multipolarities of the two gamma radiations, (L_1, L_1') and (L_2, L_2'). It turns out that the A_{kk} can be written in the factored form[7],

$$A_{kk} = A_k(\gamma_1) \cdot A_k(\gamma_2) \quad , \tag{2}$$

where $A_k(\gamma_1)$ and $A_k(\gamma_2)$ each depend on the properties of only one of the transitions of the cascade. For a mixed multipole transition, $A_k(\gamma)$ has the explicit form[7],

$$A_k(\gamma_1) = \frac{F_k(L_1 L_1 I_i I) + 2\delta(\gamma_1) F_k(L_1 L_1' I_i I) + \delta^2(\gamma_1) F_k(L_1' L_1' I_i I)}{1 + \delta^2(\gamma_1)} \quad , \tag{3}$$

where the F_k are tabulated coefficients[8] and the mixing amplitude δ is defined as the ratio of the reduced transition matrix elements for the two multipoles[7];

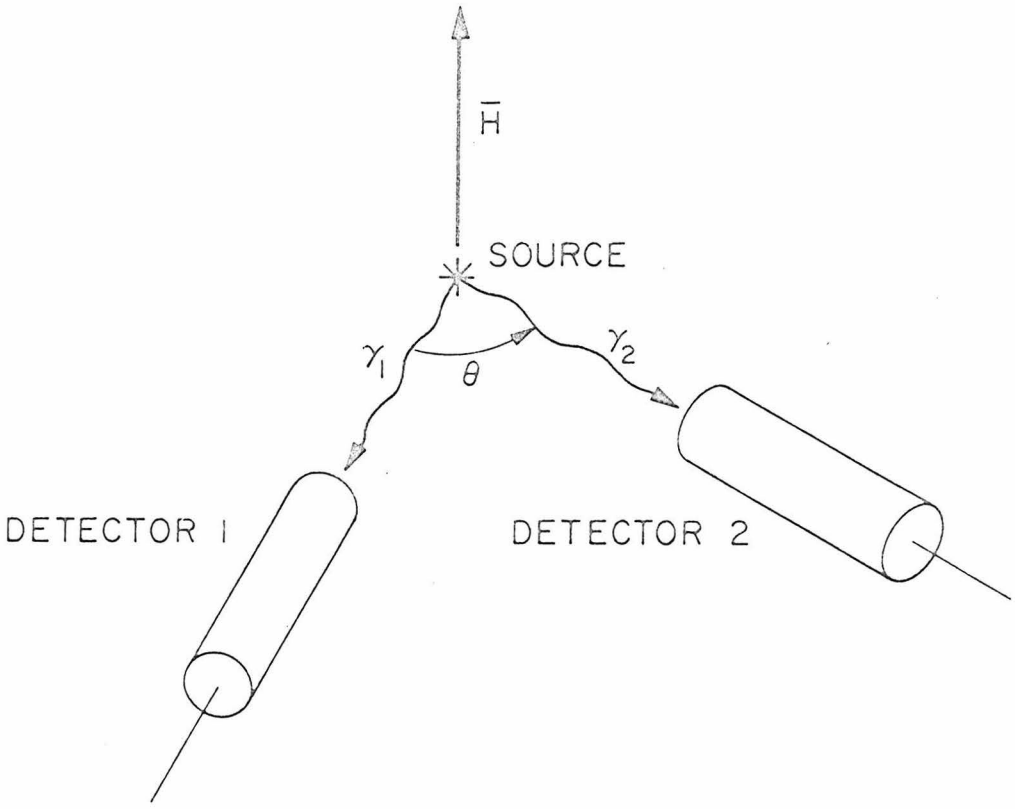

Figure 2

Geometrical arrangement of the source, detector, and magnetic field in a perturbed angular correlation experiment.

$$\delta(\gamma_1) = \langle I||L_1'\pi_1'||I_i\rangle/\langle I||L_1\pi_1||I_i\rangle \ . \qquad (4)$$

A similar expression holds for $A_k(\gamma_2)$. Thus, the measurement of A_{kk} can determine the size and sign of a mixing amplitude.

In practice, radiation detectors subtend a finite solid angle. Therefore, the detection of γ_1 and γ_2 indicates that the angle between emission directions falls in a range of angles centered about θ. Also the detection efficiency for gamma-ray pairs within this range of angles is not uniform, because the efficiency of each detector depends on the path length traversed by the radiation in the active detector volume. The replacement of A_{kk} in Eq. (1) by $Q_k^{\,1}Q_k^{\,2}A_{kk}$ is needed to account for these effects, where $Q_k^{\,1}$ and $Q_k^{\,2}$ are correction factors for the smearing of the angular correlation in the detector accepting γ_1 and γ_2, respectively. In the following, the Q_k's will not be written explicitly but are understood to be present in all experimentally measured angular correlation coefficients. The index k of the sum in Eq. (1) must satisfy the inequality

$$0 < k < \text{Min } (2I, L_1 + L_1', L_2 + L_2') \qquad (5a)$$

for mixed multipole radiation and

$$0 < k < \text{Min } (2I, 2L_1, 2L_2) \qquad (5b)$$

for pure multipole radiation. In all measurements reported here, k_{max} is not greater than 4.

II.3 Perturbation of the Angular Correlation by a Static Magnetic Interaction

The presence of an electromagnetic field at the nucleus, while it is in the intermediate state with spin I, will cause transitions among the (2I + 1) magnetic substates corresponding to different projections of the spin on the chosen direction of the quantization axis. In other words, the preferred direction of orientation of the spin vector in the intermediate state is altered, thereby changing the angular correlation. The application of a static magnetic field causes a precession of the nuclear spin about the applied field direction with the Larmour frequency

$$\bar{\omega} = - g\mu_N \bar{H}/\hbar, \tag{6}$$

in which $\bar{H}$ is the applied magnetic field, g is the nuclear g-factor of the intermediate state, and μ_N is the nuclear magneton. If $\bar{H}$ is perpendicular to the plane of the detectors (cf. Fig. 2) and γ_2 is emitted after the nucleus has been in the intermediate state for a time 't', then the angular correlation pattern will be of the form,

$$W(\theta,H,t) \propto 1 + \sum_{\substack{k=2 \\ (\text{even})}}^{k_{max}} A_{kk} P_k(\cos(\theta - \omega t)). \tag{7}$$

In the measurements described in the following chapters, the lifetime τ of the intermediate state is considerably shorter than the electronic resolving time of the apparatus. Thus, the observed correlation pattern will be that of Eq. (7), integrated over the intermediate state lifetime. The result of the integration appears as

$$\frac{1}{\tau}\int_0^\infty e^{-t/\tau}\, W(\theta,H,t)\, dt = \overline{W(\theta,H)} \propto 1 + \sum_{\substack{N=2 \\ (\text{even})}}^{k_{max}} \frac{b_N \cos(N\theta - N\Delta\theta)}{\sqrt{1 + (N\omega\tau)^2}}\,, \tag{8}$$

where $b_2 = (3A_{22}/4 + 5A_{44}/16)/(1 + A_{22}/4 + 9A_{44}/64)$,

$b_4 = (35A_{44}/64)/(1 + A_{22}/4 + 9A_{44}/64)$, and $\tan(N\Delta\theta) = N\omega\tau$.

The coincidence counting rates in the experiment are proportional to the quantity $\overline{W(\theta,H)}$. In practice, the magnetic field direction is reversed periodically and the quantity

$$\epsilon(\theta) = \frac{\overline{W(\theta,H)} - \overline{W(\theta,-H)}}{\overline{W(\theta,H)} + \overline{W(\theta,-H)}} = \frac{\sum_{\substack{N=2 \\ (\text{even})}}^{k_{max}} \frac{N\omega\tau b_N \sin(N\theta)}{1 + (N\omega\tau)^2}}{1 + \sum_{\substack{N=2 \\ (\text{even})}}^{k_{max}} \frac{b_N \cos(N\theta)}{1 + (N\omega\tau)^2}}\,, \tag{9}$$

which is independent of the normalization of the function $\overline{W(\theta,H)}$, is determined. The g-factor of the intermediate state is then deduced, using Eqs. (6) and (9), from a knowledge of $\epsilon(\theta)$, H, τ and experimentally measured values of A_{22} and A_{44}. This method of g-factor measurement is known as the "integral reversed field method of the perturbed angular correlation technique"[9].

The quantity $\omega\tau$ is referred to as the spin rotation angle, since it represents the mean angle of precession of the nuclear spin while in the intermediate state. At present, a value for $\omega\tau$ of 0.01 rad. is about the smallest one can measure with reasonable accuracy. For a

g-factor of ≈ 0.4 and a mean life of $\tau \approx 10^{-9}$ sec., Eq. (6) indicates a magnetic field of $H \approx 5$ kG may be sufficient to produce a measurable $\omega\tau$. This is the case for the measurement in ^{182}W described in Chapter IV. In the measurements on ^{169}Tm and ^{171}Tm (cf. Chapter V), the shortest lifetimes τ are approximately 8×10^{-11} sec. For these a field of at least 60 kG is needed. A laboratory magnet which produces such a large field is not necessary since the rare earth thulium atom is paramagnetic and enhances the applied field by a factor of five at the nucleus. Finally, in the measurement on ^{106}Pd where a lifetime $\tau \approx 4 \times 10^{-12}$ sec. applies, no laboratory magnet can produce the large field (≈ 500 kG) needed, nor is the palladium atom strongly paramagnetic. In this case, advantage will be taken of the large internal hyperfine field at the site of a Pd nucleus in a ferromagnetic lattice. Since $\epsilon(\theta)$ is the experimentally measured quantity, the size of the coefficients A_{kk} must of course be large enough to permit the measurement of the spin rotation.

II.4 Perturbation of the Angular Correlation by Fluctuating Electric or Magnetic Fields

In addition to fields applied by the experimenter, the nuclei under study experience magnetic fields and electric field gradients arising from their chemical environment. These fields fluctuate in time with the thermal vibrations in a solid or molecular collisions in a liquid. The fluctuations of the fields' magnitudes and directions are, in most cases, random in time. The effect of these time-dependent interactions on an angular correlation has been treated by Abragam and Pound [10]. To

characterize the randomness of the fluctuations, they define a "correlation function"[+] $G(T)$ as the ensemble average of the product $\langle f(t)f\ (t - T)\rangle$, where $f(t)$ is some scalar random function of time. The function $G(T)$ indicates the degree to which the value of 'f' at time 't' can be predicted from a knowledge of 'f' at the earlier time 't - T'. Abragam and Pound[10] assume that the form $G(T) = G(0).\exp(-T/\tau_c)$ applies to the case of a liquid source. The constant τ_c, so defined, is known as the correlation time and represents the time after which $f(t)$ has significantly changed its value. When taking the time-dependent perturbing fields into account, they find that Eqs. (1) and (7) are modified to

$$W(\theta,t) \propto 1 + \sum_{\substack{k=2 \\ (\text{even})}}^{k_{max}} \exp(-\lambda_k t)\ A_{kk}\ P_k(\cos\ \theta) \qquad (10)$$

and

$$W(\theta,H,t) \propto 1 + \sum_{\substack{k=2 \\ (\text{even})}}^{k_{max}} \exp(-\lambda_k t)\ A_{kk}\ P_k(\cos(\theta - \omega t)), \qquad (11)$$

respectively. The exponential character of the attenuation factors has been predicted by Dillenburg and Maris[11] for an interaction random in space and time, regardless of the nature, strength, or frequency of the interaction. The constant λ_k is proportional to the correlation time τ_c. Specifically, for an electric interaction[12]

+ This term is not related to the term "angular correlation".

$$\lambda_k = \frac{\tau_c}{40} \frac{(I + 1)(2I + 3)}{(2I - 1)I} \left(\frac{eQ}{\hbar}\right)^2 \left(\frac{\partial^2 V}{\partial z^2}\right)^2 [1 - (2I + 1)W(I2kI,II)], \tag{12}$$

and for a magnetic interaction[12]

$$\lambda_k = \frac{2\tau_c}{3} I(I + 1) \left(\frac{g\mu_N H_{int}}{\hbar}\right)^2 [1 - (2I + 1)W(I1kI,II)]. \tag{13}$$

The undefined quantities are the electric quadrupole moment of the intermediate state, Q, the g-factor of that state, g, the electric field gradient and magnetic field at the nucleus, $\partial^2 V/\partial z^2$ and H_{int}, respectively, and the Racah[13] coefficients, W.

The total time integrated correlation functions corresponding to Eqs. (10) and (11) are

$$\overline{W(\theta)} \propto 1 + \sum_{\substack{k=2 \\ (\text{even})}}^{k_{max}} G_{kk} A_{kk} P_k(\cos\theta) \tag{14}$$

and, the complex but manageable expression for $k_{max} = 4$,

$$\overline{W(\theta,H)} \propto 1 + \frac{1}{4} A_{22} G_{22} \left\{1 + \frac{3\cos(2\theta - 2\Delta\theta_{22})}{[1 + (2\omega\tau G_{22})^2]^{1/2}}\right\} + \tag{15}$$

$$+ \frac{1}{64} A_{44} G_{44} \left\{9 + \frac{20\cos(2\theta - 2\Delta\theta_{24})}{[1 + (2\omega\tau G_{44})^2]^{1/2}} + \frac{35\cos(4\theta - 4\Delta\theta_{44})}{[1 + (4\omega\tau G_{44})^2]^{1/2}}\right\},$$

respectively, where $\tan(N\Delta\theta_{Nk}) = N\omega\tau G_{kk}$ and $G_{kk} = 1/(1 + \lambda_k\tau)$.

In the measurement to be described on ^{106}Pd, the palladium atom is assumed to be located in a regular lattice site of cubic Fe metal.

The extremely short intermediate state lifetime, $\tau \approx 4 \times 10^{-12}$ sec., and the absence of an electric quadrupole interaction in a cubic symmetry indicate the product $\lambda_k \tau$ is very small and the integral attenuation coefficients G_{kk} are approximately unity. On the other hand, the ^{182}W, ^{169}Tm, and ^{171}Tm measurements were carried out with liquid sources. The size of the attenuation of an angular correlation in ^{182}W, in the chemical environment used here, has been measured by Körner et al.[14]. No such data are available for the case of thulium. In thulium the lifetimes of the nuclear levels are relatively long ($\approx 5 \times 10^{-10}$ sec.), and the paramagnetic atomic structure of thulium permits a strong time-dependent magnetic interaction. Thus, for a correlation time τ_c of $\approx 10^{-11}$ sec.[15] in a liquid source, the quantity $\lambda_k \tau$ could be appreciable. In Chapter V a measurement of the attenuation factor G_{22} is described which uses the fact that τ_c is roughly proportional to the viscosity of the liquid source. This assumption is based on the studies of Debye[16] on the properties of liquids made up of polar molecules and of Bloembergen et al.[17] on NMR measurements of spin-lattice and spin-spin relaxation times in liquids. The studies show that, to a good approximation, the correlation time τ_c is proportional to the ratio of viscosity to temperature.

III. MEASUREMENT OF THE MAGNETIC MOMENT OF THE SECOND EXCITED $I^\pi = 2^+$ TWO-PHONON VIBRATIONAL STATE IN ^{106}Pd

III.1 Introduction - Vibrational Models

The excited states of the even-even nucleus ^{106}Pd are populated in the decay of ^{106}Ru according to the partial decay scheme shown in Fig. 3 [18]. As is the case with most medium weight even-even nuclei, a first excited $I^\pi = 2^+$ state is observed followed by an $I^\pi = 0^+, 2^+, 4^+$ triplet of levels at approximately twice the excitation energy of the first excited state. This general level structure is predicted by the harmonic vibrational model for a spherical nucleus[19,20], which describes the first excited state as one quantum of vibrational energy $\hbar\omega$ built on the $I^\pi = 0^+$ spherical ground state. The correct spin and parity are obtained if the angular dependence of the vibratory mode is represented by the second order spherical harmonics $Y_{2\mu}(\theta\varphi)$ (i.e., a quadrupole vibration). Two non-interacting vibrational quanta or "phonons" form a degenerate triplet of states with $I^\pi = 0^+, 2^+, 4^+$ at an energy $2\hbar\omega$. This semi-classical approach treats the nucleus as a fluid-type mass. The motions of many individual nucleons are assumed to be correlated in a coherent fashion so as to produce a collective mass flow which resembles harmonic shape oscillations. The inertial and restoring force parameters, introduced in a phenomenological way, must be determined from experiment.

In addition to level energies, this macroscopic vibrational model yields predictions concerning electromagnetic transition rates between vibrational levels. Specifically, the collective quadrupole vibrational nature of the states leads to greatly enhanced electric quadrupole (E2)

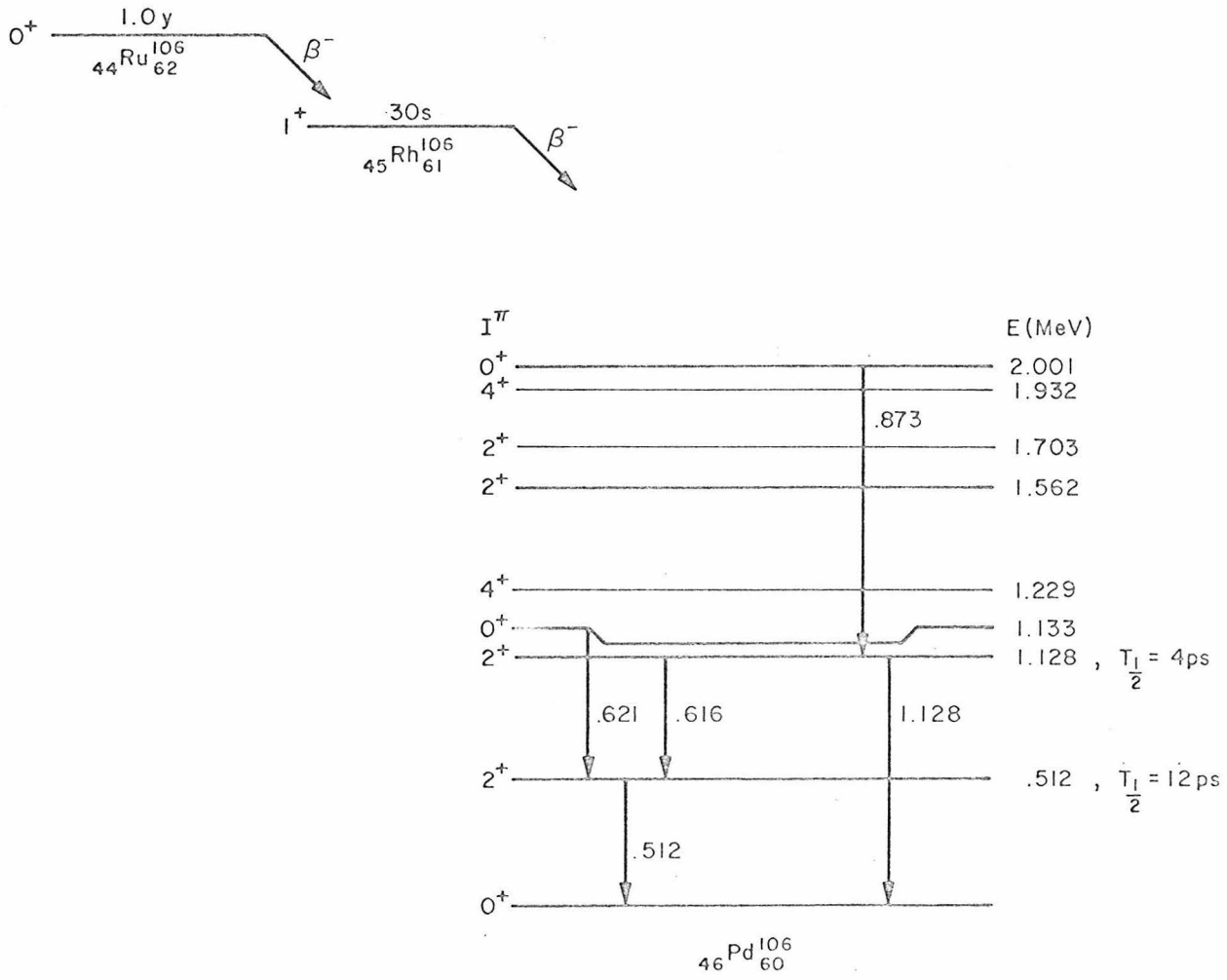

Figure 3: Partial level scheme of ^{106}Pd showing transitions of interest.

transition rates, from the second $I^{\pi} = 2^{+}$ state to the first and from the first $I^{\pi} = 2^{+}$ state to the ground state, over those expected for transitions involving a single nucleon. The ratio R of these rates defined as

$$R = B(E2:2' \rightarrow 2)/B(E2:2 \rightarrow 0) \qquad (16)$$

is predicted to be R = 2. However, an electric quadrupole transition from the second excited 2^{+} state to the ground state, which entails the destruction of two phonons, is forbidden, as is the one-phonon magnetic dipole (M1) transition from the second to the first 2^{+} state. From Table 1, which lists experimental values of the pertinent reduced transition probabilities, it is seen that the properties of ^{106}Pd are approximately those predicted for a spherical vibrational nucleus. In this scheme, the g-factor of a vibrational level (regardless of the number of phonons) is $\approx Z/A$, since the angular momentum of the nuclear fluid is carried by all nucleons and the magnetic moment is produced only by the orbital motion of the protons (neglecting intrinsic spin). The g-factors would be exactly Z/A if the nucleus were a uniformly charged liquid drop.

A microscopic model of vibrational nuclei has also been developed[21,22] which describes the excitations as coherent superpositions of many two-particle states. Short-range pairing forces and long-range quadrupole-quadrupole forces between nucleons were added to a nuclear shell model[23,24] Hamiltonian, and approximate solutions were obtained. This model, which we can call the "harmonic approximation", has the various names: Sawada's approximation, random phase approximation, method of approximate second quantisation, method of linearized

Table 1

Transition Probabilities for ^{106}Pd

Quantity	Exp. Value [a]	Single Particle Units
$B(E2;\ 2^+ \rightarrow 0^+)$	$1.29 \times 10^{-49} e^2 cm^4$	44
$B(E2;\ 2^{+'} \rightarrow 2^+)$	$1.30 \times 10^{-49} e^2 cm^4$	44
$B(E2;\ 2^{+'} \rightarrow 0^+)$	$0.29 \times 10^{-50} e^2 cm^4$	1
$\frac{B(E2;\ 2^{+'} \rightarrow 2^+)}{B(E2;\ 2^+ \rightarrow 0^+)} = R$	1.00 ± 0.37	
$B(M1;\ 2^{+'} \rightarrow 2^+)$	$\leq 1.7 \times 10^{-4}\ (nm)^2$	

a) P.H. Stelson and F.K. McGowan, Phys. Rev. 110 (1958) 489; and 121 (1961) 209.

equations of motion, and Dyson's new Tamm-Dancoff method. The inertial and restoring force parameters of the macroscopic model are replaced here by interaction force constants, some of which can be determined independently in measurements on nuclear reactions and scattering or from odd-even mass differences. The model predicts[25,26,27,28], with fair success, the energies and transition probabilities for collective vibrational states. But, because of the "harmonic approximation" method used, the E2 transition from the second 2^+ to the ground state and the M1 transition from the second 2^+ to the first 2^+ state are forbidden, and the two-phonon triplet of states is expected to be degenerate. Also, since the model represents the elemental vibrational excitation as a true boson composed of many particle pairs, each coupled to angular momentum 2^+, the two-phonon (boson) state is expected to have the same g-factor as the one-phonon level. Lombard[28] has predicted the value of $g = 0.53$ for ^{106}Pd which is close to the macroscopic model prediction of $g \approx Z/A = 0.44$.

Experimental evidence on properties of ^{106}Pd[29,1] as well as many other medium weight vibrational nuclei have shown the g-factors of the first 2^+ states to be approximately equal to but usually somewhat less than Z/A[30]. However, in these same nuclei the forbidden E2 and M1 transitions mentioned above are found to be hindered but usually present, and the ratio of the reduced transition probabilities R is found to deviate significantly from the value R = 2 predicted by the models[31]. Also, the two-phonon triplet is not found to be degenerate. Especially damaging is the recent evidence[32] that the one-phonon states of some Cd, Te, Sn, Ba, and other isotopes possess static

quadrupole deformations, which contradicts the picture of simple harmonic motion about spherical equilibrium. Two approaches to the resolution of these discrepancies have been employed. In the first, the macroscopic model is used, and an anharmonicity is assumed to exist, without regard for its physical origin, which causes the mixing of the one- and two-phonon states[33]. This technique successfully accounts for values of the ratio R, the static quadrupole moments, the non-zero values of $B(E2:2' \rightarrow 0)$, and the splitting of the two-phonon triplet, but again requires $B(M1:2' \rightarrow 2)$ to be zero. The M1 rate is forced to zero since, if the M1 transition is forbidden between the pure states, the M1 transition amplitude between the mixed states is proportional to the difference in magnetic moments of the pure states and this must be zero in the case of a hydrodynamical fluid model where all g-factors are equal.

The second, microscopic, approach to the problem is quite complex. It goes beyond the "harmonic approximation" by including phonon-phonon interaction terms in the Hamiltonian and also accounts for exchange terms and the Pauli exclusion principle for the particles forming a phonon[34]. The structure of the basic phonon resulting from these calculations is now altered so that not only are the electric quadrupole properties accounted for but the magnetic moments of the one- and two-phonon states may now differ, allowing a finite value of $B(M1:2' \rightarrow 2)$ to exist[35]. Yamamura et al.[36] have pointed out that the inclusion of the above-mentioned corrections to the "harmonic approximation" method have so severe an effect on the predicted structure of the two-phonon state that the concept of a two-phonon excitation may begin to

break down. The data in Table 1 indicate the presence of anharmonic effects in the nucleus ^{106}Pd. An experimental test of the equality of the one- and two-phonon state magnetic moments should indicate whether the two-phonon state has large components of particle configurations unrelated to a vibrational mode or whether it can be considered a true vibrational state.

III.2 Experimental Procedure and Apparatus

a. The Gamma-Gamma Cascade

Figure 3 shows a gamma-gamma cascade through the $I^{\pi} = 2^{+}$ two-phonon state at 1128 keV in ^{106}Pd appropriate for the measurement of the g-factor. The gamma-ray energies are 873 keV and 1128 keV in the cascade $0^{+}(E2)2^{+}(E2)0^{+}$. The expected angular correlation coefficients corresponding to this spin sequence are the largest known (theoretically $A_{22} = 0.357$ and $A_{44} = 1.143$). Because of inconsistencies in the literature[37] regarding the existence and placement of some gamma transitions in the ^{106}Pd level scheme, we undertook a preliminary measurement using a Ge(Li) semiconductor detector with high energy resolution. The Ge(Li) detector spectrum was stored in a 4096 channel pulse height analyzer. A portion of the resulting spectrum is shown in Fig. 4. It is evident that the only gamma transitions of substantial intensity in the energy region of interest are the 873 keV, 1050 keV and 1128 keV transitions. It is known that the 1050 keV transition does not populate a spin 0^{+} state[37,18]. Therefore, the measurement of angular correlation coefficients consistent with a $0^{+} - 2^{+} - 0^{+}$ spin sequence, to be reported in Section III.3, indicates that the 1050 keV and 873 keV transitions are not in coincidence and that no interfering

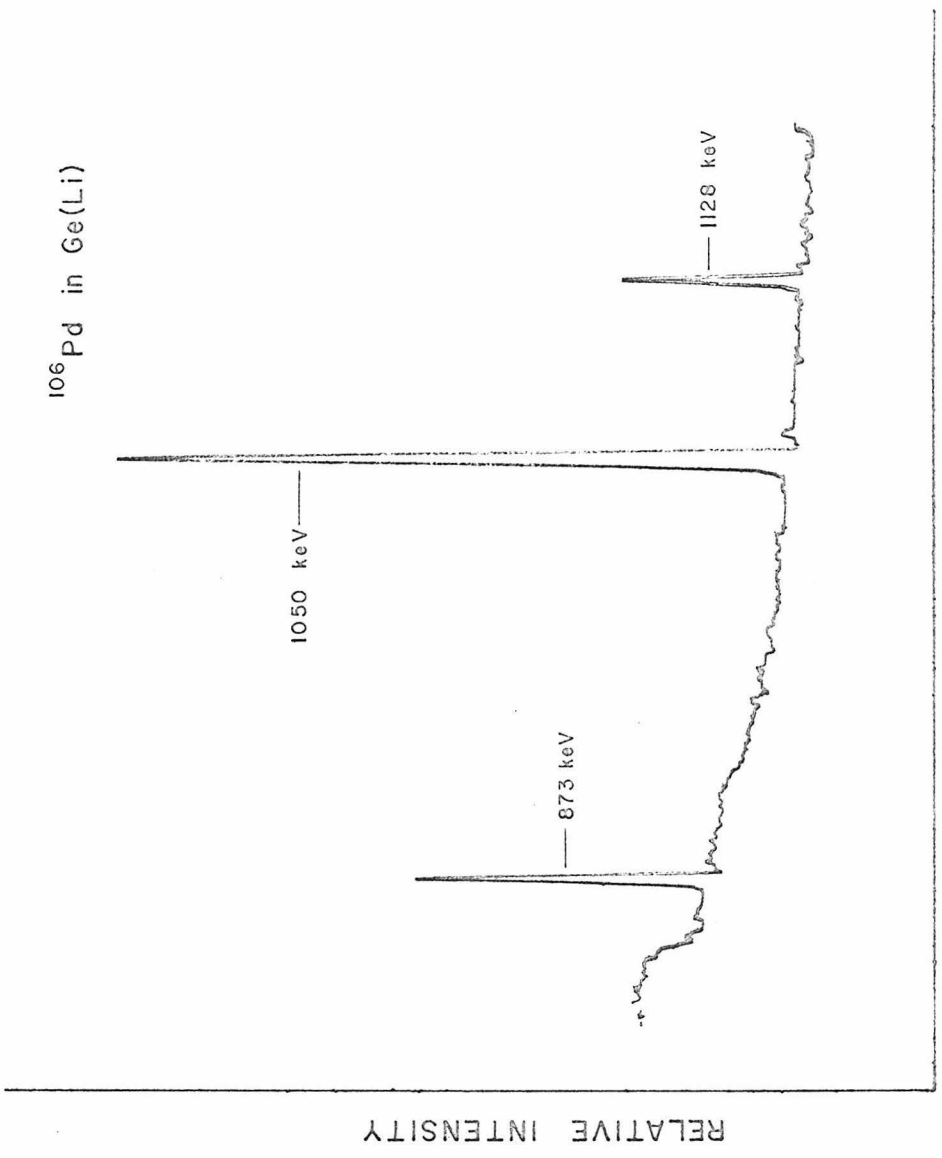

Figure 4: Portion of the gamma-ray spectrum of ^{106}Pd, observed with a Ge(Li) detector.

cascades are present in the current measurement.

The lifetime of the intermediate state is so short ($\tau = 3.5 \times 10^{-12}$ sec.[31,38]) that a very large magnetic field is needed to obtain an observable spin rotation angle. To produce this field, use is made of the large internal hyperfine field at the site of a Pd nucleus in an Fe lattice. This technique of obtaining large fields is described in Ref. (39) and in references cited there. The hyperfine fields at impurity sites in an Fe lattice have been found to vary with temperature in approximately the same way that the bulk magnetization of the host lattice varies[40]. This indicates that a sizeable contribution to the observed hyperfine fields arises from conduction electrons polarized through exchange interactions with the 3d electrons of the Fe atom. The size of the hyperfine field is also known to vary from one impurity element to another and in fact changes sign in some regions of the periodic table[40]. This effect indicates atomic core electron polarization also contributes to the observed fields. Although quantitative theoretical calculations of these fields based on the phenomena of conduction electron and core electron polarization have not proven accurate, the available empirical values of the field strengths from Mössbauer effect, nuclear magnetic resonance, nuclear orientation, and perturbed angular correlation measurements may be used in the determination of nuclear moments. In particular, the field at Pd in Fe has been measured[41] to be $H_{int} = -594 \pm 12$ kG using the spin echo technique of NMR at liquid helium temperature. This total internal field, H_{int}, is composed of the large hyperfine field mentioned above as well as the so-called Lorentz field which arises from the bulk magnetization

of the material and the field produced by nearby atoms which may possess an induced dipole moment. The small external aligning field and the demagnetization factor accounting for sample shape can usually be neglected.

b. Source Preparation and the Magnet

The parent radioactivity used in the measurement was ^{106}Ru obtained from Oak Ridge National Laboratory in the form of ruthenium trichloride in HCl solution. The solution was neutralized, and the ruthenium hydroxide precipitate was collected and placed on an Fe dish of high purity (99.99 percent). The dish was placed on a flux-concentrating silver boat in the coil of a 5 kW induction furnace and heated in a hydrogen atmosphere to reduce the hydroxide to ruthenium metal. The hydrogen was then replaced by argon gas, and the temperature raised to melt the Fe dish. Ruthenium metal is soluble in Fe[42] and dissolved with the loss of only 10 percent of the initial radioactivity. The high specific activity of the Ru sample allowed the preparation of a source with sufficient activity for the measurement ($\approx 3 \times 10^6$ decay/sec.) while maintaining a dilute solution of Ru in Fe (0.01 atomic percent Ru). The Ru-Fe alloy ingot was then placed in a hardened steel drill bushing and coined between two hardened drill blanks into the shape of a right circular cylinder of 7/32 in. diameter and approximately 1/4 in. length. The external aligning magnetic field was supplied by a small cylindrically symmetric electromagnet having a "toroidal H" geometry in which the coined source was used to complete the continuous flux return path. This magnet design minimizes external

fringing fields in the region of the radiation detectors. To further reduce the stray fields, a compensation coil, which carried an adjustable fraction of the magnet current, was wound on the magnet body. In this way, the stray field due to the magnet was reduced to less than 5×10^{-4} G in the region of the detectors. Diagrams of the melting apparatus and magnet are given in Figs. 5 and 6.

c. Detectors and Electronic Apparatus

The gamma rays were detected by two identical 3 x 3 in. NaI(Tl) scintillation crystal spectrometers including ten-stage photomultiplier tubes. The multipliers were wrapped in several layers of netic and conetic foils to minimize the influence of the small stray magnetic fields on multiplier gain, and lead collimators prevented the detection of scattered radiation by the crystals. A diagram of the photomultiplier assembly is given in Fig. 7.

Pulses from the detectors were analyzed by a slow-fast coincidence counting apparatus[43], a schematic block diagram of which is presented in Fig. 8. The photomultiplier anode pulses were split into low and high frequency components. A low level discriminator accepting the high frequency component was gated on only when the low frequency signal, whose amplitude is roughly proportional to the energy of the incident gamma ray, exceeded a threshold determined by a second discriminator. Thus, pulses corresponding to the intense 512 keV and 621 keV transitions were rejected by the fast electronics without creating excessive electronic dead time. The two low level discriminator signals, one corresponding to each detector, jointly operated a time-to-amplitude converter (TAC), whose output pulse height is proportional to the time

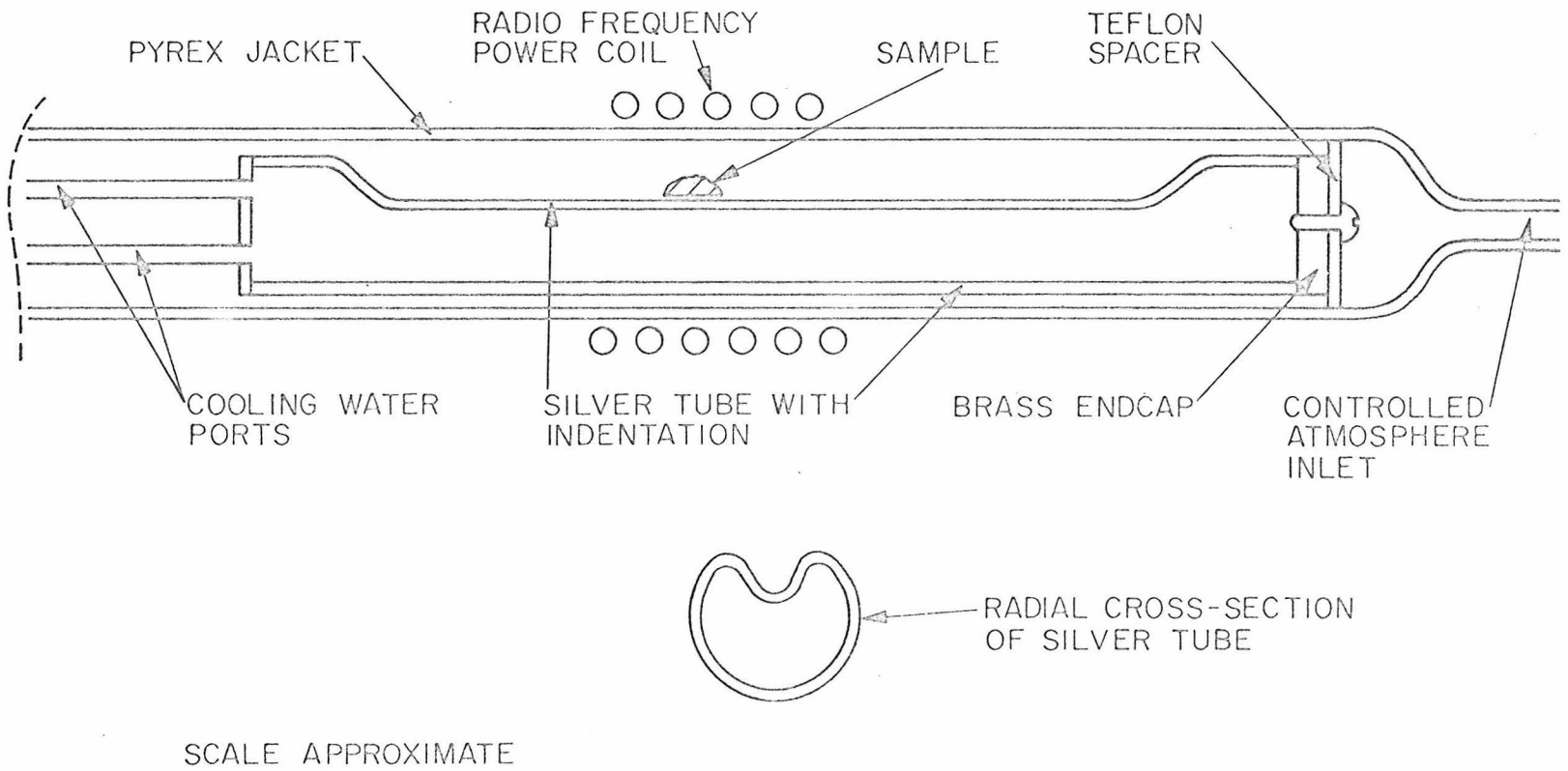

Figure 5

The silver boat and controlled atmosphere assembly used to form the Ru-Fe alloy.

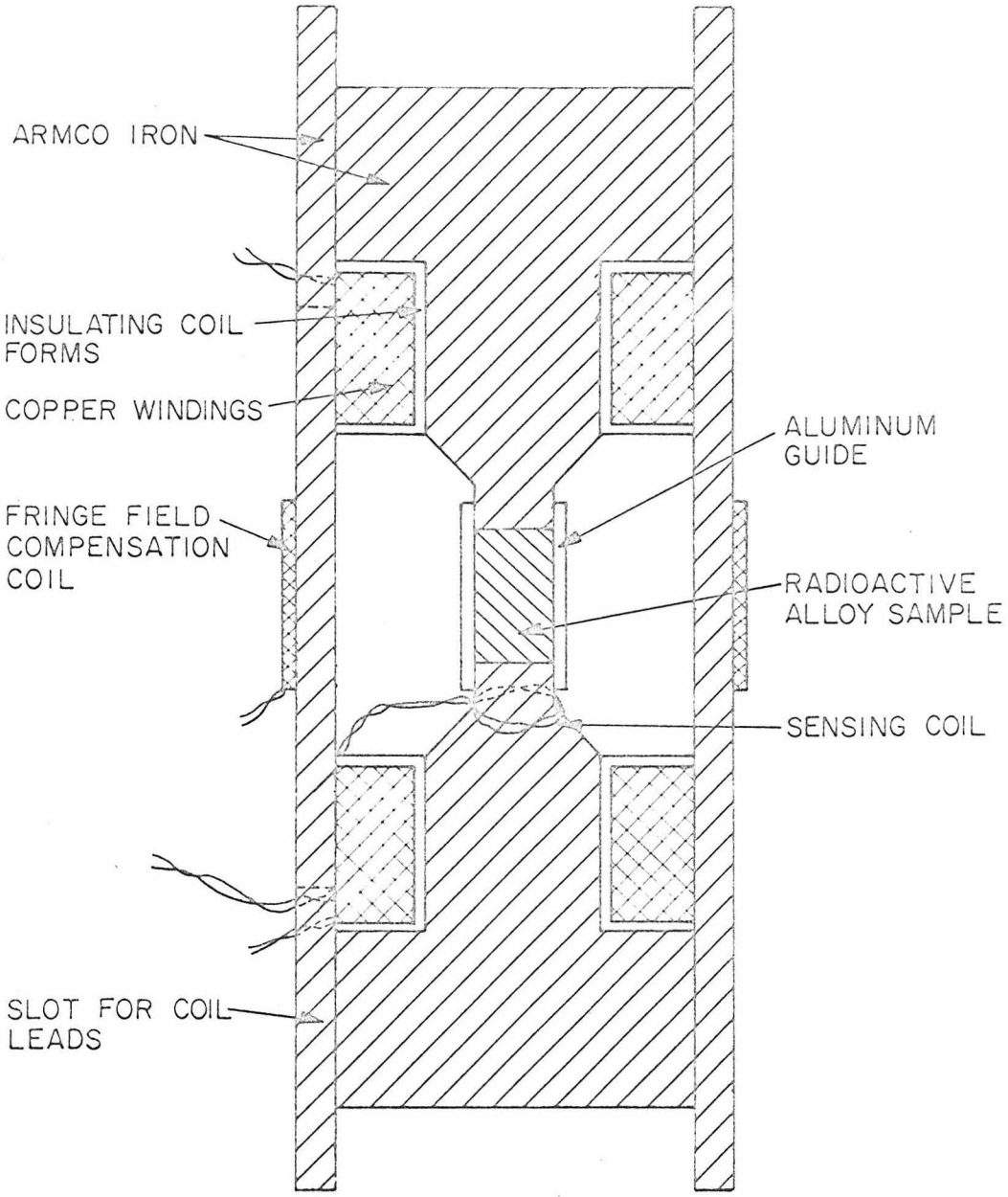

Figure 6

Cross-section of the "toroidal H" magnet used in the measurement on ^{106}Pd.

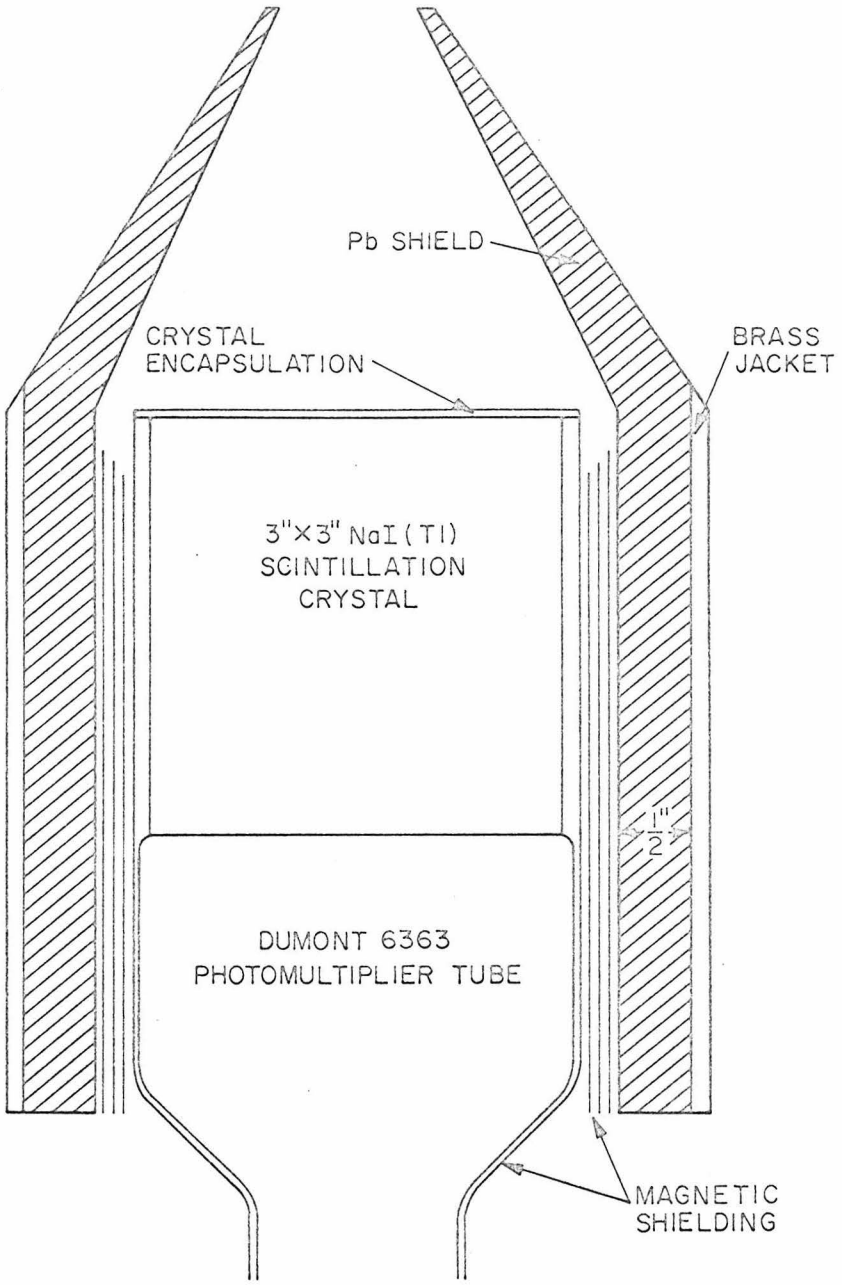

Figure 7

Cross-section of NaI(Tl) scintillation crystal spectrometer used in the measurement on ^{106}Pd.

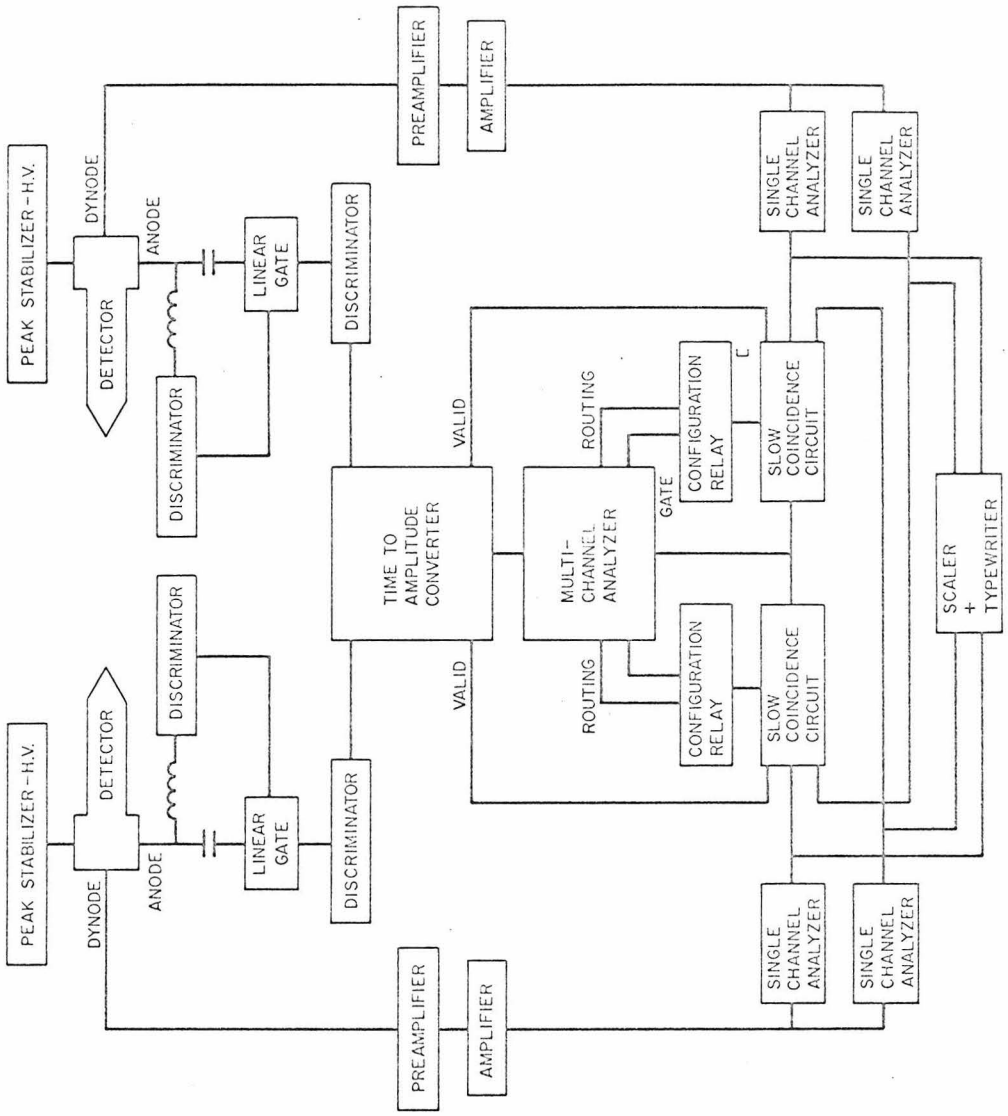

Figure 8: Flow diagram of electronic slow-fast coincidence counting system in the arrangement used for ^{106}Pd.

between the arrival of the two input signals. The photomultiplier dynode pulses, after suitable amplification and amplitude discrimination by a single-channel analyzer, were accepted by a slow (time constants of the order of 10^{-6} sec.) coincidence circuit. In addition to pulses from the single-channel analyzers, the coincidence circuit accepted a logic pulse from the TAC which indicated the successful processing of a fast pulse pair. The time spectrum provided by the TAC was stored in subsections of a 400-channel pulse height analyzer, which was gated on by the slow coincidence circuit according to the direction of aligning magnetic field or the angle between the two detectors. As can be seen from Fig. 8, each detector supplied pulses to two single-channel analyzers allowing both the 873 keV and 1128 keV gamma rays to be accepted in each detector channel. This technique doubled the rate of data collection and served to eliminate systematic errors arising from small errors in the positioning of the detectors. The NaI(Tl) scintillation spectrum as well as the settings of the single-channel analyzers is shown in Fig. 9, and a typical time-to-amplitude spectrum is given in Fig. 10.

III.3 Results

Coincidence counting rates were measured for several values of the angle between detectors to determine the angular correlation coefficients for the geometry used. The experimental values of the function $W(\theta)$ of Eq. (1) are plotted in Fig. 11, where the result of a least-squares fit to the data is also shown. The fitted values of the correlation coefficients were found to be $A_{22} = 0.262 \pm 0.007$ and

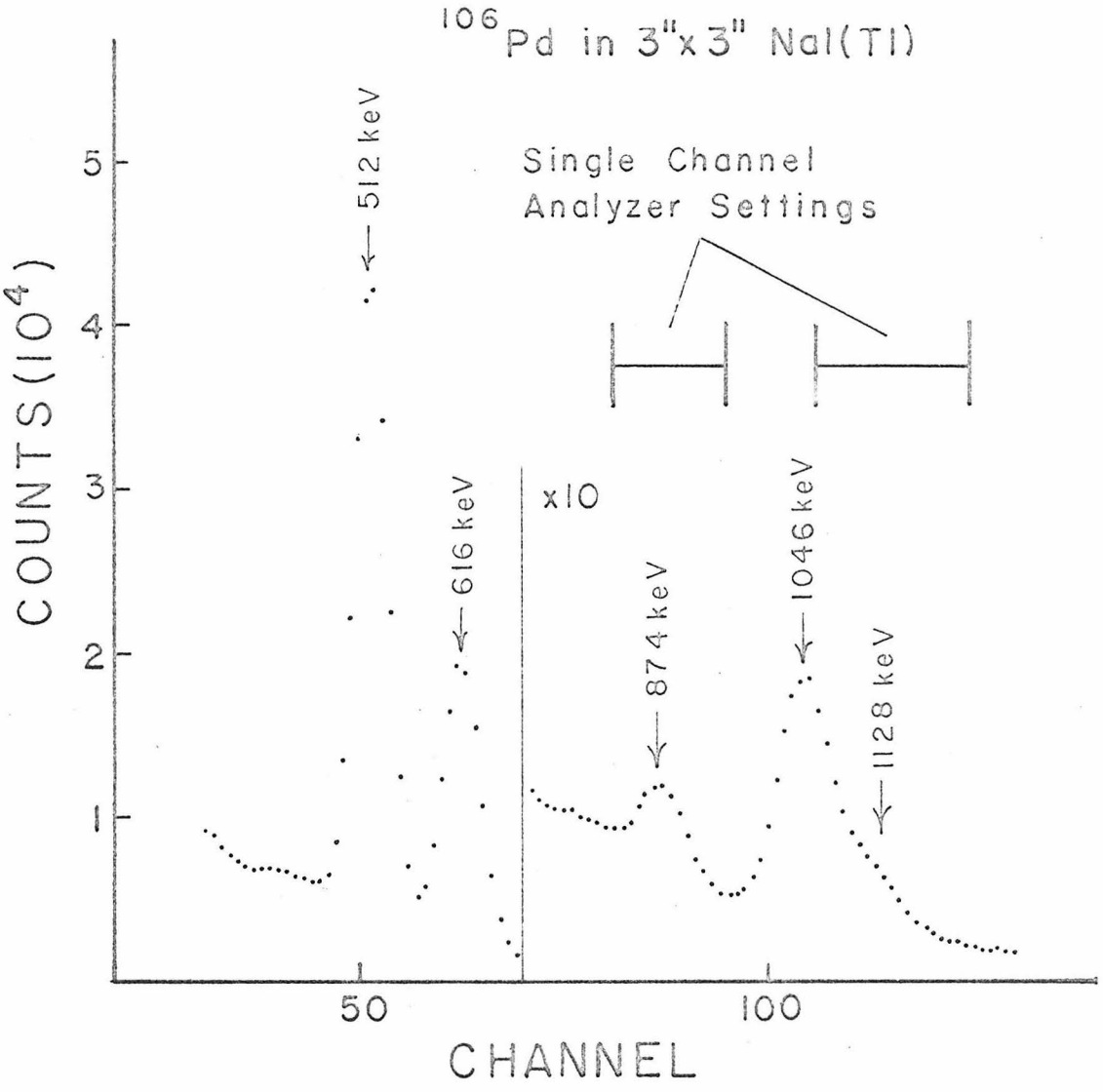

Figure 9

Gamma-ray scintillation spectrum of ^{106}Pd as observed by the detector assembly shown in Fig. 7. The settings of the single-channel analyzers are shown.

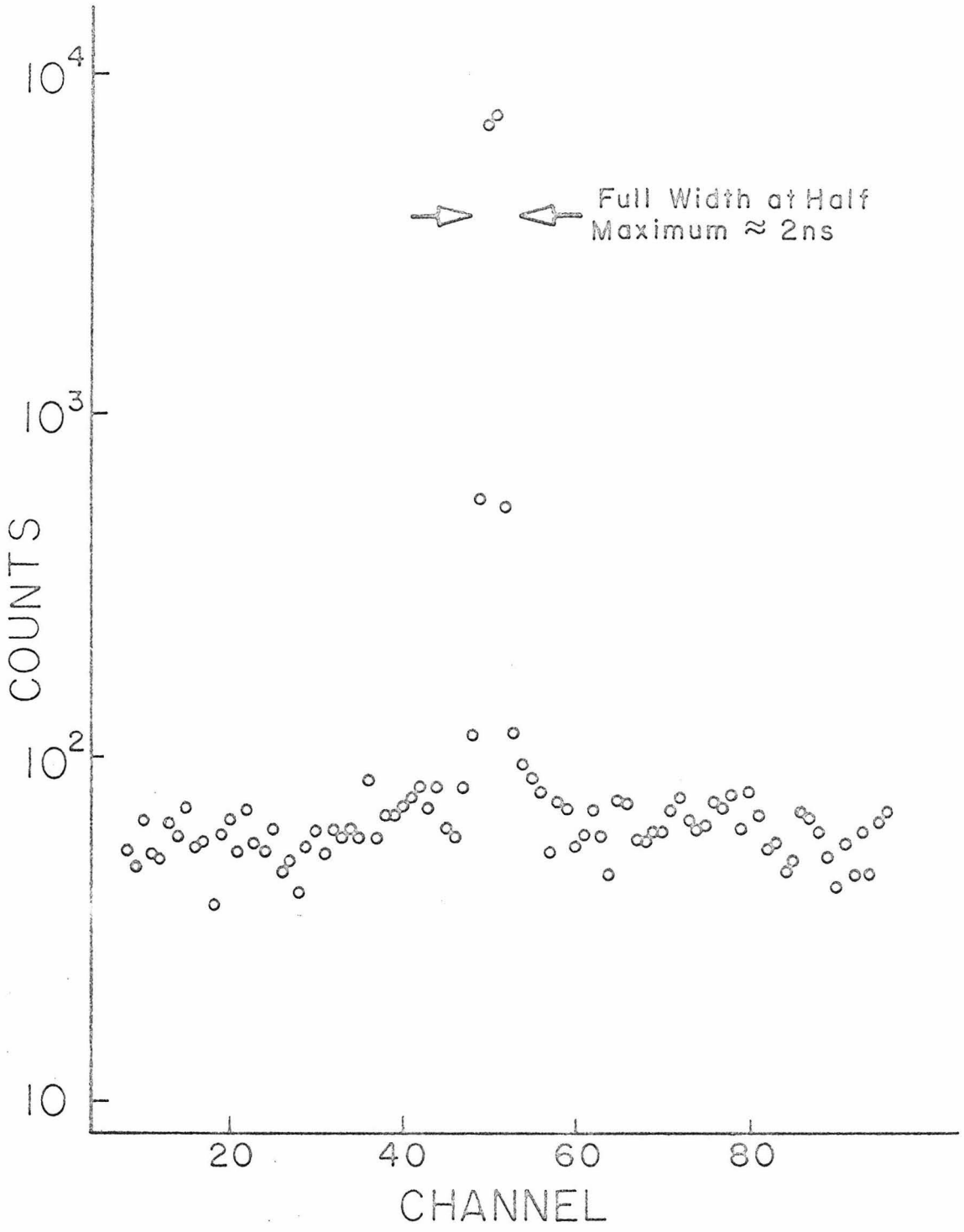

Figure 10

Typical time-to-amplitude converter pulse height spectrum as stored in the multichannel analyzer (for ^{106}Pd).

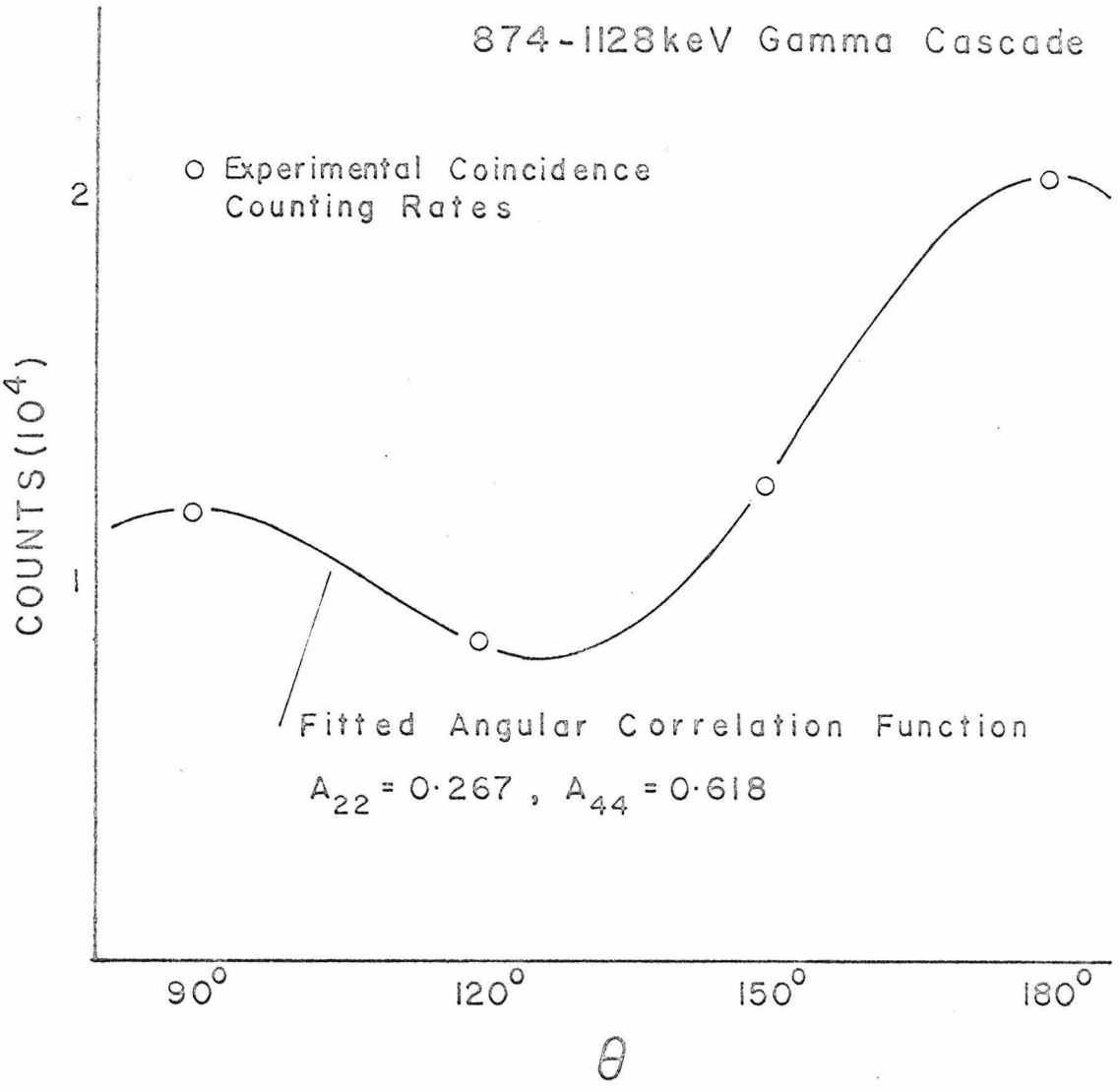

Figure 11

Plot of the experimentally measured coincidence counting rate for four angles between detectors and the theoretical function fitted to the data. The size of the plotted points is greater than the statistical error.

$A_{44} = 0.618 \pm 0.008$. The finite solid angle subtended by the detectors and small angle scattering of the gamma rays in the source and magnet material account for the difference between the observed and theoretical values of these coefficients. To measure the quantity ϵ defined in Eq. (9), the angle between the detectors was fixed at either 150° or 210° where $|\epsilon|$ is expected to be a maximum. During each experimental run, lasting one day, the magnetic field direction was reversed every three minutes. To check the effect of stray fields on the photomultiplier gain, the singles counting rates from the four single-channel analyzers were monitored and found to be independent of magnetic field direction to better than 0.01 percent.

Twenty-seven such runs were performed, each accumulating 7×10^4 coincidence counts, and the weighted average of the results yielded $\epsilon(150^{\circ}) = -\epsilon(210^{\circ}) = (0.566 \pm 0.074) \times 10^{-2}$. The statistical consistency of the data was excellent, as indicated by the normalized chi-square of 0.98. As a control experiment, the effect in the random background of the time spectrum was also calculated and was found to be $\epsilon_{random} = (-0.49 \pm 1.36) \times 10^{-3}$, consistent with a null result. The spin rotation angle $\omega\tau$, determined from ϵ, A_{22}, and A_{44} by means of Eq. (9), was $\omega\tau = (3.63 \pm 0.47) \times 10^{-3}$ rad.

The lifetime of the 1128 keV level has been deduced from Coulomb excitation experiments by Stelson and McGowan[31] to be $\tau = (5.1 \pm 1.9) \times 10^{-12}$ sec. and by Gangrksii et al.[38] to be $\tau = (3.32 \pm 0.51) \times 10^{-12}$ sec. We adopt the weighted average of $\tau = (3.46 \pm 0.49) \times 10^{-12}$ sec. The measurement of the internal hyperfine field at Pd in Fe of $H_{int} = -594 \pm 12$ kG by Kontani and Itoh[41] was conducted at the temperature

of liquid helium, whereas our measurements were performed at room temperature. To correct for the difference in temperature, we use the results of Johansson et al.[44], who found that the field at Pd in Fe shows essentially the same temperature dependence as the bulk magnetization of the Fe lattice. From their data we find the appropriate field for room temperature is $H_{int} = -573 \pm 20$ kG. Finally, using the adopted value of τ and H_{int} and our measured value of $\omega\tau$, we find from Eq. (6) that the g-factor of the 1128 keV state in ^{106}Pd is $g_{2'} = 0.370 \pm 0.071$.

Fields at impurity sites in an Fe lattice may be a function of the history of the sample and the impurity concentration. In our case, we can neglect possible concentration effects in our extremely dilute alloy; however, to check the effect of the mechanical stresses present in the source, we measured the spin rotation of the first 2^+ state at 512 keV in ^{106}Pd in the experimental configuration described above. This control experiment gave a value of $\omega\tau = (1.73 \pm 0.02) \times 10^{-2}$ rad. in excellent agreement with the earlier result of $\omega\tau = (1.76 \pm 0.03) \times 10^{-2}$ rad. obtained by Auerbach et al.[29]. Thus it appears that the field in our source is the same as that found in previous investigations. Assuming a lifetime of $\tau = (17.3 \pm 1.1) \times 10^{-12}$ sec.[31] for this state and the previously quoted value of H_{int}, we find $g_2 = 0.365 \pm 0.028$. In addition, the ratio of the moments of the one- and two-phonon states is now found to be $g_{2'}/g_2 = 1.01 \pm 0.20$, a value independent of the assumed strength of the internal hyperfine field.

III.4 Conclusion

The results indicate that the g-factor of the second excited $I^{\pi} = 2^{+}$ state in ^{106}Pd is slightly less than Z/A and is equal to the g-factor of the first excited 2^{+} state, within reasonable limits of error. This agrees with the predictions of the macroscopic model described in Section III.1 for both the pure harmonic assumption and the modified version which allows the mixing of one- and two-phonon states through anharmonic terms. The result is also consistent with the microscopic "harmonic approximation" model. From the equality of the g-factors and the very small, if not zero, value of $B(M1:2' \rightarrow 2)$ (cf. Table 1), we can conclude that, although the microscopic model extended to include corrections to the "harmonic approximation" is needed to account for the Fermi statistics of a system of nucleons, the detailed particle configuration of the two-phonon $I^{\pi} = 2^{+}$ state is not altered by these corrections to the extent predicted by Yamamura et al.[36]. Unfortunately, no quantitative predictions of the second excited 2^{+} level moment based on this microscopic model are available for comparison.

IV MEASUREMENT OF THE MAGNETIC MOMENT OF AN $I^{\pi} = 2^{-}$ TWO-QUASIPARTICLE STATE IN ^{182}W

IV.1 Introduction - Rotational Model and Strong Coupling

Nuclei with mass numbers in the range $150 < A < 190$ have long been known to possess static quadrupole shape deformations and to display energy level schemes corresponding to rotational excitations[45,19]. The phenomenological rotational model developed by Bohr and Mottelson[19] accounts very well for observed properties of rotational bands. Individual nucleon orbits in the deformed potential have been computed by Nilsson[46] and Rassey[47]. Upon each intrinsic configuration of particle orbits is built a rotational band whose energies (with one exception described in Chapter V) follow the $I(I + 1)$ spacing rule for a rigid rotator. The deformed nucleus ^{182}W, whose partial level scheme is shown in Fig. 12 [18], displays a well-formed rotational band built on the $I^{\pi} = 0^{+}$ ground state. Above 1 MeV, the energy levels become quite dense and consist of rotational bands built on vibrational and particle excitations of the deformed core. The $I^{\pi} = 2^{-}$ level at 1289 keV has been identified[48] as the lowest state of a "K = 2" rotational band. Its intrinsic structure assignment[49] of $p_{5/2^{+}}[402]$ $p_{9/2^{-}}[514]$ has been confirmed by comparison of the 1289 keV M2 transition rate with those between corresponding single particle states in neighboring odd-mass nuclei[50]. The quantum number K is the projection of the total angular momentum on the symmetry axis of the rotationally symmetric nucleus and is a good quantum number in the rotational model. The designations $p_{5/2^{+}}[402]$ and $p_{9/2^{-}}[514]$ indicate

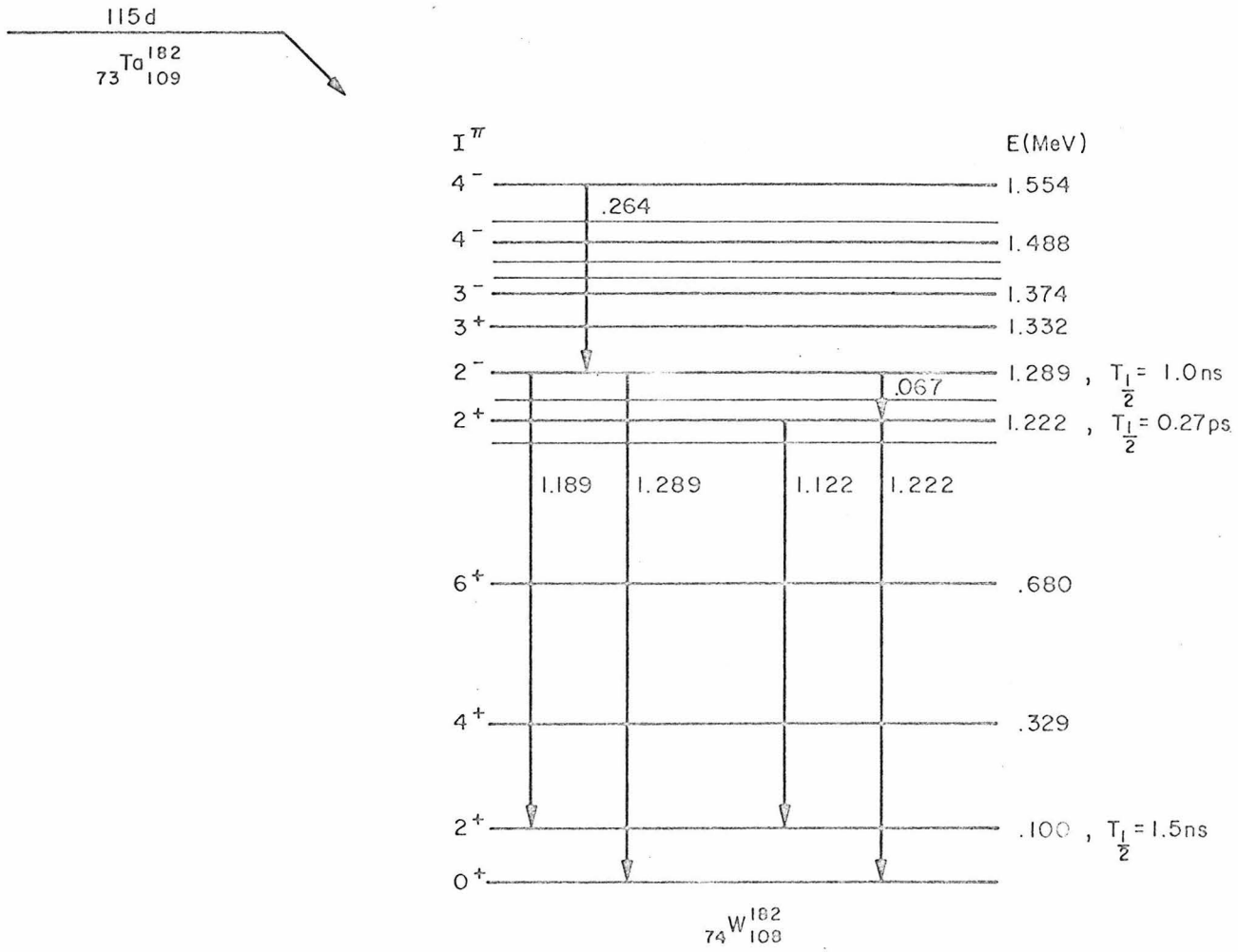

Figure 12

Partial level scheme of ^{182}W showing transitions of interest.

that two-proton quasiparticles[+] have been excited from the even-even core into the single particle Nilsson[46] orbits $[402]5/2^+$ and $[514]9/2^-$, respectively. The first orbit has angular momentum projection $\Omega_1 = 5/2$ on the nuclear symmetry axis, and the second has $\Omega_2 = 9/2$. The value of $K = \Omega_2 - \Omega_1 = 2$ is thus obtained for the rotational band. A band with $K = \Omega_1 + \Omega_2 = 7$ has not been positively identified, but may occur at a higher excitation energy than the K = 2 band. A state at 1961 keV with $I^\pi = 7^-$ is a likely candidate.

Only two parameters, g_K and g_R, are needed to describe the magnetic properties of a K = 2 rotational band. The quantity g_R is the rotational or collective g-factor of the core as a whole, and g_K is the contribution of the intrinsic particle structure. In order to investigate the way in which the two excited protons couple to the even core and to each other, an experimental determination of g_K is desirable. In particular, the "strong-coupling" rule[52], which neglects particle-particle interactions and assumes each particle to be independently coupled to the deformed core, can be tested.

Grigor'ev et al.[48] have deduced magnetic dipole transition rates among the first three levels of the K = 2 rotational band from a measured lifetime and internal conversion and gamma-ray transition intensities. In doing so, the intrinsic electric quadrupole moment for

---

+ In accounting for the effect of the short-range pairing force between like particles in nuclei, it was found that, in order to retain the simple Nilsson orbital picture, a new mathematical construct called a quasiparticle had to be introduced[51]. For our purposes the difference between particle and quasiparticle is not important.

the K = 2 band was assumed to be the same as that of the ground state K = 0 band. From the deduced M1 transition rates within the band, which in the rotational model are given by[20,19]

$$B(M1:I_iK \rightarrow I_fK) = \frac{3}{4\pi} K^2 (I_i 1K0 | I_f K)^2 (g_K - g_R)^2 \text{ nm}^2, \tag{17}$$

the value of $|g_K - g_R|$ was determined. Thus a measurement of the magnetic moment of a state in the band, which can be expressed as[19]

$$\mu_I = g_R I + (g_K - g_R) \frac{K^2}{I + 1} , \tag{18}$$

will allow the direct determination of g_K. We therefore undertook the measurement of the magnetic moment of the $I^\pi = 2^-$ band head using the general technique described in Chapter II.

IV.2 Experimental Procedure and Apparatus

a. The Gamma-Gamma Cascade and the Magnet

From the level scheme of Fig. 12, it is seen that two gamma-gamma cascades through the 1289 keV $I^\pi = 2^-$ level can be used: namely, the 264 - 1289 keV cascade with the spin sequence $4^-(E2)2^-(M2)0^+$ and the 264 - 1189 keV cascade with the spin sequence $4^-(E2)2^-(E1)2^+$ are appropriate. The measured halflife of the 2^- level of $T_{1/2} = (1.00 \pm 0.05) \times 10^{-9}$ sec.[53] is large enough for a measurable spin rotation to be produced using an external magnetic field. A water cooled electromagnet was fabricated which supplies a field greater than 30 kG in a 1 mm pole gap. A diagram of the magnet assembly is given in Fig. 13. The iron magnet body, which serves as a flux return path, was

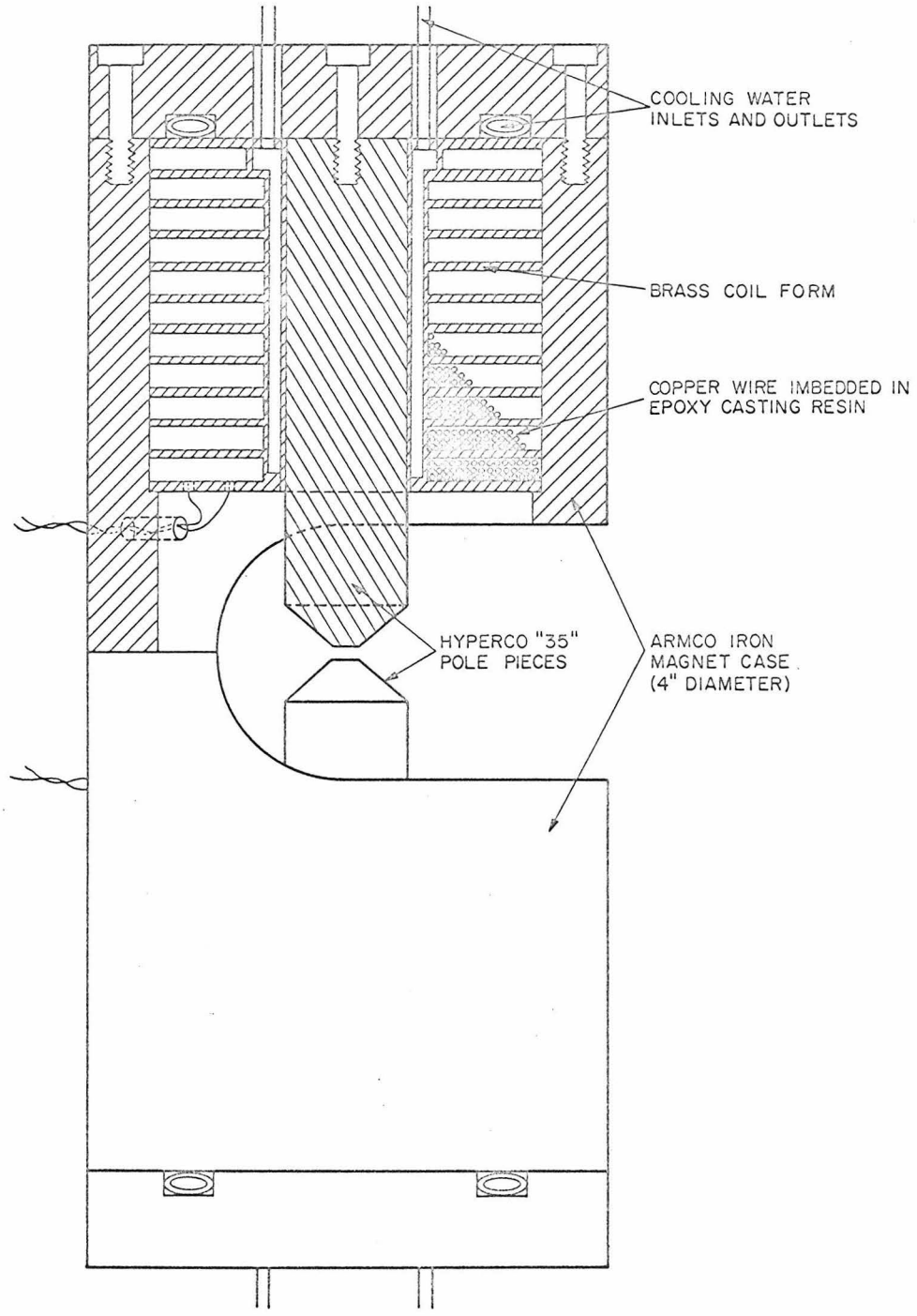

Figure 13

Cutaway view of the high-field electromagnet used in the ^{182}W experiment.

designed to minimize external fringing fields. A current of approximately 30 amperes was drawn from the secondary coils of a direct current generator, and field reversal was accomplished by reversing the small current in the primary coils. In this way, the problem of arc suppression, which arises when the current through an inductive load is abruptly changed, was avoided.

b. Source Preparation and Detectors

Radioactive ^{182}Ta($T_{1/2}$ = 115 days) was produced by thermal neutron capture on ^{181}Ta at the Materials Testing Reactor of the Idaho Nuclear Corporation. The source material was allowed to decay until the double neutron capture product ^{183}Ta ($T_{1/2}$ = 5 days) could not be detected. The Ta metal was then dissolved in hydrofluoric acid and sealed in a thin-walled (0.004 in.) polyethylene sack which was placed in the pole gap of the magnet. A 4 x 4 in. NaI(Tl) scintillation crystal coupled to a magnetically shielded CBS 7819 photomultiplier tube was used to detect the high-energy gamma rays. The 264 keV gamma ray, on the other hand, cannot be resolved by a NaI(Tl) detector to the exclusion of other interfering gamma transitions. Therefore to detect the 264 keV radiation, a Ge(Li) semiconductor detector operating at liquid nitrogen temperature was used. A schematic diagram of the detectors is given in Fig. 14.

c. Electronics

The electronic slow-fast coincidence counting system used was similar to that described in the previous chapter with two exceptions. Namely, both gamma rays could not be accepted symmetrically in both detectors since the NaI(Tl) detector could not resolve the 264 keV

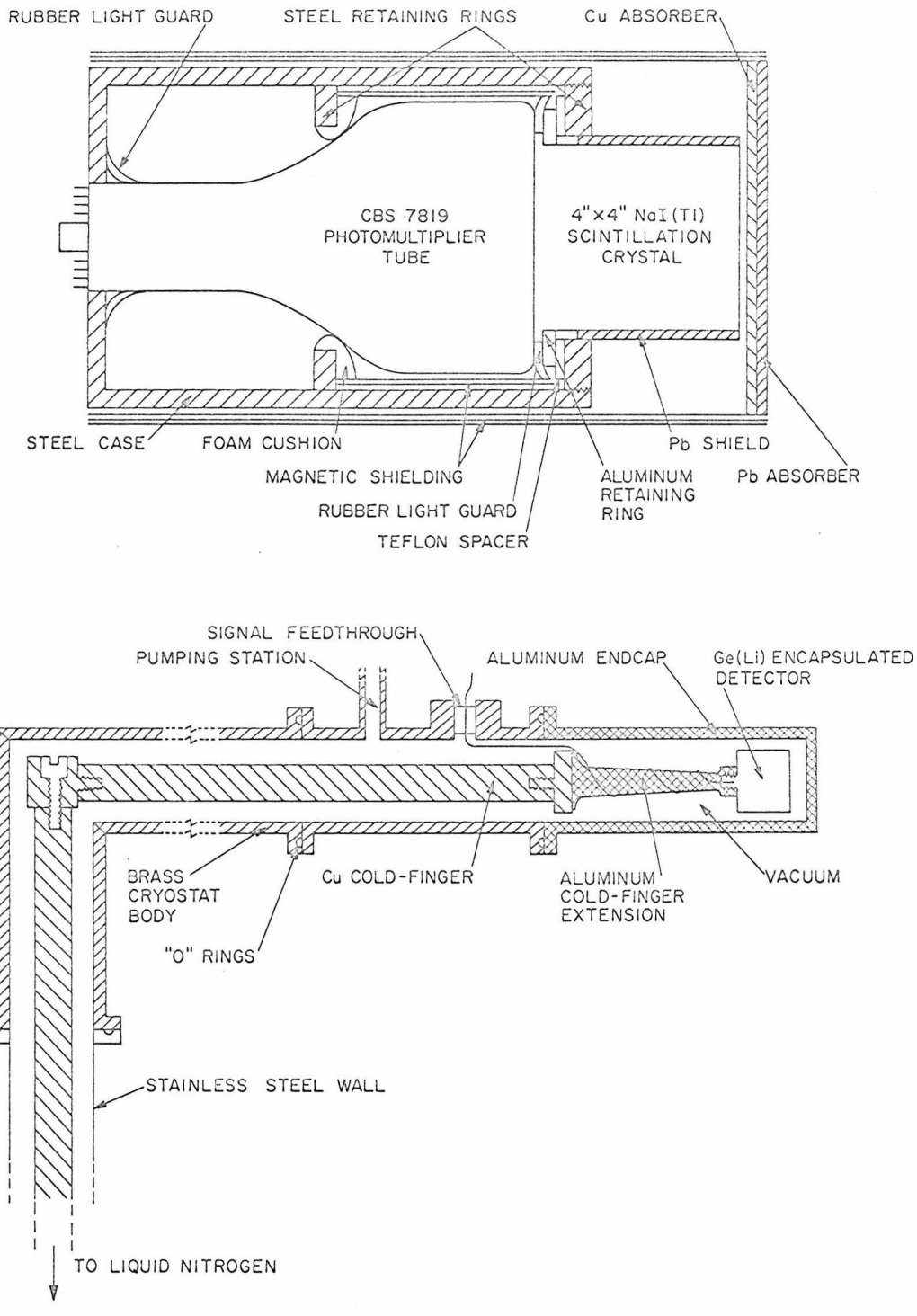

Figure 14

Cross-sectional diagram of the NaI(Tl) and Ge(Li) detector assemblies used in the ^{182}W experiment.

radiation, and no single-channel analyzer was needed in the slow NaI(Tl) channel. The energy selection for the NaI(Tl) spectrum was provided by a fast integral discriminator. Figure 15 shows a block diagram of the electronic apparatus, and Figs. 16a and 16b display the spectra in each detector and the spectral regions selected by the electronics. The signal from the time-to-amplitude converter was stored in subsections of the 400-channel pulse height analyzer according to the angle between detectors or the magnetic field direction as described in the previous chapter. A typical time spectrum is shown in Fig. 17. The best time resolution of a system containing a Ge(Li) detector is somewhat worse than that possible with two NaI(Tl) detectors (cf. Fig. 10). This is due, in part, to the greater sensitivity of the shape of the leading edge of pulses from the Ge(Li) system to the electronic noise. The large size of the NaI(Tl) crystal employed and the integral energy discrimination also contributed to the width of the prompt coincidence peaks shown in Fig. 17.

IV.3 Results

Based on tabulated values of theoretical angular correlation coefficients[54] for all cascades accepted by the electronics, it is expected that the coefficient A_{44} for the cascades used is at least an order of magnitude smaller than A_{22} and can be neglected. Therefore the ratio $W(\theta)/W(90^{\circ})$ (cf. Eq. (1)) was measured for several values of θ, and for each measurement, the coefficient A_{22} was computed. The weighted average of all measurements was $A_{22} = 0.0265 \pm 0.0022$, uncorrected for the finite solid angle subtended by the detectors. The results of an

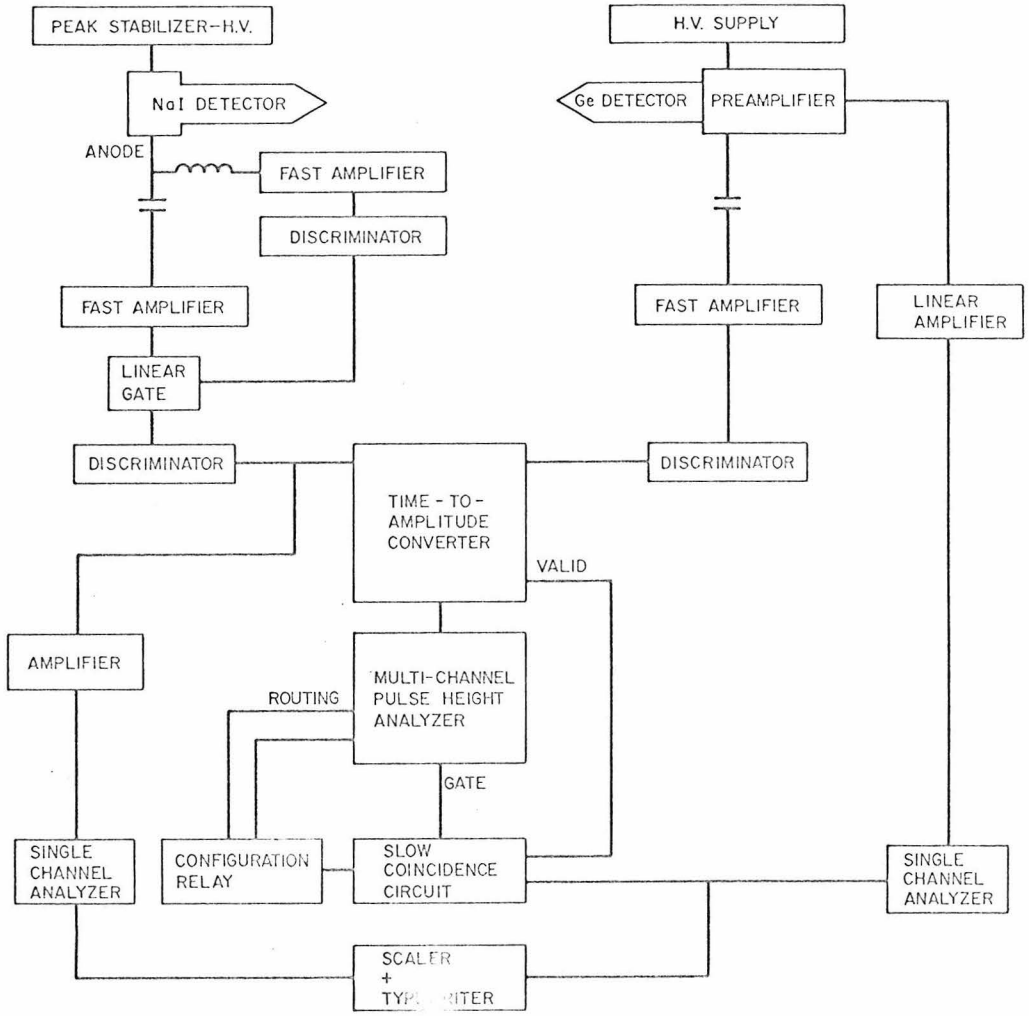

Figure 15: Flow diagram of electronic slow-fast coincidence counting system in the arrangement used for ^{182}W.

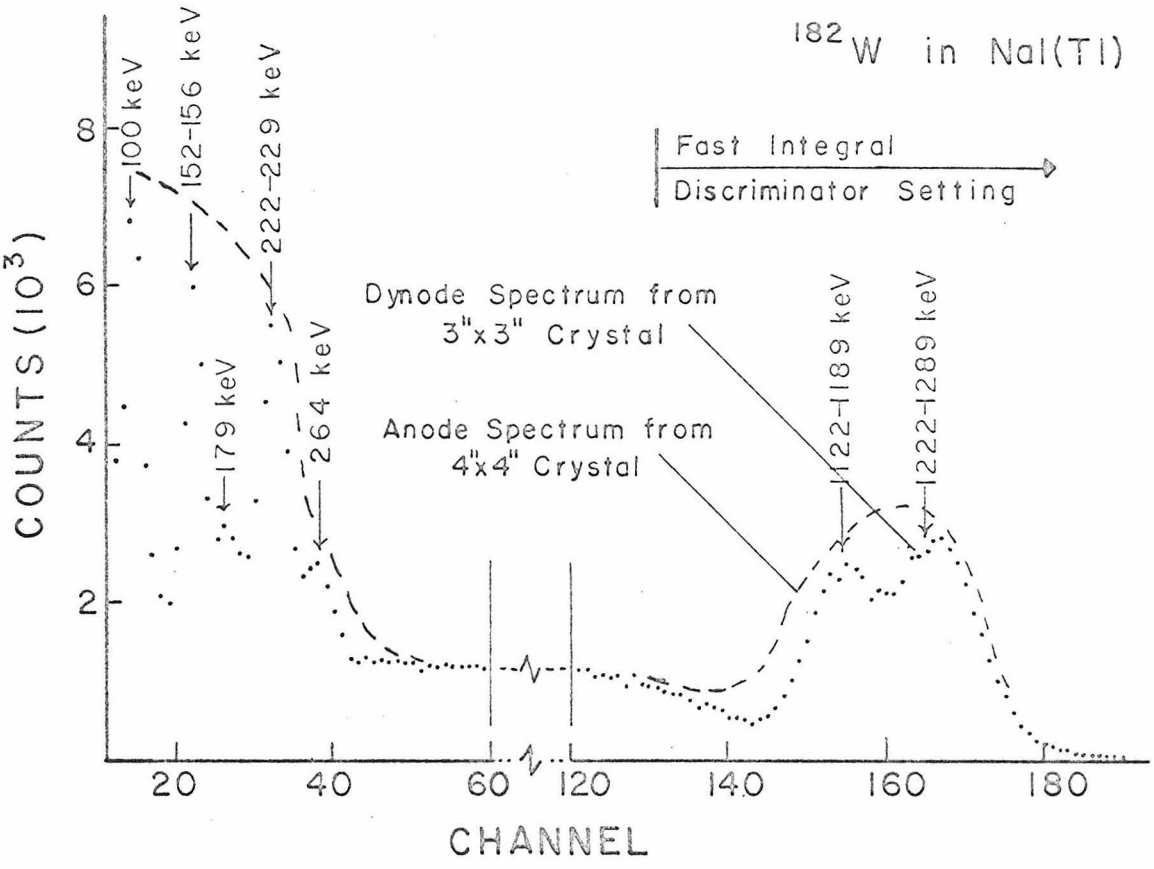

Figure 16a

Gamma-ray scintillation spectrum of ^{182}W showing setting of fast integral discriminator.

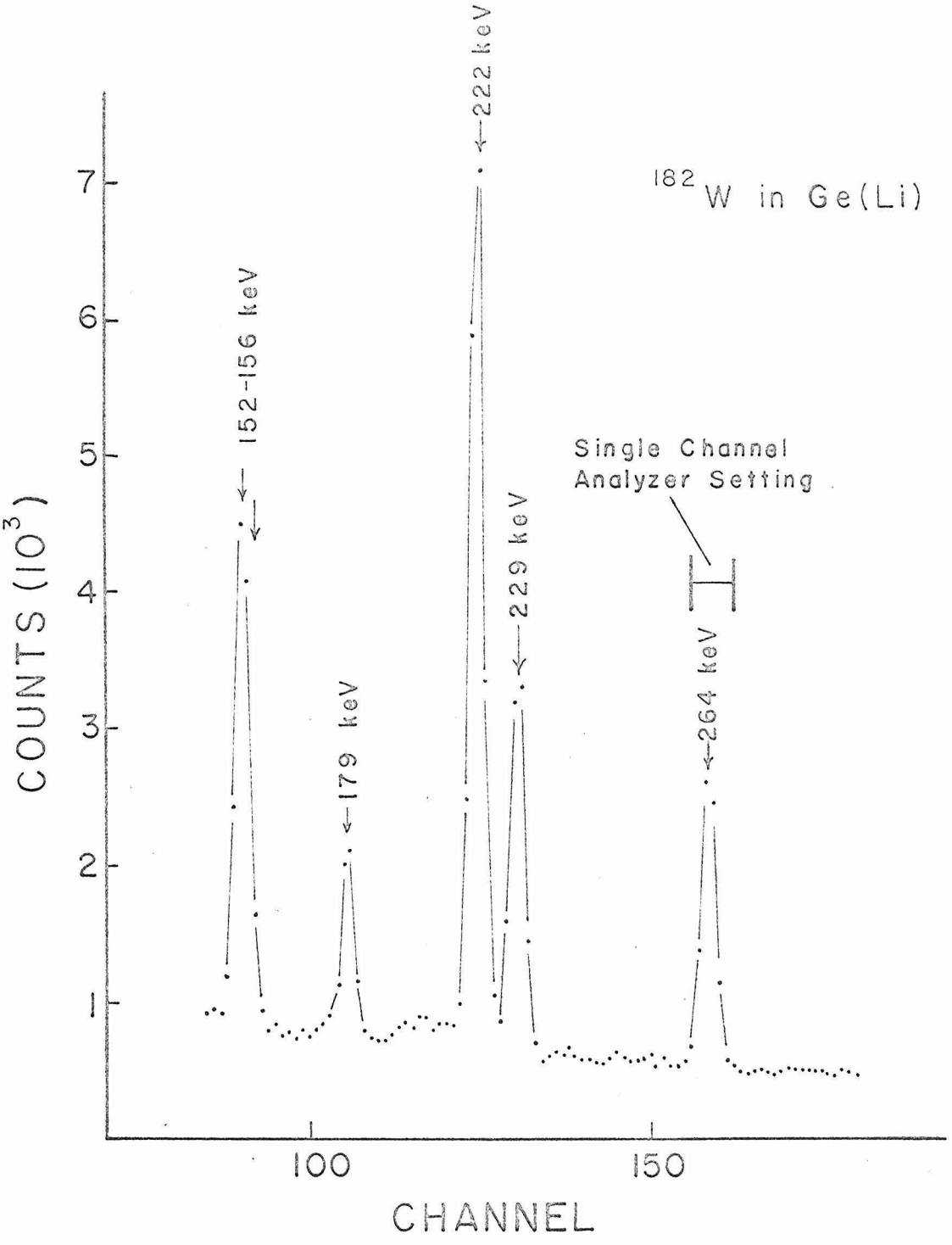

Figure 16b

Portion of the gamma-ray spectrum of ^{182}W as observed in the Ge(Li) detector shown in Fig. 14. The setting of the single-channel analyzer is shown.

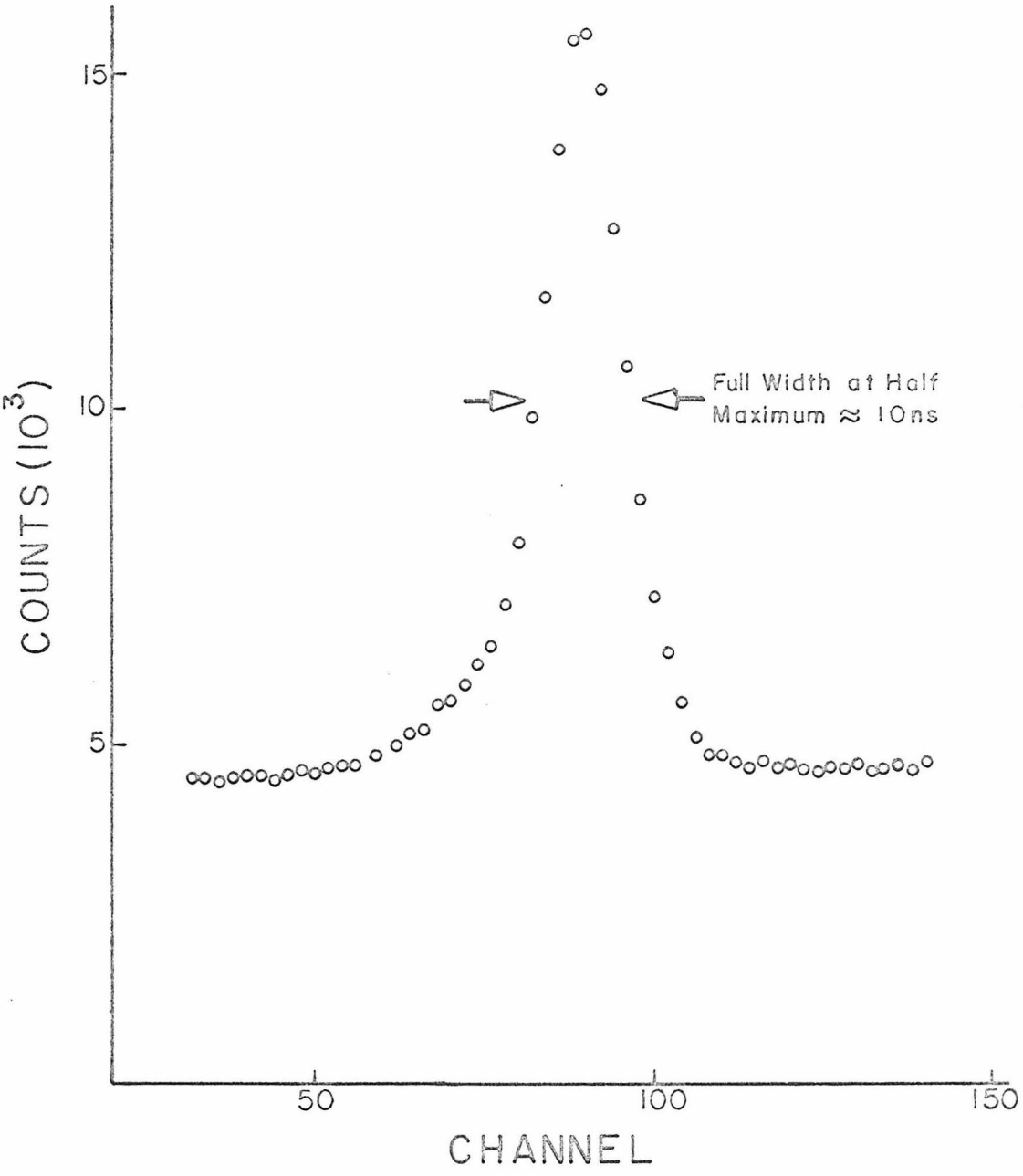

Figure 17

Typical time-to-amplitude converter pulse height spectrum as stored in the multichannel analyzer (for ^{182}W).

angular correlation measurement by Körner et al.[14] have shown that the attenuation of A_{22} due to fluctuating fields is small compared to our statistical errors. The correction for this effect can therefore be neglected. The small value of A_{22} is not only due to the finite solid angle effect, but is also due in large part to dilution of the correlation by gamma cascades other than the two previously mentioned. From Figs. 12 and 16a, one sees that the 1222 keV and 1122 keV radiations are accepted with the 1289 keV and 1189 keV gammas in the NaI(Tl) detector. These are in coincidence with the 264 keV gamma ray through an undetected intense 67 keV (E1) transition. Although these competing cascades serve to dilute the measured angular correlation, they do not interfere with the spin rotation measurement since they pass through the state of interest and undergo the same precession as the direct cascade. The fact that the competing cascades also pass through the $I^{\pi} = 2^{+}$ state at 1222 keV does not influence the measurement because the lifetime of that 2^{+} level is too short (3×10^{-12} sec.) to contribute a measurable precession.

The measurement of the field effect ϵ (cf. Eq. (9)) was performed in six two-day runs, each collecting 5×10^{5} coincidence counts. The weighted average of the results was $\epsilon(135^{\circ}) = (-0.435 \pm 0.092) \times 10^{-2}$. Using Eq. (9) and the experimental values of ϵ and A_{22}, a spin rotation angle of $\omega\tau = -0.116 \pm 0.026$ rad. was found. The magnetic field strength was measured using a "flip coil" composed of five turns of copper wire which was alternately inserted and withdrawn from the pole gap of the magnet. The induced current was measured with a ballistic galvanometer and compared with results from a standard magnetic field. In

this way, the field was found to be $H_{ext} = 32.5 \pm 0.3$ kG. With this value of H_{ext} and the measured lifetime of $\tau = (1.44 \pm 0.07) \times 10^{-9}$ sec.[53], Eq. (6) yields a value for the g-factor of the $I^{\pi} = 2^{-}$ level of $g = 0.52 \pm 0.12$ corresponding to a magnetic moment of $\mu = 1.04 \pm 0.24$ nm.

IV.4 Conclusion

In order to compare the experimental value of μ_{2^-} with the prediction of the strong-coupling approximation[52], we must calculate the value of g_K in the strong-coupling limit and assume a value of g_R appropriate for the deformed nuclear core. The details of our calculation of g_K are given in Appendix A. Recent values of Nilsson wavefunction amplitudes and single particle magnetic parameters[55] for the proton orbits in question were obtained for a deformation parameter derived from the observed ground state rotational band intrinsic quadrupole moment of $Q_0 = 6.57 \pm 0.06$ barn[56]. The values of g_K computed from the relation (cf. App. A, Eq. (9A))

$$Kg_K = \Omega_2 g_2 - \Omega_1 g_1 \qquad (19)$$

were $g_K = 0.906$, assuming the free nucleon value of the proton spin g-factor, and $g_K = 0.953$, if $g_s^{eff} = 0.6\, g_s^{free}$ is assumed to account for spin polarization effects+ [59]. The even-even core of ^{182}W, when two

+ A systematic study of the magnetic moments of states in rotational bands of odd mass nuclei [57] has shown that the Nilsson model can successfully predict these moments only if $g_s^{eff} = 0.6 g_s^{free}$ is assumed for the nucleon spin g-factor. This apparent quenching of the nucleon spin is produced by a residual spin-spin interaction between the valence nucleon and the nucleons in the deformed core[58].

protons are excited into unpaired single particle states, is that of the ground state of ^{180}Hf. We can assume the value of g_R appropriate to our problem is $g_R = 0.34 \pm 0.03$ which is the experimentally measured value for ^{180}Hf [60]. This assumption is justified by the fact that nuclear model calculations of collective g_R-factors[61] have shown that the addition of a proton in an outer orbital of ^{180}Hf does not materially change the predicted value of g_R. Insertion of the above values of g_K and g_R into Eq. (18) yields predicted values of $\mu_{2^-} = 1.44$ nm for $g_s = g_s^{free}$ and $\mu_{2^-} = 1.50$ nm for $g_s = 0.6\, g_s^{free}$. Our measurement of $\mu_{2^-} = 1.04 \pm 0.24$ nm is considerably smaller than the strong-coupling limit prediction.

If we utilize the reported value of $|g_K - g_R| = 0.50 \pm 0.11$ by Grigor'ev et al.[48] and our value of μ_{2^-}, the parameters g_K and g_R can be deduced separately without recourse to specific measurements in other nuclei or to theoretical calculations. Values of $g_R = 0.18 \pm 0.14$ and $g_R = 0.86 \pm 0.14$ are obtained, in this way, from Eq. (18) assuming the sign of $(g_K - g_R)$ to be positive or negative, respectively. Only the smaller value of g_R is in reasonable agreement with the systematic trends of g_R values[61] in this region of nuclei. We therefore adopt a positive sign for $(g_K - g_R)$ and re-order Eq. (18) to read

$$g_K = \frac{\mu}{I} + (g_K - g_R)\left[1 - \frac{K^2}{I(I+1)}\right], \qquad (20)$$

from which we arrive at a value of $g_K = 0.69 \pm 0.13$. Again our value is considerably smaller than that predicted in the strong-coupling limit.

One explanation for the observed discrepancy is the breakdown of the strong-coupling scheme because of a residual proton-proton interaction which cannot be neglected. The only other available measurement of a two-quasiparticle state magnetic moment in an even-even deformed nucleus was performed in ^{172}Yb(62) where good agreement was found with the strong-coupling prediction. This, to some extent, supports our hypothesis of a residual interaction in ^{182}W because the residual interaction is expected to become less significant relative to coupling with a deformed core as the deformation of the core increases(52) and the deformation of ^{172}Yb is considerably greater than that of ^{182}W.+

+ The deformation parameter β, defined by $R = R_0 [1 + \beta Y_{20}(\theta,\varphi)]$, which specifies the spheroidal shape of the nuclear surface, is related to the intrinsic electric quadrupole moment by $Q_0 \propto ZR_0^2\beta$, where R_0 is the mean nuclear radius. From known values of the quadrupole moments(62,56), we find that $\beta(^{172}\text{Yb})/\beta(^{182}\text{W}) \approx 1.3$.

V. MEASUREMENTS ON THE GROUND STATE ROTATIONAL BANDS OF ^{169}Tm AND ^{171}Tm

V.1 Introduction

The highly deformed nuclei, ^{169}Tm and ^{171}Tm, exhibit well-formed K = 1/2 ground state rotational bands built on the [411] 1/2 Nilsson orbital. The spectroscopic properties of these bands have been previously studied by many workers. In this chapter, we report measurements of the magnetic moments of the $I^{\pi} = 7/2^{+}$ and $I^{\pi} = 5/2^{+}$ band members in each nucleus, the E2/M1 mixing amplitude of the $5/2^{+} \rightarrow 3/2^{+}$ transition in ^{169}Tm, and some relative gamma-ray intensities in the decay of ^{171}Er. As can be seen from the partial level schemes of ^{169}Tm and ^{171}Tm given in Figs. 18 and 19[18], respectively, the spacing of the few lowest energy levels does not follow the I(I + 1) rule for a rigid rotator. This behavior is characteristic of a K = 1/2 rotational band. It arises from the fact that the Hamiltonian in the unified+ model description may be written as[20]

$$H = H_{intr} + \frac{\hbar^2}{2\mathcal{I}} (\vec{I}^2 - I_0^2) - \frac{\hbar^2}{2\mathcal{I}} (I_+ j_- + I_- j_+) , \quad (21)$$

where H_{intr} is essentially the Nilsson Hamiltonian and $\vec{I}$ is the total angular momentum with a z-component in the nuclear body fixed frame of I_0. The $I_\pm$ and $j_\pm$ are the total and intrinsic angular momentum raising and lowering operators, respectively. $\mathcal{I}$ is the effective moment of inertia of the deformed nucleus. The I(I + 1) spacing rule arises from the second term in Eq. (21). The third term represents a coupling energy between the collective rotational motion and the intrinsic

---

+ The term unified model is commonly used to refer jointly to the rotational model and Nilsson model.

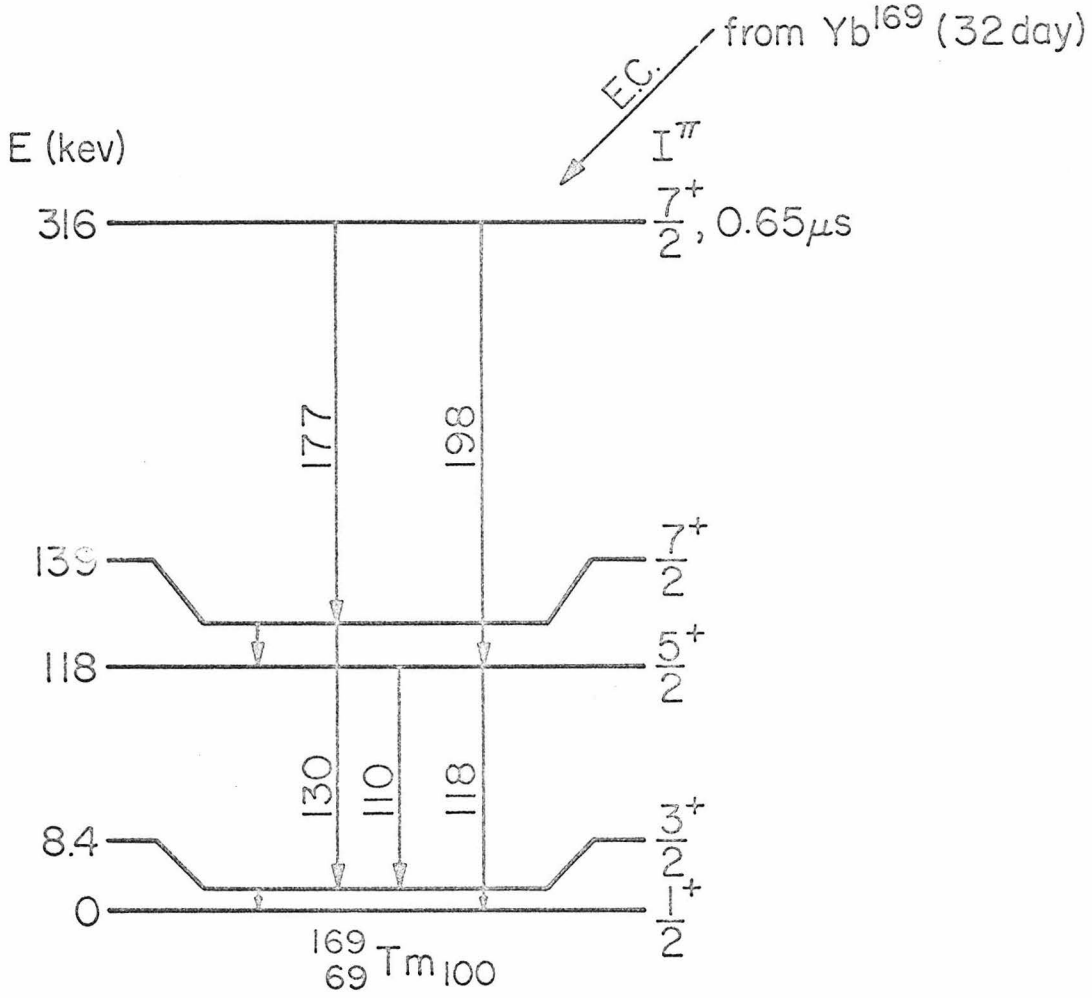

Figure 18

Partial level scheme of ^{169}Tm showing transitions of interest.

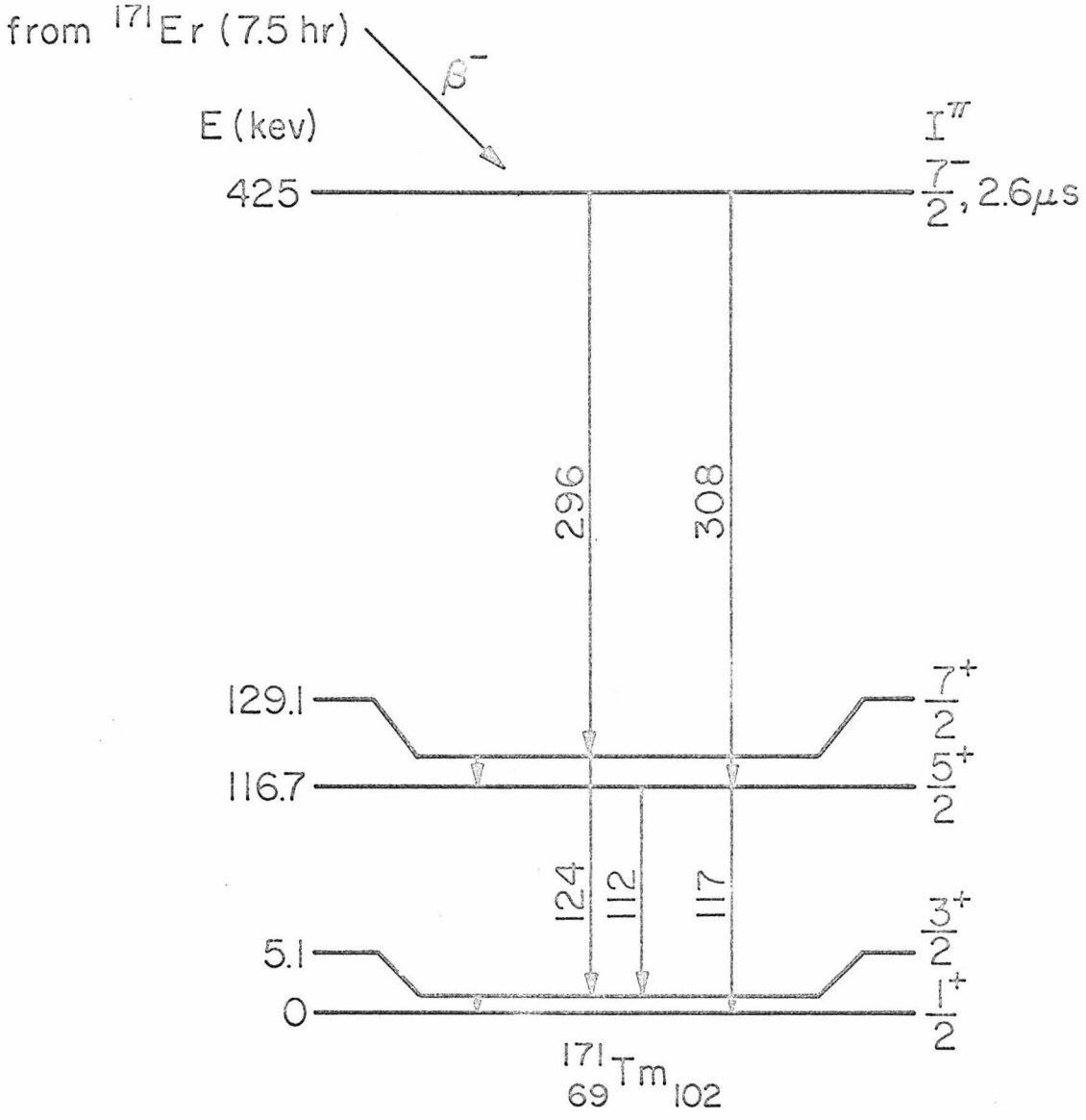

Figure 19

Partial level scheme of ^{171}Tm showing transitions of interest.

nuclear motion, usually referred to as the Coriolis interaction energy. To lowest order, it gives rise to couplings between rotational bands with $\Delta K = \pm 1$ and is normally treated in first order perturbation theory.

The symmetrized eigenfunctions of this Hamiltonian, neglecting the Coriolis term, are given by[20]

$$\psi^{I}_{MK} = \frac{1}{4\pi}\sqrt{(2I+1)}\ (D^{I}_{M,K}\ \chi_K + (-1)^{I+K}\ D^{I}_{M-K}\chi_{-K}), \qquad (22)$$

in which D^{I}_{MK} are the well-known rotation matrices and the χ_K are the eigenstates of H_{intr}. Now it is evident that the $\Delta K = \pm 1$ Coriolis interaction will couple the two terms in Eq. (22) if $K = 1/2$. In other words, the Coriolis term in Eq. (21) has non-zero diagonal matrix elements for a $K = 1/2$ band and thus changes the simple $I(I+1)$ energy spacing rule to[20]

$$E_{total} = E_{intr} + \frac{\hbar^2}{2\mathcal{S}}[I(I+1) + a(-1)^{I+1/2}(I+1/2)]. \qquad (23)$$

The parameter 'a', defined by the intrinsic matrix element,

$$a = -\langle\chi_{1/2}|j_{+}|\chi_{-1/2}\rangle, \qquad (24)$$

is the famous energy decoupling factor for $K = 1/2$ bands. It is this unique level spacing feature which accounts for the very small difference in energy of the $I^{\pi} = 5/2^{+}$ and $7/2^{+}$ states in these bands (cf. Figs. 18 and 19). This in turn has been the major obstacle to accurate measurements of the magnetic moments of those states using the methods of Chapter II. Our use of a high resolution Ge(Li) semiconductor detector has overcome this obstacle and permitted the accurate deter-

mination of the $5/2^+$ and $7/2^+$ level moments in ^{169}Tm and the $7/2^+$ level moment in ^{171}Tm and the first measurement of the $5/2^+$ level moment in ^{171}Tm.

The magnetic properties of a K = 1/2 band are also unique in that, in addition to the two parameters g_K and g_R discussed in the previous chapter, a third parameter b_0 is required in the rotational model description of the band. A presentation of the relevant rotational model formulas and of the determination of the model parameters from the measurements reported here and from results of other investigations is deferred to Chapter VI.

V.2 Source Preparation, Magnet, and Electronics

The radioactive source used for measurements on ^{169}Tm was ^{169}Yb which decays by electron capture with a half-life of 32 days. It was produced by thermal neutron capture on natural ytterbium oxide which contains 0.14% ^{168}Yb. The sample was allowed to age until the ^{175}Yb ($T_{1/2} \approx 4$ days), which is also produced in the natural oxide, had decayed. The source used for measurements on ^{171}Tm was ^{171}Er which decays by β^- emission with a half-life of 7.5 hours. Several sources were needed because of the short half-life of ^{171}Er. Each one was prepared by thermal neutron capture on erbium oxide enriched to 96% ^{170}Er. Short irradiation times of 12 hours were used to minimize the production of ^{172}Er ($T_{1/2} \approx 40$ hours) by double neutron capture. In both the case of ^{169}Yb and ^{171}Er, the radioactive oxides were dissolved in hydrochloric acid and sealed in a thin-walled polyethylene sack as in the previous case of ^{182}W. The high field electromagnet used was

also the same as that described in the previous chapter.

In the majority of the measurements to be described, a 3 x 3 in. NaI(Tl) crystal spectrometer, identical to those used for ^{106}Pd (cf. Fig. 7), and a 2.2 cm dia. x 0.5 cm deep Ge(Li) semiconductor detector, identical to that used for ^{182}W (cf. Fig. 14), were used to detect the cascading gamma rays.

For the most part the electronic instrumentation was similar to that employed in the ^{182}W experiment. Figures 20 and 21 show block diagrams of the electronics for two different configurations. In the first (Fig. 20), the time-to-amplitude spectrum is stored in the pulse height analyzer as was the case in the previous chapters, and in the second (Fig. 21), the Ge(Li) spectrum is stored. Since some aspects of the electronics and detector arrangement varied from one case to another, the details of the experimental configurations are described in the sections pertaining to the individual measurements.

V.3 Measurements in ^{169}Tm

a. Measurement of the Magnetic Moment of the 138.9 keV $I^{\pi} = 7/2^{+}$ State in ^{169}Tm.

The gamma-gamma cascade used was the 177-130 keV cascade with spin sequence $7/2^{+}$(M1 + E2) $7/2^{+}$(E2) $3/2^{+}$ which is shown in Fig. 18. The g-factor of the $7/2^{+}$ intermediate state was measured by two methods. In method I, the 177 keV photopeak of the NaI(Tl) scintillation spectrum was selected in a single-channel analyzer as shown in Fig. 22. A second single-channel analyzer selected those pulses from the time-to-amplitude converter which corresponded to a fast coincidence. A

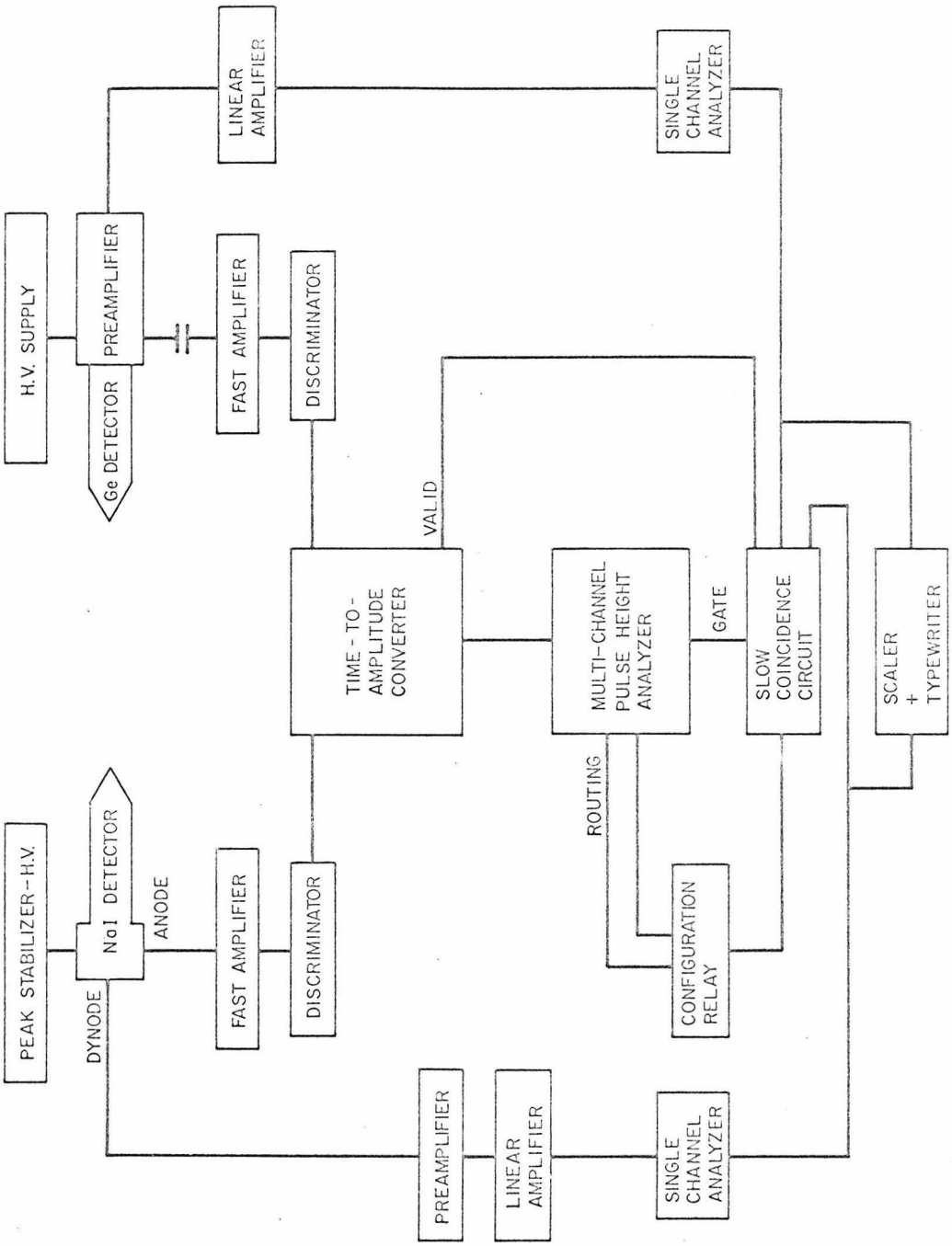

Figure 20: Flow diagram of electronic slow-fast coincidence counting system in the time-to-amplitude spectrum storage mode for the measurements in Tm.

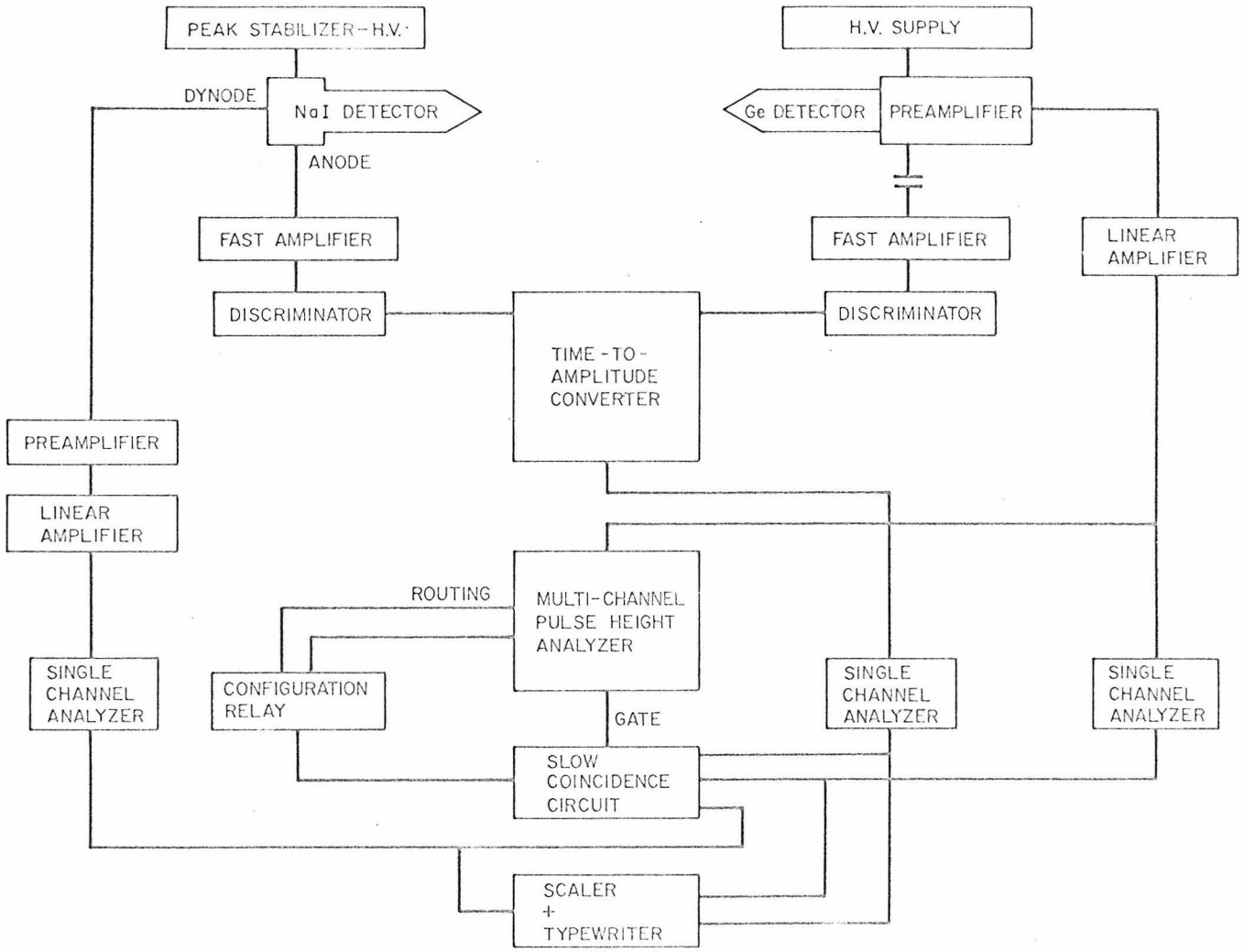

Figure 21: Flow diagram of electronic slow-fast coincidence counting system in the Ge(Li) coincidence spectrum storage mode for the measurements in Tm.

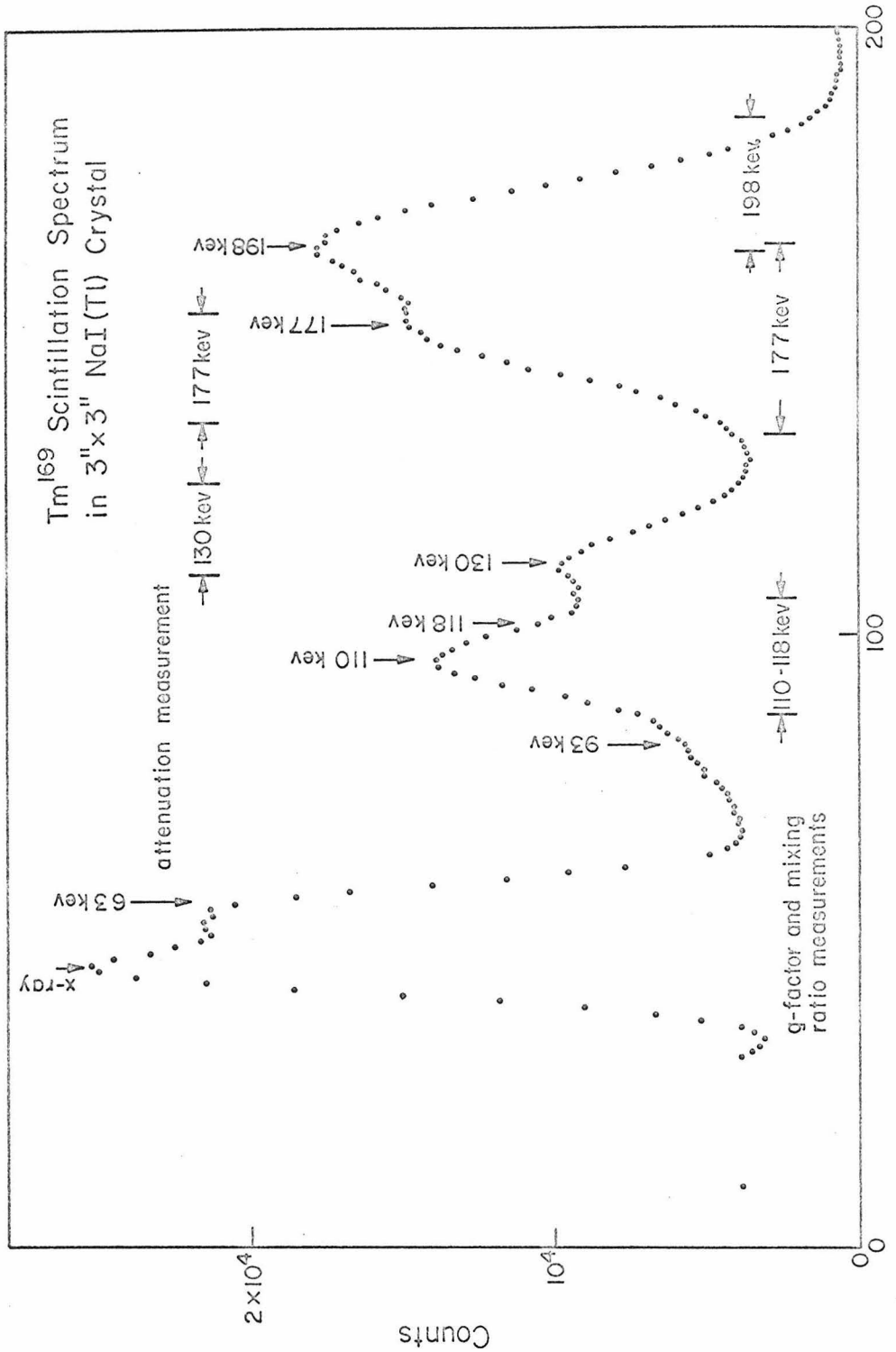

Figure 22: Gamma-ray scintillation spectrum for ^{169}Tm as observed in NaI(Tl). The single-channel analyzer settings for all measurements are shown.

portion of the Ge(Li) spectrum from 90 to 280 keV was stored in subsections of the 400-channel pulse height analyzer in coincidence with the outputs of the single-channel analyzers. The experimental arrangement is that depicted in Fig. 21. Corrections for random coincidences were determined by comparing the 177 keV and 198 keV photopeak intensities in the Ge(Li) coincidence spectra with the corresponding intensities in a Ge(Li) spectrum measured without coincidence requirements.

Intensities were extracted from a least-squares fit of the experimental coincidence spectrum to a multi-parameter function describing the Ge(Li) line profile on a sloping background. A typical fitted spectrum is shown in Fig. 23. Coincidence spectra were collected for several angles between detectors with no magnetic field and at a fixed angle of 135° when the magnetic field direction was periodically reversed. The 130 keV coincidence photopeak intensity, after random subtraction, was used in Eq. (14) to compute the angular correlation coefficients and in Eq. (15) to find the observed spin rotation angle. The results are listed in Table 2a.

In method II, all conditions were essentially identical to those in method I except that the time-to-amplitude spectrum was stored in the pulse height analyzer in coincidence with the outputs of the single-channel analyzer for the NaI(Tl) spectrum and a second single-channel analyzer accepting the 130 keV photopeak in the Ge(Li) spectrum. The arrangement is that shown in Fig. 20. It can be seen from Table 2a that the results of the two methods are in excellent agreement.

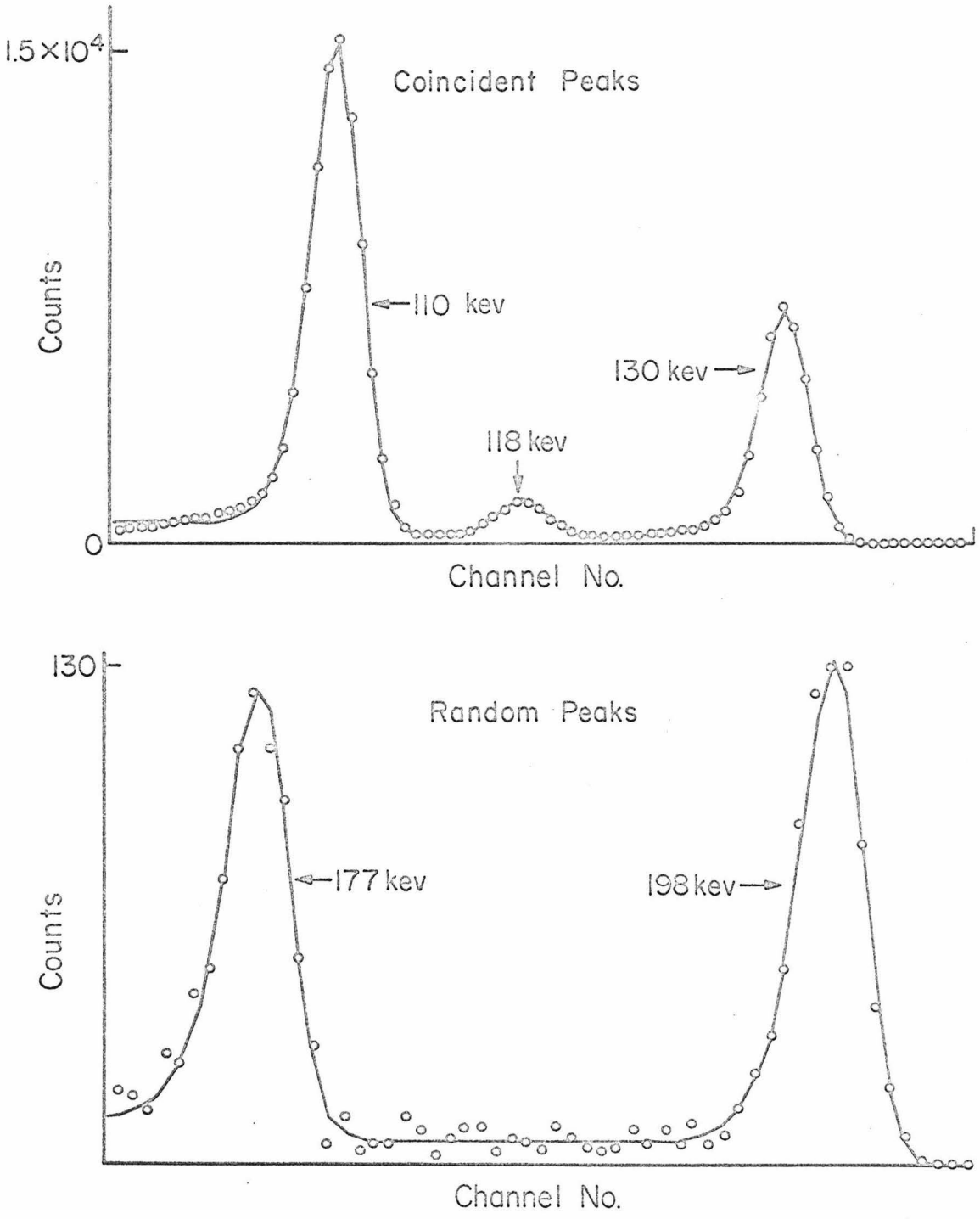

Figure 23

Typical fitted Ge(Li) coincidence spectrum of ^{169}Tm. The open circles are experimentally measured data and the straight line segments connect fitted points which are not shown.

Table 2

Results of Magnetic Moment Measurements in ^{169}Tm

2a: The $I^{\pi} = 7/2^{+}$ State

Quantity	Method I	Method II	Weighted Average
A_{22} (a)	0.229 ± 0.003	0.208 ± 0.004	
A_{44} (a)	0.045 ± 0.006	0.022 ± 0.004	
$\epsilon(135^{o})$ (%)	4.258 ± 0.098	3.706 ± 0.136	
$\omega\tau$(rad.) (b)	-0.134 ± 0.007	-0.133 ± 0.006	-0.133 ± 0.004
$\mu\tau(10^{-10}$ nm-sec)			6.00 ± 0.24
μ(nm)			1.33 ± 0.07

2b: The $I^{\pi} = 5/2^{+}$ State

Quantity	Method I	Method II	Weighted Average
A_{22} (a)	0.293 ± 0.004	0.222 ± 0.009	
A_{44} (a)	-0.020 ± 0.006	0.009 ± 0.010	
$\epsilon(135^{o})$ (%)	0.857 ± 0.096	-0.72 ± 0.16	
$\omega\tau(10^{-2}$ rad.)	-2.17 ± 0.24	-2.25 ± 0.60	-2.18 ± 0.22
$\mu\tau(10^{-11}$ nm-sec)			7.02 ± 0.71
μ(nm)			0.79 ± 0.08

(a) Experimental values not corrected for attenuation or geometrical effects.

(b) Corrected for attenuation of the angular correlation according to Sec. V.3b.

The configuration of the atomic electrons of thulium is such that the Tm^{3+} ion has a non-zero atomic magnetic dipole moment, which arises from the resultant spin and orbital angular momentum of a partially filled 4f electronic subshell. It is the alignment of this atomic moment in an external magnetic field which accounts for the bulk paramagnetic susceptibility of thulium compounds in the solid state. The incomplete 4f subshell also produces a large magnetic field at the site of the thulium nucleus. The hyperfine interaction of the nuclear moment with this field is well-known from optical spectra.

In a short time (see below) after the decay of ^{169}Yb in the liquid solutions of $YbCl_3$, the chemical environment of the thulium daughter is that of $TmCl_3$. The trivalent state of the thulium ion in chloride solution is the only known valence state at standard conditions of temperature and pressure. In liquid, the direction of the large field at the nucleus fluctuates randomly in time, in the absence of an external field, with a rate corresponding to the effective collision frequency in the liquid. The collision frequency is inversely proportional to the correlation time τ_c (defined in Sec. II.4) or, alternatively, to the electronic relaxation time for paramagnetic ions in liquid. This time is 10^{-12} to 10^{-13} sec. or shorter at room temperature[63]. When $\tau_c \ll \tau$ (the intermediate state lifetime), as is the case for the measurements reported here, the time average of the hyperfine field over the lifetime of the intermediate state is zero.

In the presence of an externally applied field, the degeneracy of the magnetic substates of the 4f subshell is removed (Zeeman effect),

with the substate corresponding to alignment of the hyperfine and external fields being lowest in energy. For this case, the time average of the component of the hyperfine field along the direction of the external field is non-zero. The size of this additional effective field has been computed as a function of temperature by Günther and Lindgren[63] for the Tm^{3+} ion under the assumption that the ion is in thermal equilibrium with its environment. The assumption of thermal equilibrium during the intermediate state lifetime is valid in our case since it is achieved in times of the order of τ_c and $\tau_c \ll \tau$. Thus the value of the paramagnetic enhancement factor β, defined by $H_{eff} = \beta H_{ext}$, calculated in ref. (63) is applicable to the Tm^{3+} ion in the liquid source at room temperature.

The effect of preceding decays, such as the electron capture decay of ^{169}Yb, can drastically alter the charge state of the thulium ion. The capture of a K-electron, for example, results in the spontaneous shake-off of outer electrons followed by the emission of several x-rays and Auger electrons as the electron vacancy propagates to the outer electronic shells. The electromagnetic lifetime of a vacancy in an inner shell is of the order of 10^{-16} sec., whereas that for an outer optical level is about 10^{-8} sec [63]. The optical levels, however, decay much more rapidly through emission of Auger electrons and through induced de-excitation by collisions in times of the order of τ_c. It is assumed, of course, that in the liquid there are a sufficient number of electrons available from nearby ions to fill the vacancies in the thulium ion. It can be seen from Fig. 18 that after the ^{169}Yb decay, the thulium nucleus remains in

the long-lived 316 keV state for 10^{-7} to 10^{-6} sec., which is more than enough time for the electronic configuration to return to its ground state. The above considerations indicate that a value of β taken from ref. (63) is applicable to the present experiment[†]. For the measurements in ^{171}Tm presented below, the above arguments also apply.

+ The value of β computed for Tm^{3+} in ref. (63) is particularly accurate ($\sim$ 2%) since it does not depend on the numerical evaluation of an atomic radial matrix element.

The value of $\mu_{7/2}\,\tau_{7/2}$ was computed, using Eq. (6), from the measured value of H = (32.57 ± 0.30) kG for the external magnetic field, G_{22} = 0.956 ± 0.012 for the angular correlation attentuation factor (cf. Sec. V.3b), and a paramagnetic enhancement factor for Tm at 35°C of β = 4.98[63]. The temperature of 35°C in the pole gap of the electromagnet was measured using a 0.01 in. diameter glass bead thermistor enclosed in a polyethylene sack and inserted in the pole gap in place of the radioactive source. The measured resistance of the thermistor was then compared with a resistance versus temperature calibration curve determined with the aid of a temperature controlled bath to be described in the following section. The mean life of the $7/2^+$ state has been measured to be τ = 0.464 ± 0.020 ns[+] by Sundström et al.[64], τ = 0.420 ± 0.101 ns by Blaugrund[65], and τ = 0.417 ± 0.035 ns by McAdams et al.[66]. If we adopt the weighted average τ = 0.452 ± 0.018 ns, this yields a magnetic moment for the $7/2^+$ state of $\mu_{7/2}$ = 1.33 ± 0.07 nm. This value is in good agreement with that of Bowman et al.[67] who reported $\mu_{7/2}$ = 1.31 ± 0.18 nm.

b. Attenuation of the Angular Correlation through the 138.9 keV State

The angular correlation coefficients for the $7/2^+$(177 keV) $7/2^+$ (130 keV) $3/2^+$ cascade were measured as a function of temperature. The source used was an HCl solution of $YbCl_3$ sealed in a glass capsule. The source was immersed in a mineral oil bath in a thin-walled glass dewar where the temperature was maintained with an accuracy of ± 0.2°C by a mercury column thermostat in conjunction with resistive heating

+ The unit ns stands for 1 x 10^{-9} seconds.

elements. Figure 24 shows the dewar and temperature regulating assembly. Gamma rays were detected in the two 3 x 3 in. NaI(Tl) scintillation spectrometers and processed with the electronic apparatus used in the measurement on ^{106}Pd (cf. Figs. 7 and 8). The geometrical configuration of the apparatus was not changed throughout the measurement. The single-channel analyzers selected the low energy portion of the 177-198 keV doublet and high energy portion of the 110-118-130 keV triplet with NaI(Tl) spectrum as shown in Fig. 22.

The angular correlation was measured at temperatures of 30°C, 60°C, and 90°C. It is expected that, over this range of temperatures and for small attenuations, the attenuation of the angular correlation coefficients is proportional to the viscosity of the solute[15]. In Fig. 25, we plot the experimentally determined value of $G_{22}A_{22}$ as a function of the viscosity of water at the above temperatures. No correction for geometrical effects has been made. A straight line was fitted to the data and $G_{22}(35^{\circ}C)$ was determined to be $G_{22}(35^{\circ}C) = 0.956 \pm 0.012$. The statistical accuracy in the determination of A_{44} did not permit G_{44} to be experimentally determined. G_{44} can, however, be deduced from the value of G_{22} if an assumption is made concerning the form of the perturbing interaction and use is made of Eqs. (12) and (13). The corrections to the experimental values of $\omega\tau$, however, were found to be insensitive to the nature of the assumed interaction (pure electric or pure magnetic). The appropriate value of G_{22} for the $7/2^+$ state in ^{171}Tm was determined from the above value for the $7/2^+$ state in ^{169}Tm by scaling according to the ratio of the lifetimes of the two states. Effects of attenuation were neglected in measurements on the

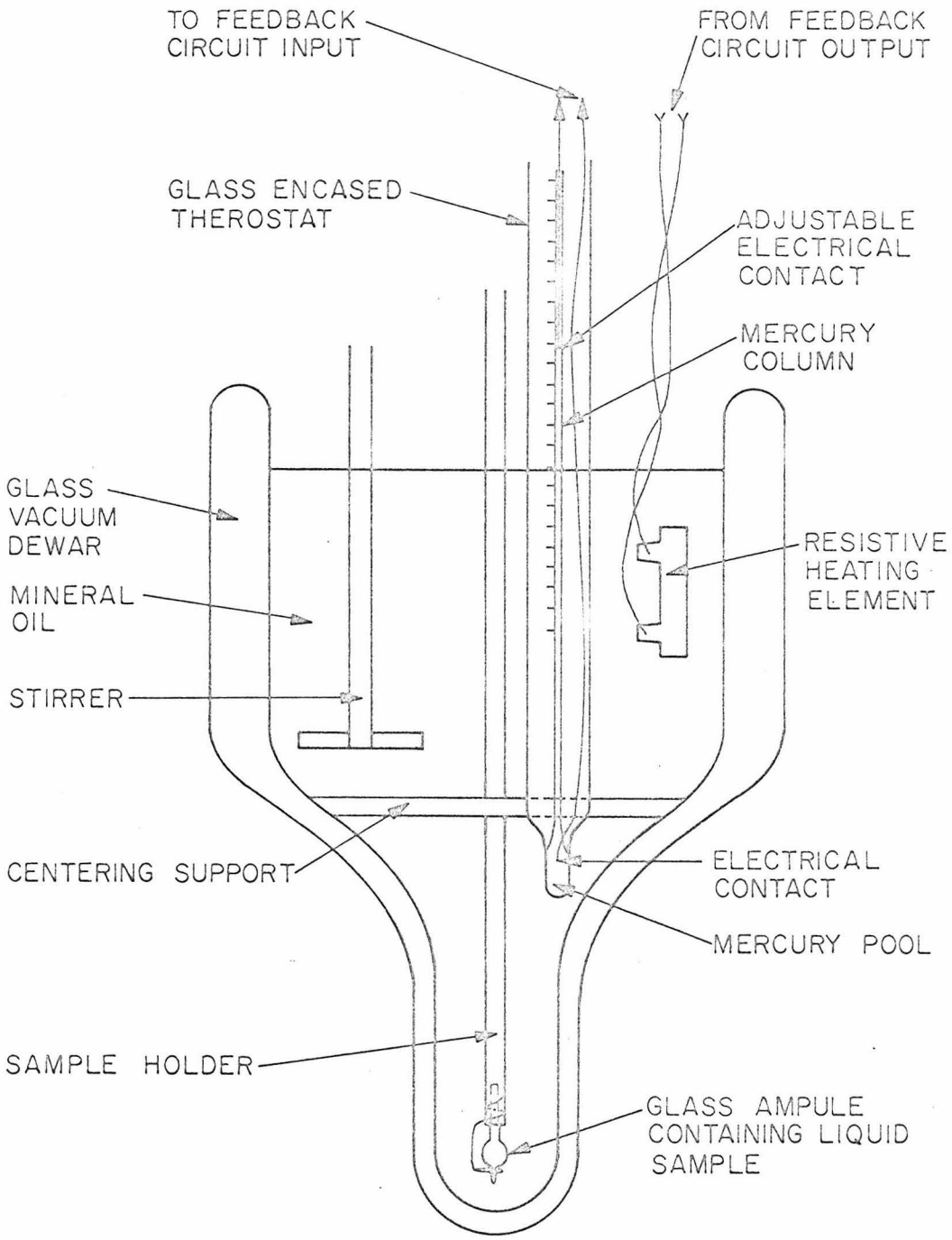

Figure 24

Diagram of the dewar and temperature regulator assembly used in the measurement of the attenuation of the angular correlation in ^{169}Tm.

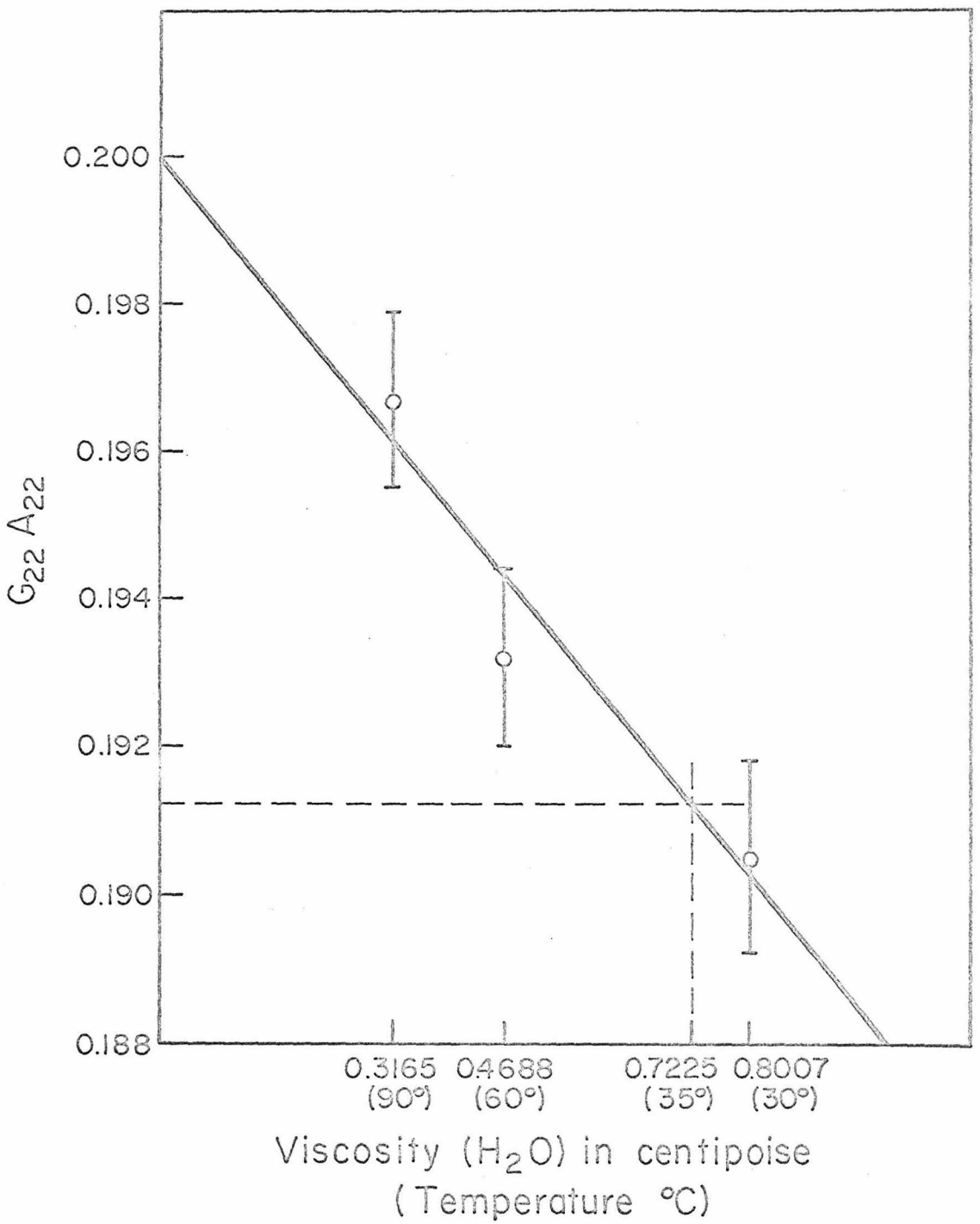

Figure 25

Plot of the attenuated angular correlation coefficient $G_{22}A_{22}$ versus the viscosity of the liquid source. At zero viscosity $G_{22} = 1$.

shorter lived $I^{\pi} = 5/2^{+}$ states.

c. Measurement of the Magnetic Moment of the 118.2 keV $I^{\pi} = 5/2^{+}$ State in ^{169}Tm

In this measurement, the 198-110 keV gamma-gamma cascade (cf. Fig. 18) with spin sequence $7/2^{+}$(M1 + E2) $5/2^{+}$(M1 + E2) $3/2^{+}$ was used and, as in the case of the 138.9 keV state, two methods were employed to measure the g-factor of the $5/2^{+}$ intermediate state. Method I was similar to method I for the 138.9 keV state in that the Ge(Li) coincidence spectrum was stored in coincidence with the output of a single-channel analyzer which selected the prompt coincidence region of the time-to-amplitude spectrum. The single-channel analyzer for the NaI(Tl) spectrum was set to accept the 198 keV line as shown in Fig. 22. Angular correlation coefficients and the spin rotation angle were determined from the photopeak intensity of the 110 keV line in the Ge(Li) coincidence spectrum, using Eqs. (6) and (9). The results are listed in Table 2b.

It is evident from Fig. 22 that the window selecting the 198 keV NaI(Tl) photopeak also accepts a small number of pulses from the 177 keV transition. We estimated the effects of this interfering cascade to be small; however, as an experimental check, the spin rotation was measured by a second method (II). The time-to-amplitude spectrum was stored in the multichannel pulse height analyzer in coincidence with single-channel analyzers selecting the 198 keV photopeak in the Ge(Li) spectrum and the 110-118 keV photopeaks in the NaI(Tl) spectrum as shown in Fig. 22. The results of this measurement are also summarized in Table 2b.

The mean life of the $5/2^+$ state has been measured to be $\tau = 0.0895 \pm 0.0040$ ns by Blaugrund et al.[68] and $\tau = 0.0909 \pm 0.0101$ ns by McAdams et al.[66]. Adopting the weighted average $\tau = 0.0897 \pm 0.0037$ ns and neglecting attentuation of this angular correlation, our quoted value of $\omega\tau$, with the aid of Eq. (6), yields a magnetic moment of $\mu_{5/2} = 0.79 \pm 0.08$ nm. This value is in fair agreement with that of Bowman et al.[67] who found $\mu_{5/2} = 0.61 \pm 0.12$ nm, and Manning and Rogers'[69] value of $\mu_{5/2} = 0.50 \pm 0.15$ nm.

d. Measurement of the E2/M1 Mixing Amplitude of the 109.8 keV Transition in ^{169}Tm.

Apparatus identical to that employed above was used to measure the angular correlation coefficient A_{22} for the 198-110 keV cascade with spin sequence $7/2^+$(M1 + E2) $5/2^+$(M1 + E2) $3/2^+$. The electromagnet was removed to reduce the effects of scattering, and the single-channel analyzer settings and mode of data collection and analysis were the same as in method I described in the previous section. In order to extract a mixing amplitude, the experimental angular correlation coefficient must be corrected for the finite solid angle subtended by the detectors. The geometrical correction factors, discussed in Section II.2, were computed for the geometry used, following a method prescribed by Frauenfelder and Steffen[70]. The result was $Q_2^1 Q_2^2 = 0.846$. After applying this correction, the measured value of A_{22} was found to be $A_{22}(7/2^+ \rightarrow 5/2^+ \rightarrow 3/2^+) = 0.347 \pm 0.006$. The coincidence photopeak intensity of the 118 keV line in the Ge(Li) spectrum was also extracted from the data in order to determine the correlation coefficient for the 198-118 keV cascade with spin sequence $7/2^+$(M1 + E2)

$5/2^+$(E2) $1/2^+$. The result was $A_{22}(7/2^+ \rightarrow 5/2^+ \rightarrow 1/2^+) = -0.295 \pm 0.016$ after applying the geometrical correction.

From Eq. (2), it is seen that the above coefficients can be written as $A_{22}(7/2^+ \rightarrow 5/2^+ \rightarrow 3/2^+) = A_2(198\ \text{keV}) \cdot A_2(110\ \text{keV})$ and $A_{22}(7/2^+ \rightarrow 5/2^+ \rightarrow 1/2^+) = A_2(198\ \text{keV}) \cdot A_2(118\ \text{keV})$. Thus, the unknown $A_2(198\ \text{keV})$ factor is absent in the ratio of the two experimental values. In addition, $A_2(118\ \text{keV})$ for a pure E2 multipole transition can be found in tables of F_K coefficients (cf. Sec. II.2). The value of $A_2(110\ \text{keV})$, determined in this way, was found to be $A_2(110\ \text{keV}) = 0.628 \pm 0.041$. Figure 26 shows a graphical display of Eq. (3) from which the value of $\delta(\text{E2/M1}) = -0.15 \pm 0.02$ is seen to correspond to the value of $A_2(110\ \text{keV})$ quoted above. This value is in excellent agreement with previous measurements[71]. The second root of Eq. (3) shown in Fig. 26 was rejected on the ground that it is totally inconsistent with results of measurements on internal conversion electron subshell intensity ratios for the 110 keV transition.

V.4 Measurements in ^{171}Tm

a. Measurement of the Magnetic Moment of the 129.1 keV $I^\pi = 7/2^+$ State in ^{171}Tm

The detectors and electronic apparatus used for this measurement were the same as those described above. Only the arrangement displayed in Fig. 21 was employed. In the present case, the 296-124 keV gamma-gamma cascade with spin sequence $7/2^-$(E1) $7/2^+$(E2) $3/2^+$, which is shown in Fig. 19, was used. The single-channel analyzer accepting the NaI(Tl) spectrum selected the composite 296-308 keV photopeak as

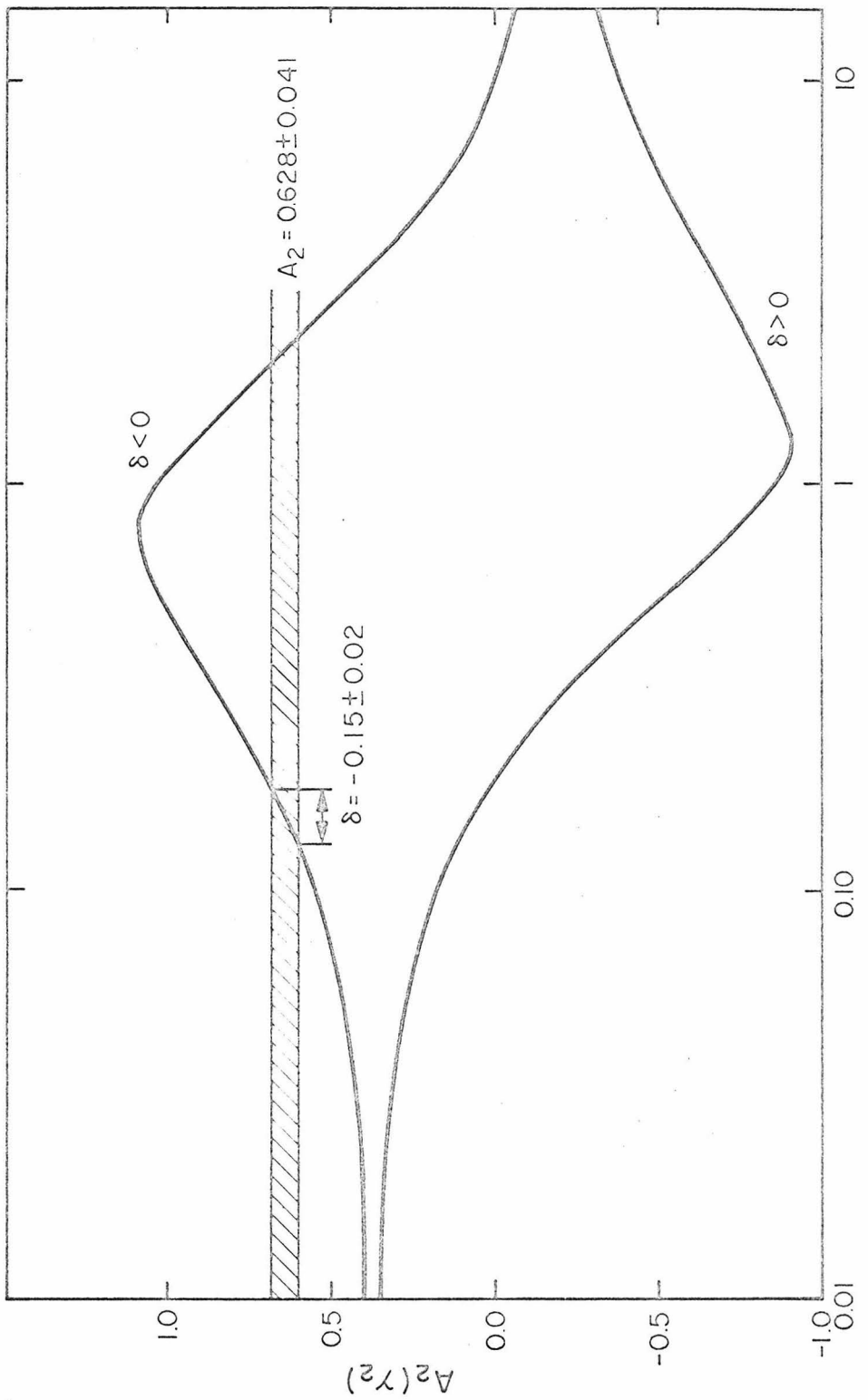

Figure 26: Plot of $A_2(\gamma_2)$ versus the mixing amplitude $\delta(E2/M1)$. The experimentally determined value is shown.

shown in Fig. 27. No interference from the 308 keV transition is seen since it is not in coincidence with the 124 keV transition. The Ge(Li) coincidence spectrum was stored in the multichannel analyzer, and random corrections were determined from the intensities of the 296 keV and 308 keV photopeaks as previously described. A typical fitted Ge(Li) coincidence spectrum is shown in Fig. 28. The fitted values of the 124 keV photopeak intensities in the Ge(Li) coincidence spectrum were used, with Eqs. (14) and (15), to evaluate the angular correlation coefficients and spin rotation angle listed in Table 3a.

During the measurement of the angular correlation function and the mean spin rotation angle, the experimental configuration was periodically switched between two states; that is, either the angle between the detectors or the magnetic field direction was changed every three minutes throughout any given run. This was also the case in all previously described measurements. The coincidence counting rate, in this case, however, decayed exponentially (neglecting dead time effects in the electronics which were found to be small) with the 7.5 hour half-life of the parent activity. For such a short half-life, the change in source strength from one three-minute period to the next cannot be neglected. In Appendix B, the effect of the decay on the accumulated coincidence counts is demonstrated, and the necessary correction factors are computed. These corrections, for the present measurement, never effected more than a ten percent change in an experimental value.

The lifetime of the 129.1 keV $7/2^+$ state has been measured by

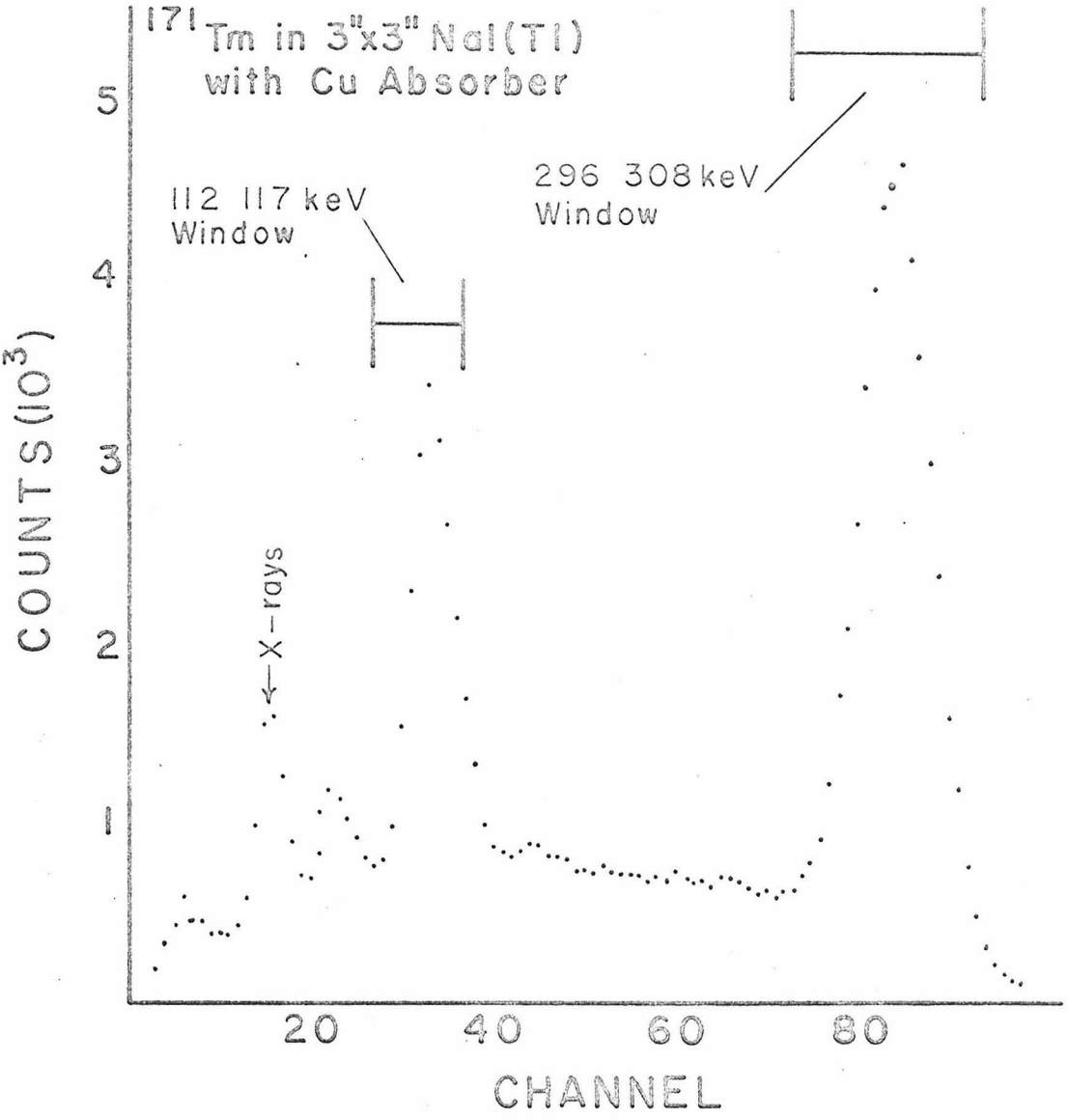

Figure 27

Gamma-ray scintillation spectrum of ^{171}Tm in the 3 x 3 in. NaI(Tl) crystal. The settings of the single-channel analyzers are shown.

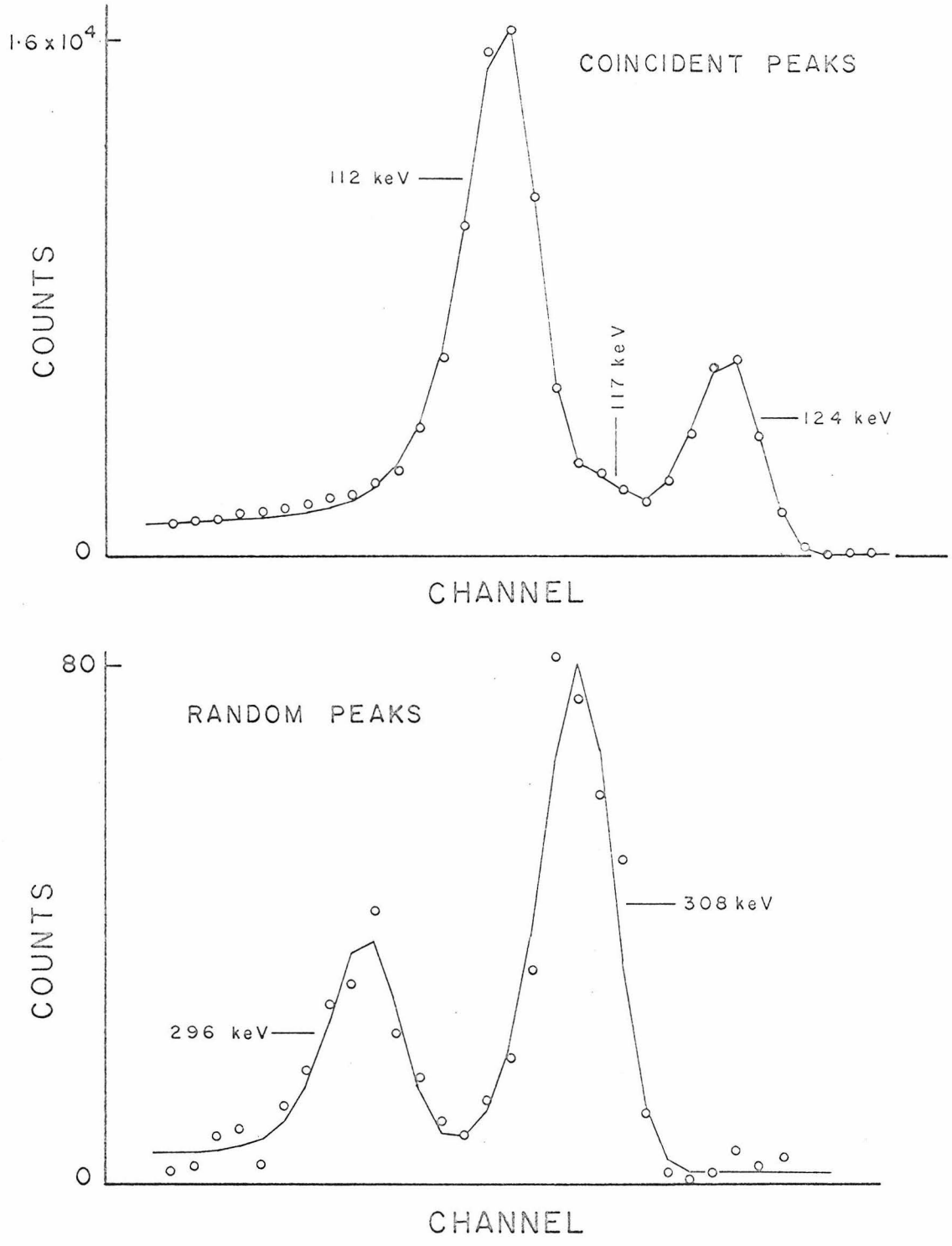

Figure 28

Typical fitted Ge(Li) coincidence spectrum of ^{171}Tm. The open circles are experimentally measured data and the straight line segments connect fitted points which are not shown.

Table 3

Results of Magnetic Moment Measurements in ^{171}Tm

3a: The $I^{\pi} = 7/2^{+}$ State

Quantity	Value
A_{22} (a)	0.151 ± 0.005
A_{44} (b)	-0.004 ± 0.009
$\epsilon(140.5^{\circ})$ (%)	3.04 ± 0.19
$\omega\tau$ (rad.) (c)	-0.168 ± 0.015
$\mu\tau(10^{-10}$ nm-sec)	7.56 ± 0.67
μ(nm)	1.44 ± 0.14

3b: The $I^{\pi} = 5/2^{+}$ State

Quantity	Set I	Set II	Weighted Average
A_{22} (a)	0.070 ± 0.006	0.066 ± 0.007	
A_{44} (b)	0	0	
$\epsilon(135^{\circ})$ (%)	-0.285 ± 0.160	-0.17 ± 0.09	
$\omega\tau(10^{-2}$ rad.)	-2.77 ± 1.57	-1.75 ± 0.94	-2.02 ± 0.80
$\mu\tau(10^{-11}$ nm-sec)			6.5 ± 2.6
μ(nm)			0.81 ± 0.37

(a) Experimental value not corrected for attentuation or geometrical effects.

(b) A_{44} is expected to be zero.

(c) Corrected for attenuation of the angular correlation according to Sec. V.3b.

Sundström et al.[72] to be $\tau = 0.523 \pm 0.022$ ns.+ With this value of τ, the previously quoted values of H and β, and an attentuation coefficient $G_{22} = 0.949 \pm 0.013$, the value of $\omega\tau$ from Table 3a yields a magnetic moment of $\mu_{7/2} = 1.44 \pm 0.14$ nm. This is in disagreement with a previous measurement of $\mu_{7/2} = 0.94 \pm 0.18$ nm which was performed without the aid of a Ge(Li) detector by Agarwal et al.[74].

b. Measurement of the Magnetic Moment of the 116.7 keV $I^{\pi} = 5/2^{+}$ State in ^{171}Tm

The 308 keV photopeak in the NaI(Tl) spectrum cannot be selected in a single-channel analyzer without a large interfering contribution from the 296 keV transition. Therefore, in order to perform this measurement, the 308 keV gamma ray was selected in the Ge(Li) channel where the detection efficiency for that energy is quite small. In addition, with a single-channel analyzer selecting the low energy side of the composite 112-117-124 keV photopeak in the NaI(Tl) spectrum, as shown in Fig. 27, two cascades through the $5/2^{+}$ state are observed: these are the 308-117 keV cascade with spin sequence $7/2^{-}$(E1) $5/2^{+}$(E2) $1/2^{+}$ and the 308-112 keV cascade with spin sequence $7/2^{-}$(E1) $5/2^{+}$ (M1 + E2) $3/2^{+}$, both of which are shown in Fig. 19. The anisotropy of the composite angular correlation was found to be small and of the order of 10 percent. Data were collected by storing the time spectrum as in method II for the $5/2^{+}$ state in ^{169}Tm. The strong sources used in this measurement necessitated the inclusion of time-dependent electronic

---

+ A measurement of τ by Leming[73] has not been included because of its preliminary nature.

dead time effects in the correction for source decay. That is to say, the fraction of the time during which the electronics were busy and could analyze no new pulses from the detectors decreased as the source decayed. Approximate corrections for this effect were derived from the observed time dependence of singles counting rates, which were monitored throughout each run. The results of this initial measurement are listed in Table 3b (set No. 1).

In an attempt to improve the accuracy of the measurement, the experiments were repeated with two modifications. First, the 3 x 3 in. NaI(Tl) detector was replaced by a 1/4 x 1.5 in. NaI(Tl) crystal coupled to a 5 in. Lucite light guide. A diagram of this assembly is shown in Fig. 29. This change resulted in a decrease of the total counting rate in the NaI(Tl) channel without decreasing the detection efficiency for the low energy gamma-ray group. In this way, the effect of electronic dead time was reduced. The light guide was necessary to remove the photomultiplier tube from regions of high fringing field. A typical NaI(Tl) scintillation spectrum obtained with this assembly is given in Fig. 30. Secondly, a new configuration switching pattern was employed. Whereas previously the magnetic field direction or angle between detectors was changed at equal time intervals as shown in Fig. 31 (pattern A), a new pattern (pattern B in Fig. 31) was used. It is shown in Appendix B that the use of pattern B compensates for the effect of time-dependent dead times as well as source decay up to terms of order $(T_c/\tau_{source})^2$. The results of this second measurement are also displayed in Table 3b (set no. 2).

From the weighted average of the two measurements and the life-

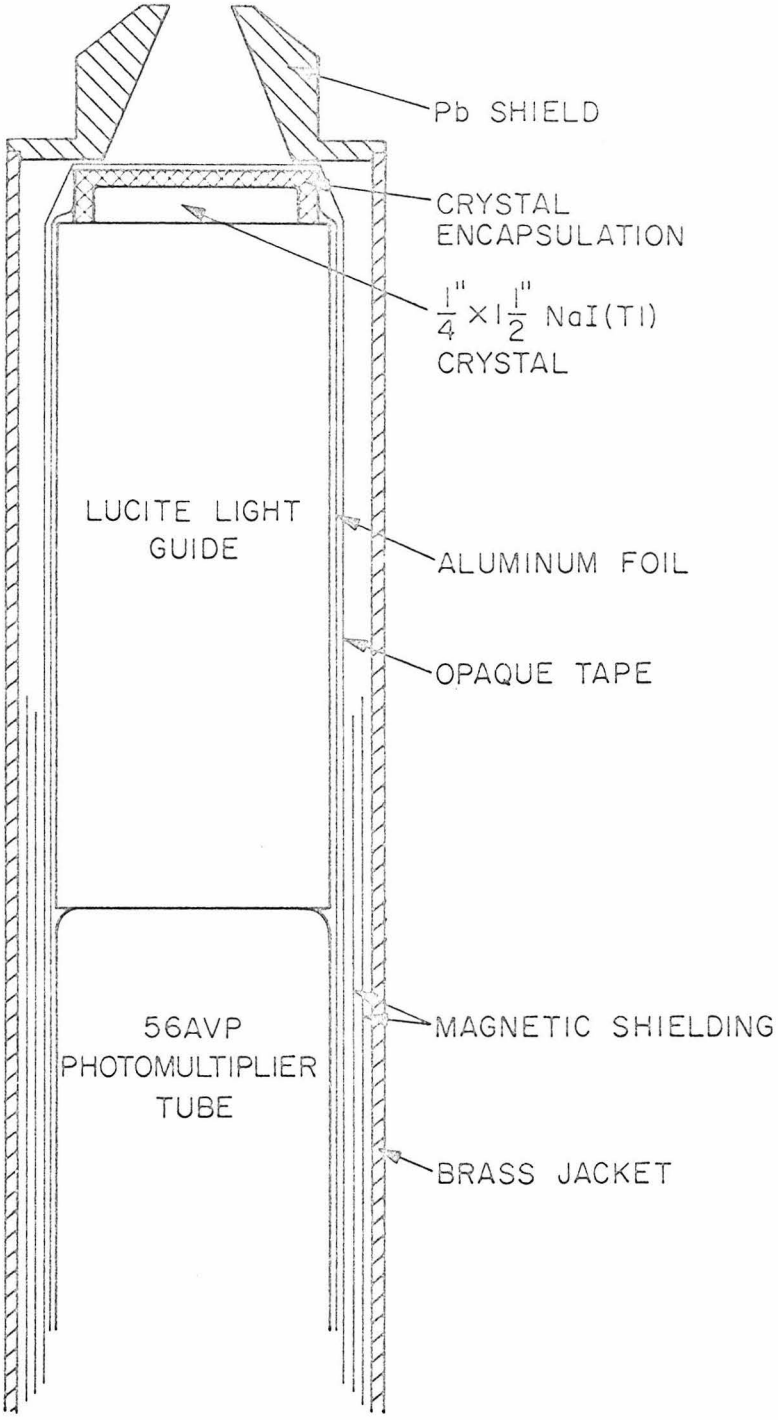

Figure 29

Cross-section of $\frac{1}{4}$ x 1 $\frac{1}{2}$ in. NaI(Tl) scintillation crystal spectrometer and Lucite light guide used in the measurement of the $\frac{5}{2}^+$ level moment in ^{171}Tm.

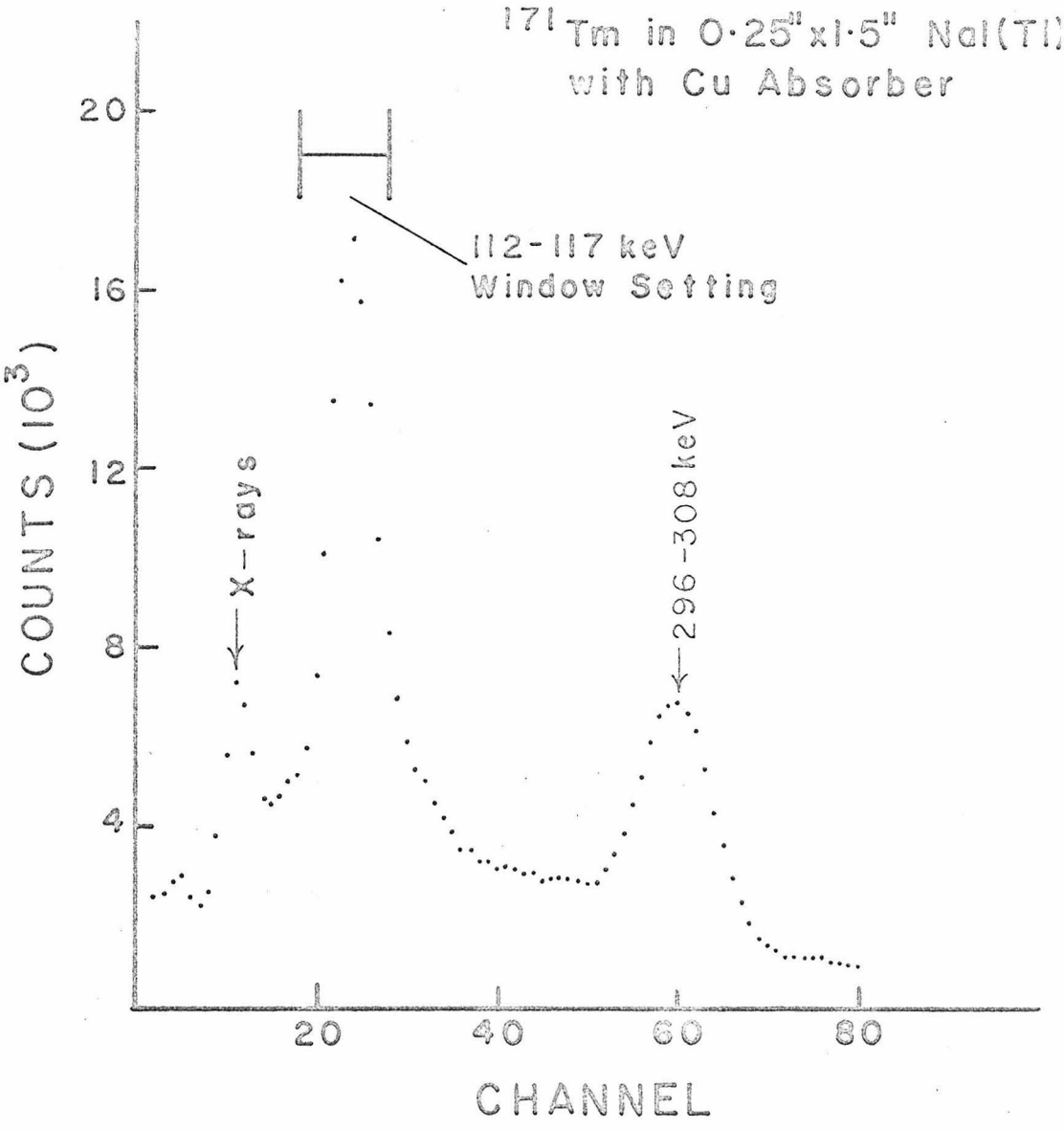

Figure 30

Gamma-ray scintillation spectrum of ^{171}Tm observed in the detector shown in Fig. 29. The single-channel analyzer setting is shown.

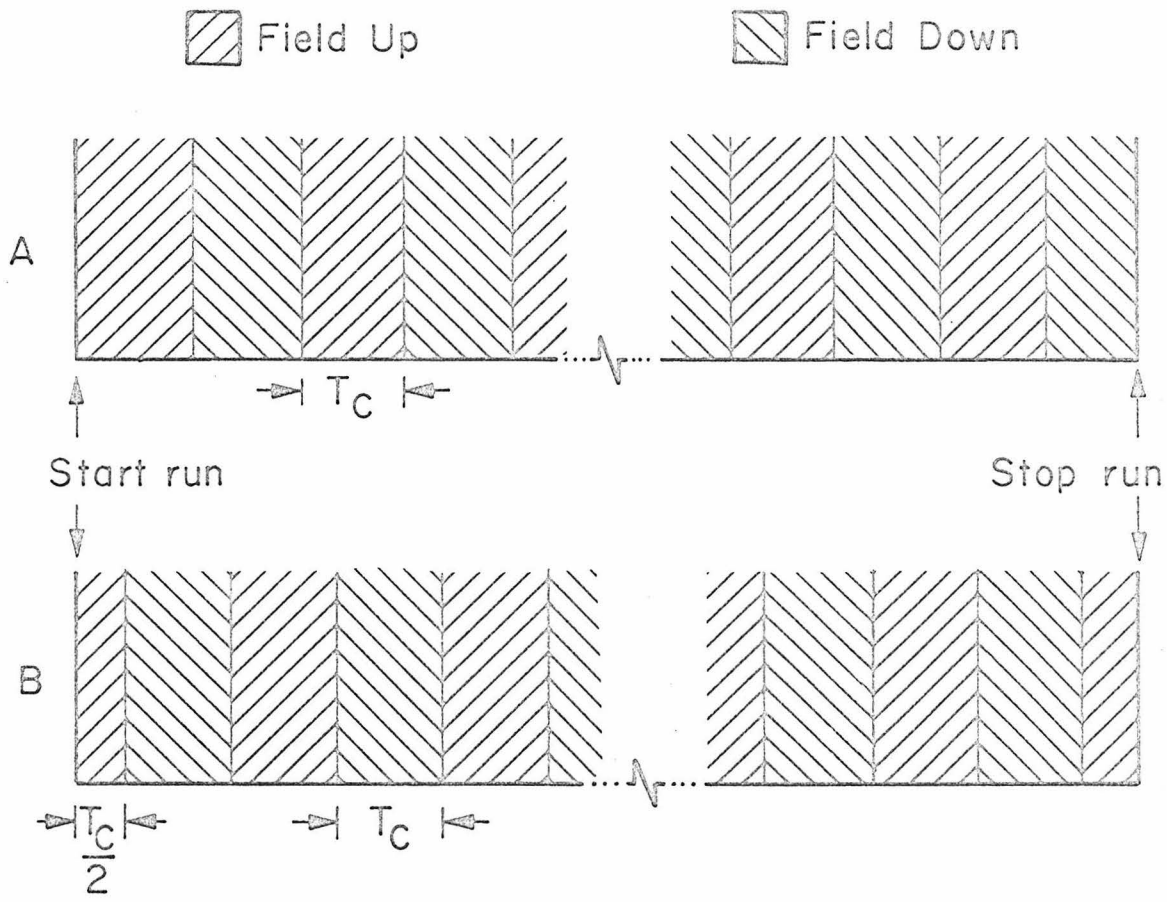

Figure 31

Normal (A) and improved (B) configuration switching patterns used in the measurements on ^{171}Tm.

time of $\tau_{5/2} = 0.080 \pm 0.019$ ns measured by Sundström et al.[72], we find the magnetic moment of the $5/2^+$ state to be $\mu_{5/2} = 0.81 \pm 0.37$ nm.

c. Measurement of Branching Ratios from the 129.1 keV $I^\pi = 7/2^+$ and 116.7 keV $I^\pi = 5/2^+$ States in ^{171}Tm

These measurements were performed using a 5 cm^2 area x 1 cm deep Ge(Li) detector having an energy resolution of 1.8 keV at 100 keV. The low energy portion of the measured spectrum is shown in Fig. 32. Photopeak intensities were determined by a multi-parameter least-squares fit to the experimental spectrum. The intensity and energy calibrations and fitting procedures are described by Varnell[75]. Experimentally measured intensities are given in Table 4. The crossover-to-cascade gamma intensity ratio $\lambda_{5/2} = I_\gamma(117 \text{ keV})/I_\gamma(112 \text{ keV})$ for the $5/2^+$ state at 116.7 keV is taken directly from the table as $\lambda_{5/2} = 0.115 \pm 0.005$. To extract the branching ratio information concerning the $7/2^+$ state at 129.1 keV, we use the experimental value of $I_\gamma(296 \text{ keV})/I_\gamma(124 \text{ keV}) = 3.00 \pm 0.13$ from the table and total conversion coefficients of $\alpha_T(296;E1) = 0.0196$ and $\alpha_T(124;E2) = 1.379$ interpolated from Ref. (76). Under the assumption that all beta and gamma-ray feeding of the 129.1 keV level other than through the 296 keV transition amounts to 2 percent of the 296 keV total transition intensity[18], we obtain a total intensity crossover-to-cascade ratio for the $7/2^+$ state of $I_T(129.1 \text{ keV})/I_T(12.4 \text{ keV}) = 3.22 \pm 0.58$. These measurements disagree with recent values of Megli et al.[77] but are in good agreement with those of Geiger et al.[78].

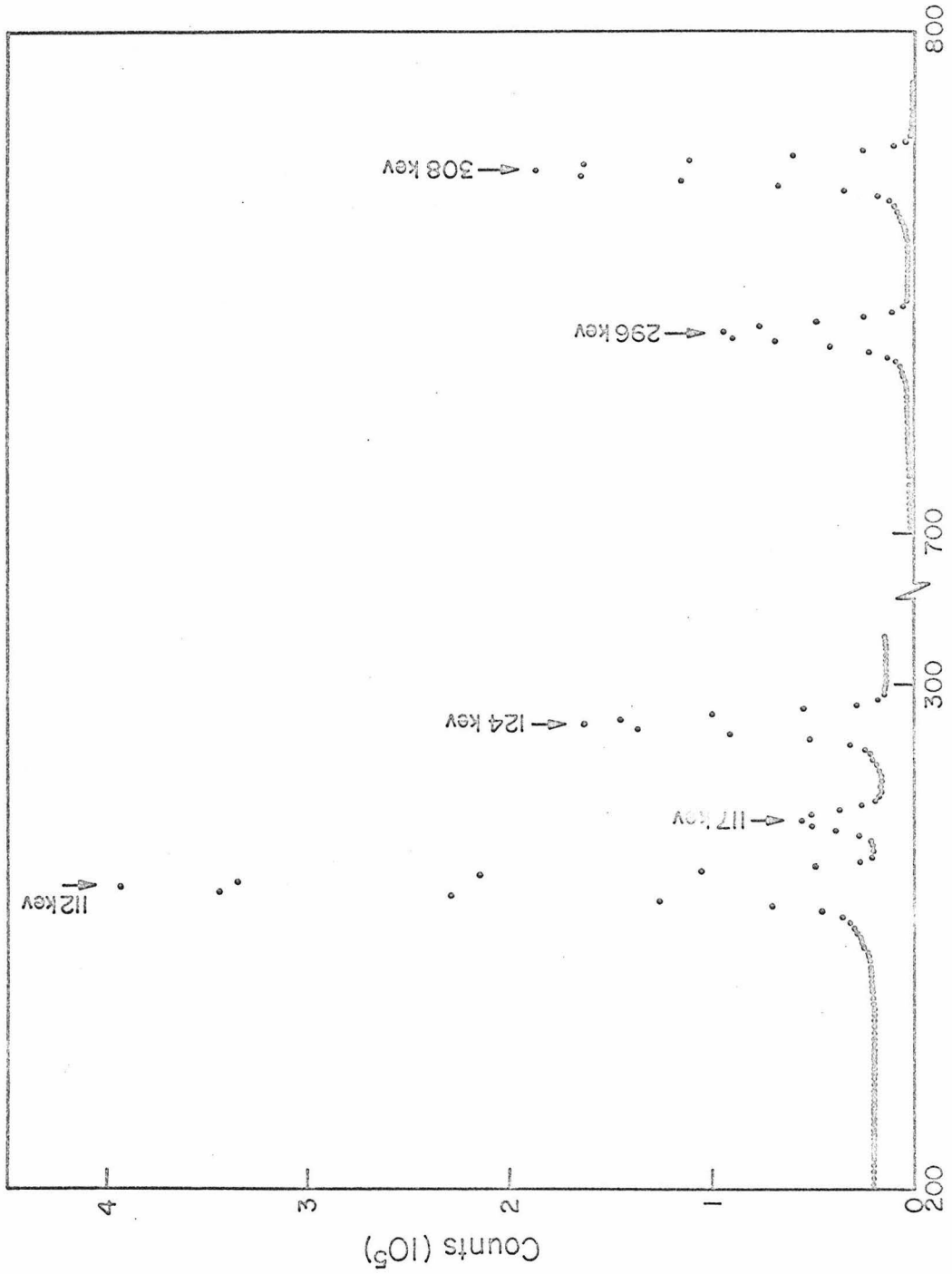

Figure 32: The portion of the gamma-ray spectrum of ^{171}Tm observed in a Ge(Li) detector, used to determine relative intensities.

Table 4

Relative Gamma-Ray Intensities for the Five Most Intense Transitions in ^{171}Tm

Energy (keV)	Intensity [a]
111.6	341.8
116.7	39.2
124.0	152.9
295.6	459.
308.2	1000.

a) Intensities are accurate to better than 3%

VI. ANALYSIS OF THE PROPERTIES OF THE GROUND STATE ROTATIONAL BANDS IN ^{169}Tm AND ^{171}Tm

VI.1 Introduction

In this chapter, the results of the measurements presented in the previous chapter in conjunction with other recent data will be used to determine the electromagnetic parameters of the rotational model for the K = 1/2 bands of ^{169}Tm and ^{171}Tm. The values of the parameters will then be used to determine some single particle matrix elements in the description of the intrinsic structure of the ground states of the two thulium nuclei.

The magnetic moment of an odd-mass nucleus contains a contribution from the collective motion of the nucleus and one from the orbital motion and intrinsic moment of the unpaired odd nucleon. The intrinsic moment of a free nucleon is related to its intrinsic spin by the nucleon spin g_s-factor; $g_s^{free} = 5.58$ for a proton and $g_s^{free} = -3.83$ for a neutron. Measurements of nuclear magnetic moments have shown, however, that use of the free nucleon value of the spin g-factor to compute the contribution of the unpaired nucleon spin to the magnetic moment is not appropriate. The semi-empirical value of $g_s^{eff} \approx 0.6\, g_s^{free}$ has been found to reproduce measured moments fairly well[57].

For the case of most deformed odd-mass nuclei, the magnetic moment is specified by Eq. (18), where g_R accounts for the collective rotational motion of the deformed nucleus and g_K represents the contribution of the odd nucleon. Under the usual assumption of independent quasiparticles occupying single particle Nilsson orbits, the parameter g_K is given by

$$g_K^K = g_\ell K + (g_s - g_\ell)\ \langle\nu|S_0|\nu\rangle, \qquad (25)$$

where g_ℓ and g_s are the orbital and spin g-factors of the odd nucleon and $\langle\nu|S_0|\nu\rangle$ is the expectation value of the spin component along the nuclear symmetry axis when the odd nucleon is in the single particle state $|\nu\rangle$. Thus, the introduction of an effective g_s factor in place of g_s^{free} in Eq. (25) is actually a phenomenological means of accounting for a renormalization of the spin matrix element $\langle\nu|S_0|\nu\rangle$. Mottelson[79] and Nilsson and Prior[80] have suggested that the renormalization is caused by a spin-dependent residual interaction between the odd nucleon and the nucleons in the even-even core. The interaction tends to align spins of like nucleons antiparallel and those of unlike nucleons parallel to the odd nucleon spin. Since the sign of the neutron and proton magnetic moments are opposite, this polarization of core nucleons always tends to reduce (quench) the spin contribution of the odd nucleon to the nuclear magnetic moment. Microscopic model calculations of this effect carried out by Bochnacki and Ogaza[81] have reproduced the semi-empirical value of $g_s^{eff} \approx 0.6\ g_s^{free}$.

For the special case of a K = 1/2 rotational band, Eq. (18) for the magnetic moment must be modified to read[20]

$$\mu_I = g_R I + \frac{(g_K - g_R)}{4(I+1)}\ [1 + (-1)^{I+1/2}(2I+1)b_0], \qquad (26)$$

where the additional "magnetic decoupling" parameter b_0 is defined by the relation

$$(g_K - g_R)b_0 = -(g_\ell - g_R^0)a + (g_s - g_\ell)\langle\nu|S_+|\bar{\nu}\rangle. \qquad (27)$$

In this formula, g_R^0 is the collective g_R-factor of the core[+], S_+ is the raising operator for the spin angular momentum, $\langle\nu|$ is the single particle state with spin projection K = 1/2, and $|\bar{\nu}\rangle$ is the symmetric state with K = - 1/2. Bochnacki and Ogaza[82] have pointed out that the effect of spin polarization on the matrix elements of the transverse spin component S_+ is not the same as the effect on those of S_0. In other words, the value of g_s needed in Eq. (27) to account for the renormalization of $\langle\nu|S_+|\bar{\nu}\rangle$ is different from the g_s value needed in Eq. (25). Their calculation[82,83] of the two g_s-factors for thulium nuclei agreed with those derived from experimentally determined values of g_K, g_R, g_R^0 and b_0, but the experimental values were not altogether accurate.

In the following sections, least-squares fits to determine the values of g_K, g_R, and b_0 are described, and accurate values of the two g_s-factors characterizing "longitudinal" and "transverse" spin polarization are found. Also determined, is the value of a correction term to the rotational model expressions for electric quadrupole transition rates, which has, for the most part, been ignored in previous investigations.

VI.2 Determination of Rotational Model Parameters

a. Rotational Model Formulas

The relevant electromagnetic properties of a K = 1/2 rotational

---

+ The parameter g_R represents the collective rotational g-factor for the entire nucleus including the odd nucleon, whereas g_R^0 is conventionally taken to represent the collective rotational g-factor for only the even-even nuclear core.

band as in ^{169}Tm and ^{171}Tm are described by the following relations[84,20]:

$$\mu_I = g_R I + \frac{(g_K - g_R)}{4(I+1)} [1 + (-1)^{I+1/2}(2I+1)b_0] \quad (26)$$

$$B(M1;I+1 \rightarrow I) = \frac{3}{16\pi} (g_K - g_R)^2 \frac{2I+1}{4(I+1)} [1 + (-1)^{I+3/2} b_0]^2 \quad (28)$$

$$B(E2;I+2 \rightarrow I) = \frac{15}{512\pi} \frac{(2I+1)(2I+3)}{(I+1)(I+2)} Q_0^2 [1 + (-1)^{I-1/2} \sqrt{\frac{2}{3}}\, q/Q_0]^2 \quad (29)$$

$$B(E2;I+1 \rightarrow I) = \frac{15}{256\pi} \frac{2I+1}{I(I+1)(I+2)} Q_0^2 [1 + (-1)^{I-1/2}(I+1) \cdot \sqrt{\frac{2}{3}}\, q/Q_0]^2. \quad (30)$$

The quantities g_K, g_R, b_0, Q_0, and q are parameters in the rotational description. The parameter Q_0 is the intrinsic electric quadrupole moment, and q is formally present as an "electric decoupling" term and is retained here for completeness. All experimentally measured electromagnetic properties of the K = 1/2 band can be written in terms of these parameters with the aid of the above relations and, in some instances, with tabulated values of internal conversion coefficients[76] and level energies[18].

b. Least-Squares Fitting Procedure

The parameters of the rotational model were determined by least-squares fits to statistically independent experimental data. For example, the measurement of the magnetic moment of a state by the perturbed angular correlation technique actually measures the quantity $\mu\tau$,

the product of moment and lifetime. Rather than use the value of μ in the least-squares fit[85,86], the error in which has been increased through the uncertainty in the mean life τ and is statistically correlated with the error in τ, we use the experimental quantity $\mu\tau$. A typical expression computed for the $7/2^+$ state in ^{169}Tm appears as

$$\mu_{7/2}\tau_{7/2} = \left(\frac{7}{2} b_1 + \frac{1}{18} b_2 + \frac{4}{9} b_3 \right) / \{ (4.012 \times 10^6 r + 133.6t) \cdot$$

$$[1 + (52.7 + 0.1354\, t/r)/(1 + 3.330 \times 10^{-5} t/r)] + 2.538 \times 10^7 v \}. \quad (31)$$

In the above, abbreviations $b_1 = g_R$, $b_2 = g_K - g_R$, $b_3 = (g_K - g_R)b_0$, $r = (g_K - g_R)(1 + b_0)$, $t = Q_0^2 \left(1 + \frac{7q}{\sqrt{6}\, Q_0}\right)^2$, and $v = Q_0^2 \left(1 - \frac{2q}{\sqrt{6}\, Q_0}\right)^2$ have been used, and the values of the appropriate transition energies[18] and theoretical conversion coefficients[76] have been inserted explicitly. This unique procedure takes full advantage of the accuracy of all experimental values.

In order to fit data to expressions of such complexity in which the parameters enter non-linearly, a modified version of a fitting program found on the IBM SHARE LIBRARY (No. 3094) was used. The algorithm followed by this program has been described by its author, D.W. Marquardt[87].

Data used in the fits represent weighted averages of recent experimental values. In those cases where individual measurements appear inconsistent, the adopted errors have been aritificially increased to obtain statistical consistency.

c. Results of the Fit for ^{169}Tm

The electromagnetic properties and their adopted experimental values are given in columns 1-3 of Table 5. As will be discussed later, the value of the parameter q in relations (29) and (30) above may be expected to be zero. Therefore, the first fit (Fit I) to the experimental data was performed with q constrained to equal zero. The results, listed in column 4 of Table 5, show fair agreement with experiment, but a value of 3.0 for the normalized chi-square indicates that the assumed theoretical expressions are not sufficient to reproduce the data within current experimental precision. A second fit (Fit II), the results of which are given in column 5 of the table, was therefore performed in which the parameter q was allowed to vary. In this second fit, the value of normalized chi-square decreased to a more acceptable value of 1.8.

It is evident from the resulting values of the parameters for Fit. I and Fit II, shown in column 7 of Table 5, that the magnetic parameters g_R, g_K, and b_0 are not sensitive to the value of q, whereas the intrinsic quadrupole moment Q_0 is significantly larger when q is allowed to vary. The accuracy of the fitted values of g_R, g_K, and b_0 has been substantially improved over that of previous analyses[85,86]. In Fit II, a non-zero value for q is found (cf. Ref. 86). To check the sensitivity of the fitted value of q to the value of each datum, fifteen fits to fourteen data points were performed, and q was found to be insensitive to the omission of any single datum. Some possible origins of a non-zero value of q are suggested in a later section.

Table 5

Results of Fits of Unified Model to Experimental Properties of Ground State Rotational Band in ^{169}Tm

Quantity	Units	Exp. value [e]	Fit I	Fit II	References [g]	Results of Fit I [f]
$\mu_{1/2}$	nm	-0.2308 ± 0.0008	-0.2306	-0.2308	(1), (2) & (3)	g_R = 0.403 ± 0.006
$\mu_{3/2}/\mu_{1/2}$	-	-2.308 ± 0.055	-2.240	-2.282	(4) & (5)	g_K = - 1.62 ± 0.02
$\mu_{5/2}/\tau_{5/2}$	10^{-10} nm·sec	0.702 ± 0.071	0.662	0.665	Present work	b_0 = - 0.142 ± 0.005
$\mu_{7/2}\ \tau_{7/2}$	10^{-10} nm·sec	6.00 ± 0.24	6.56	6.33	Present work	Q_0 = 7.67 ± 0.06 barns
$\tau_{3/2}$ [a]	10^{-10} sec	54.1 ± 2.7	59.0	60.2	(6), (7), (8) & (9)	$g_{s_\ell}^{eff}/g_s^{free}$ = 0.798 ± 0.010
$\tau_{5/2}$	10^{-10} sec	0.897 ± 0.037	0.895	0.893	(10) & (7)	$g_{s_t}^{eff}/g_s^{free}$ = 0.475 ± 0.017
$\tau_{7/2}$	10^{-10} sec	4.52 ± 0.18	4.60	4.39	(11), (12) & (7)	
B(E2; 5/2 → 1/2)	$10^{-48} e^2 \cdot cm^4$	1.123 ± 0.023	1.171	1.147	(13)	Results of Fit II [f]
$\delta^2(7/2 \rightarrow 5/2)$	10^{-3}	0.75 ± 0.37	0.65	0.57	(14) & (15) [b]	g_R = 0.406 ± 0.006
$\delta^2(5/2 \rightarrow 3/2)$	10^{-3}	25.6 ± 1.2	22.1	25.7	(16) & present work [c]	g_K = - 1.60 ± 0.02
$\delta^2(3/2 \rightarrow 1/2)$	10^{-3}	1.08 ± 0.05	0.97	0.94	(14) & (15) [d], (17)	b_0 = - 0.147 ± 0.005
$I_\gamma^{5/2\text{-}1/2}/I_\gamma^{5/2\text{-}3/2}$	-	0.104 ± 0.004	0.110	0.107	(18),(19) & (20)	Q_0 = 7.79 ± 0.06 barns
$I_{tot}^{7/2\text{-}3/2}/I_{tot}^{7/2\text{-}5/2}$	-	2.75 ± 0.42	2.20	2.44	from compilation of Ref. (6)	q/Q_0 = - 0.030 ± 0.008
$I_\gamma^{9/2\text{-}5/2}/I_\gamma^{9/2\text{-}7/2}$	-	0.486 ± 0.023	0.506	0.492	(21), (19) & (20)	$g_{s_\ell}^{eff}/g_s^{free}$ = 0.790 ± 0.011
$I_\gamma^{13/2\text{-}9/2}/I_\gamma^{13/2\text{-}11/2}$	-	1.22 ± 0.10	1.17	1.14	(21) & (20)	$g_{s_t}^{eff}/g_s^{free}$ = 0.467 ± 0.017
Normalized χ^2			3.0	1.8		

(a) Value of α_T = 270 is assumed in fit, based on subshell ratios of Ref. (17) and tables of Ref. (15).

(b) Used $L_I/(L_{II} + L_{III})$ and $M_I/M_{II\text{-}V}$ of Ref. (14).

(c) δ^2 recalculated using Ref. (15) where appropriate.

(d) Used $M_I/(M_{II} + M_{III})$ of Ref. (14)

(e) Represents weighted avg. of quoted references, with increased error if individual measurements show inconsistency.

(f) Used a g_R^0 (^{168}Er) = 0.331 ± 0.010 from Ref. (22).

(g) References cited with this table are listed on the following page.

References for Table 5

(1) G. Ritter, Phys. Rev. 128 (1962) 2238.

(2) D. Giglberger and S. Penselin, Z. Physik 199 (1967) 244.

(3) S. Penselin (1963), as tabulated by I. Lindgren in Perturbed angular correlations (Amsterdam, 1964) p. 397.

(4) M. Kalvius, P. Kienle, H. Eicher, W. Wiedemann and C. Schüler, Z. Physik 172 (1963) 231.

(5) R.L. Cohen, Phys. Rev. 134 (1964) A94.

(6) T. Sundström, J. Lindskog, J.O. Lindström and P. Sparrman, Ark. Fysik 26 (1964) 361.

(7) R.E. McAdams, G.W. Eakins and E.N. Hatch, Nuclear Phys. 82 (1966) 449.

(8) H. Beekhuis and H. DeWaard, Physica 24 (1958) 767.

(9) D. Bloess and F. Münnich, Z. Naturforsch. 18a (1963) 1028; and H. Blechschmidt, Phys. Verhandl. 12 (1961) 185.

(10) A.E. Blaugrund, V. Dar, and G. Goldring, Phys. Rev. 120 (1960) 1328.

(11) T. Sundström, P. Sparrman, J.O. Lindström and J. Lindskog, Ark. Fysik 26 (1964) 377.

(12) A.E. Blaugrund, Phys. Rev. Letters 3 (1959) 226.

(13) M.C. Olesen and B. Elbek, Nuclear Phys. 15 (1960) 134.

(14) K.N. Shliagin and P.S. Samoilov, Sov. Phys. JETP 7 (1958) 20.

(15) R.S. Hager and E.C. Seltzer, Internal Conversion Tables, Nuclear Data A4 (1968).

(16) V.M. Kel'man, R. Ys. Matskhvarishvili, B.K. Preobrazhenskii, V.A. Romanov and V.V. Tuchkevich, Sov. Phys. JETP 10 (1960) 456;
J.W. Michelich, Phys. Rev. 103 (1956) 1285;
Z. Grabowski, J.E. Thun and B. Lindström, Z. Physik 169 (1962) 303;
M. Martin, P. Marmier and J. de Boer, Helv. Phys. Acta 31 (1958) 435; and
D. Ashery, A.E. Blaugrund, R. Kalish, J.S. Sokolowski and Z. Vager, Nuclear Phys. 67 (1965) 385.

(17) T.A. Carlson, P. Erman and K. Fransson, preprint.

(18) P. Alexander and F. Boehm, Nuclear Phys. 46 (1963) 108.

(19) F. Boehm, G. Goldring, G.B. Hagemann, G.D. Symonds and A. Tveter, Physics Letters 22 (1966) 627.

(20) G.G. Seaman, E.M. Bernstein and J.M. Palms, Phys. Rev. 161 (1967) 1223.

(21) J. de Boer, Nuclear Phys. 61 (1965) 675.

(22) E. Münch, D. Quitmann and S. Hüfner, Z. Naturforsch., 21a (1966) 847.

d. Results of the Fit for ^{171}Tm

Data on electromagnetic properties of ^{171}Tm are less abundant and less precise than those available for ^{169}Tm. Table 6 displays the data and results of fits performed as in the above case. The measured values of mixing ratios of Bocquet[88] and of Geiger et al.[78] are not in agreement. Fits IA and IIA utilize the data of Bocquet, and IB and IIB use those of Geiger et al. The two sets of mixing ratios allow equally good fits, and more accurate data are needed to decide between them. Nevertheless, the new value of the $7/2^+$ state magnetic moment has permitted the first determination of a unique set of magnetic parameters with reasonable accuracy. It can also be seen in Table 6 that the experimental data are not sufficiently precise in this case to uniquely determine the value of q. Fit IIB does, however, yield a value of q whose sign is consistent with that found for ^{169}Tm.

VI.3 Interpretation of the Rotational Model Parameters in Terms of Single Particle Matrix Elements

a. Transverse and Longitudinal Effective Spin g-Factors

The magnetic parameters, g_K and b_0, for a K = 1/2 band can be related to single particle matrix elements in the following way[20,82];

$$g_K = g_\ell + 2(g_{s_\ell}^{eff} - g_\ell)\langle K = \tfrac{1}{2}|S_0|K = \tfrac{1}{2}\rangle \qquad (32)$$

$$(g_K - g_R)b_0 = -(g_\ell - g_R^0)a + (g_{s_t}^{eff} - g_\ell)\langle K = \tfrac{1}{2}|S_+|K = -\tfrac{1}{2}\rangle. \qquad (33)$$

Here, $g_\ell = 1$ is the orbital g-factor associated with the odd proton, g_R^0 is related to the rotational g-factor of the even core, and

Table 6

Results of Fits of Unified Model to Experimental Properties of the Ground State Rotational Band in ^{171}Tm

Quantity	Units	Experimental values	Fit IA	Fit IIA	Fit IB	Fit IIB	References (b)
$\mu_{1/2}$	nm	-0.277 ± 0.005	-0.228	-0.229	-0.227	-0.227	(1)
$\mu_{5/2}\tau_{5/2}$	10^{-10} nm·sec	0.65 ± 0.26	0.70	0.70	0.67	0.67	Present work
$\mu_{7/2}\tau_{7/2}$	10^{-10} nm·sec	7.56 ± 0.67	8.28	8.34	7.46	7.35	Present work
$\tau_{5/2}$	10^{-10} sec	0.80 ± 0.19	0.90	0.89	0.94	0.96	(2)
$\tau_{7/2}$	10^{-10} sec	5.23 ± 0.21	5.21	5.21	5.20	5.19	(2)
$\delta^2(7/2\text{-}5/2)$	10^{-3}	0.55 ± 0.12	0.37	0.39			(3)
		0.33 ± 0.05			0.31	0.28	(4)
$\delta^2(5/2\text{-}3/2)$	10^{-3}	25.5 ± 2.0	26.6	25.7			(3)
		30. ± 3.			26.4	29.1	(4)
$\delta^2(3/2\text{-}1/2)$	10^{-3}	0.66 ± 0.10	0.56	0.57			(3)
		0.36 ± 0.06			0.46	0.46	(4)
$\frac{I_{tot}^{7/2\text{-}3/2}}{I_{tot}^{7/2\text{-}5/2}}$		2.90 ± 0.32	2.99	2.94	2.52	2.73	Present work and (4)
$\frac{I_{\gamma}^{5/2\text{-}1/2}}{I_{\gamma}^{5/2\text{-}3/2}}$		0.111 ± 0.005	0.113	0.115	0.112	0.110	Present work and (4)
Norm χ^2			0.88	0.99	1.12	0.97	

Fit	g_R	g_K	b_0	Q_0(b)	q/Q_0	$g_{s_\ell}^{eff}/g_s^{free}$	$g_{s_t}^{eff}/g_s^{free}$ (a)
IA	0.432 ± 0.028	-1.42 ± 0.04	-0.22 ± 0.02	8.11 ± 0.18	-	0.724 ± 0.033	0.406 ± 0.047
IIA	0.435 ± 0.028	-1.43 ± 0.04	-0.22 ± 0.02	8.14 ± 0.18	0.008 ± 0.014	0.723 ± 0.033	0.406 ± 0.047
IB	0.398 ± 0.028	-1.49 ± 0.04	-0.18 ± 0.02	7.93 ± 0.17	-	0.762 ± 0.033	0.497 ± 0.046
IIB	0.391 ± 0.028	-1.46 ± 0.04	-0.18 ± 0.02	7.89 ± 0.17	-0.022 ± 0.015	0.760 ± 0.033	0.487 ± 0.046

(a) The value of $g_R^0 = 0.329 \pm 0.25$ of Ref. (5) was used to compute effective g_s factors.

(b) References cited in this table are listed on the following page.

References for Table 6

(1) B. Budick, I. Maleh and R. Marrus, Phys. Rev. 135 (1964) B1281.

(2) T. Sundström, J.O. Lindström, P. Sparrman and J. Lindskog, Ark. Fysik 26 (1964) 397.

(3) J.P. Bocquet, J. de Phys. 26 (1965) 795.

(4) J.S. Geiger, R.L. Graham and M.W. Johns, BAPS 13, No. 4 (1968) 672; and private communication.

(5) J.D. Kurfers and R.P. Scharenberg, Phys. Rev. 161 (1967) 1185.

$a = - \langle K = 1/2 | j_+ | K = - 1/2 \rangle$ is the energy decoupling factor. If the matrix elements of S_0 and S_+ are to be interpreted as single particle matrix elements for the [411] 1/2 Nilsson orbital, then the nucleon spin g-factors, $g_{s_\ell}^{eff}$ and $g_{s_t}^{eff}$, must replace the free nucleon value, g_s^{free}, to account for effects of spin polarization on the even core by the odd proton. We have extracted the values of the two spin g_s-factors in a manner identical to that used by Bochnacki and Ogaza[82,83] for ^{169}Tm and ^{171}Tm, and the results are given in Tables 5 and 6, respectively.

The procedure used in extracting the g_s^{eff} values from relations (32) and (33) above was as follows. The values of the single particle matrix elements of the spin operator were computed using recent values of Nilsson wavefunction amplitudes[55] and a deformation derived from the fitted value of Q_0. Following Bochnacki and Ogaza, corrections to g_K due to mixing of the [411] 1/2 band with K = 3/2 bands through the Coriolis interaction were computed from the difference between the fitted values of g_R and recent experimental values of g_R^0 for the neighboring even-even nuclei. The adopted values of g_R^0 were $g_R(^{168}\text{Er}) = 0.331 \pm 0.010$[89] and $g_R(^{170}\text{Er}) = 0.329 \pm 0.025$[90], respectively, for the analysis of ^{169}Tm and ^{171}Tm data. The experimental values of the energy decoupling factors, $a(^{169}\text{Tm}) = - 0.7795 \pm 0.0006$ and $a(^{171}\text{Tm}) = - 0.864 \pm 0.001$, were taken from Refs. (86) and (91). The errors quoted in Tables 5 and 6 for the values of the effective spin g_s-factor were computed from the errors in the fitted rotational parameters, taking into account the cross-correlations among their errors.

Bochnacki and Ogaza have predicted the values of the effective spin g_s-factors for Tm by considering the coherent part of the spin-spin interaction of the odd proton with the nucleons in the even core. Their results are[82,83]

$$g_{s_\ell}^{eff}/g_s^{free} = 0.713 \quad \text{and} \quad g_{s_t}^{eff}/g_s^{free} = 0.572.$$

It is seen in Table 5 that our results in ^{169}Tm, although confirming the expected relative magnitude, disagree in both the transverse and longitudinal cases with the above numerical predictions. In ^{171}Tm (Table 6), the transverse values for all of the fits are in disagreement. The longitudinal effective spin g_s-factor disagrees with the prediction only in the cases IB and IIB. Several approximations could account for the observed disagreement with predicted values.

In the calculation of the experimental values of $g_{s_\ell}^{eff}$ and $g_{s_t}^{free}$, the Coriolis mixing of the [411] 1/2 band with other K = 1/2 bands, which can renormalize g_K and b_0, was neglected. Secondly, in interpreting the quantity g_R^0 mentioned above as the rotational g_R-factor of the neighboring even-even nucleus, the effects of blocking+ of the [411] 1/2 level in the odd Tm nuclei are neglected. And finally, the use of the experimental values of the energy decoupling factor 'a' rather than those computed from Nilsson wavefunctions is not clearly justified, since the experimental values of 'a' for the [411] 1/2 bands in ^{167}Tm, ^{169}Tm, and ^{171}Tm show a dependence on deformation

---

+ The term "blocking" implies that the level in question may not be occupied by particles from the even core. This restriction on the states into which core nucleons may scatter alters the rotational motion of the core.

opposite to that predicted by the Nilsson model. This anomalous behavior of 'a' has been successfully explained by Feifrlik[54], who introduced an interaction between quasiparticles which renormalizes the $\langle K = 1/2 | j_+ | K = -1/2 \rangle$ matrix element. Renormalization of spin matrix elements due to this interaction was not taken into account by Bochnacki and Ogaza[82].

There is available an alternate method of correcting g_K and b_0 for Coriolis mixing with K = 3/2 bands and other K = 1/2 bands. The corrections may be calculated directly from Nilsson wavefunction amplitudes, single particle energies, and factors which account for the short-range pairing forces[93]. Such a calculation was performed for the case of ^{169}Tm, and the g_s^{eff} factors redetermined. The values found were

$$g_{s_t}^{eff}/g_s^{free} = 0.477 \quad \text{and} \quad g_{s_\ell}^{eff}/g_s^{free} = 0.811,$$

which vary slightly from the results of Fit I, shown in Table 5. Thus the observed discrepancies between the experimental values and the predictions of Bochnacki and Ogaza must arise from the use of experimental values for the decoupling parameter 'a' and the rotational g-factor g_R^0 and not from the neglect of the Coriolis mixing with other K = 1/2 bands.

b. Discussion of the Parameter q

Bohr and Mottelson[84] have indicated that, in the evaluation of electric quadrupole matrix elements in the rotational model formalism, an extra term arises in the cases of K = 1/2 and K = 1 bands (see expressions (29) and (30)). The quantity q appearing in these terms is

formally defined as $q = \langle K = 1/2 | \mathcal{M}(E2,1) | K = -1/2 \rangle$, where $\mathcal{M}(E2,\mu)$ is the μ^{th} spherical tensor component of the electric quadrupole operator defined with respect to the nuclear body fixed axes. Analysis performed by Dzhelepov and Dranitsyna[86] indicated that q may differ from zero, and the present fits have verified this, q being approximately three percent of Q_0 in the case of ^{169}Tm.

It can be shown, however, that although q is formally present in the rotational model, the value of the matrix element, $\langle K = 1/2 | \mathcal{M}(E2,1) | K = -1/2 \rangle$, is identically zero. To prove this result, only time reversal invariance, the Hermiticity of the E2 operator, and symmetries of vector addition coefficients need to be invoked after expansion of the single particle wavefunction in a spherical basis. The proof is given in Appendix C. The experimentally determined value of q must therefore be attributed to admixtures of other single particle configurations into the [411] 1/2 orbital. Two types of admixtures can be suggested. The first is the ordinary Coriolis mixing of the [411] 1/2 band with other K = 1/2 and K = 3/2 bands. Small admixtures of this type simply renormalize the magnetic parameters g_K, g_R, and b_0, leaving relations (26) and (28) unchanged. But, in the electric case several new spin-dependent terms enter, some of which contain spin-dependent phases. The expressions describing B(E2) would, in this case, no longer be those of relations (29) and (30) but would be similar in that small terms, whose signs alternate with I, are added to correct the value of Q_0.

Admixtures of a second type, which would leave relations (29) and (30) unchanged and give a non-zero q, can arise from a mechanism dis-

cussed by Soloviev and Vogel [94]. They conclude that intrinsic states of odd mass deformed nuclei, such as the [411] 1/2 state, may contain sizable admixtures of a collective γ-vibrational+ phonon excitation. The departures from axial symmetry in the γ-vibration would lead to a non-zero value of the matrix element

$$q = \langle 411\ \tfrac{1}{2} + [411\ \tfrac{3}{2},\ Q_2^{\,2}]_{1/2} | \mathcal{M}(E2,1) | 411 - \tfrac{1}{2} + [411\ \tfrac{3}{2},\ Q_2^{\,2}]_{-1/2} \rangle .$$

The notation indicates that a γ-vibrational phonon $Q_2^{\,2}$, coupled to a particle in the state [411] 3/2 to give a net K = 1/2, is mixed into the [411] 1/2 state. A prediction of the value of q on this basis would prove useful in determining the physical origin of our fitted value, but no such prediction is available as yet.

VI.4 Conclusion

The rotational model parameters of the K = 1/2 ground state rotational band in ^{169}Tm have been precisely determined by means of a least-squares fit to all recent experimental data including the measurements reported here. Further, more accurate experimental data may now be used to investigate deviations from the pure rotational model such as the above-mentioned correction to the electric quadrupole moment. Although we have determined the rotational parameters of the K = 1/2 band of ^{171}Tm with reasonable accuracy, significant improvement could be realized through the use of more precise experimental data. In particular, the measurement of the mixing ratios of

---

+ Deformed nuclei can suuport two types of vibrational modes. The β-vibration is the same as that described in Chapter III except that the equilibrium is deformed rather than spherical. The γ-vibration entails fluctuations away from the axially symmetric nuclear shape, and a γ-vibrational phonon, denoted $Q_2^{\,2}$, carries an angular momentum projection of 2 on the symmetry axis.

the 5, 12, and 112 keV transitions may be improved, and a more accurate measurement of the magnetic moment of the $I^{\pi} = 5/2^{+}$ state may be possible through the use of the large internal hyperfine magnetic fields at Tm in a ferromagnetic lattice. Finally, we have confirmed the qualitative agreement with experiment of the predictions of Bochnacki and Ogaza[82,83] regarding spin polarization effects but have found that a more reliable method of computing the renormalization of single particle magnetic matrix elements from the experimental data is needed.

APPENDIX A

Computation of g_K for the Two-Proton State in ^{182}W in the Strong Coupling Limit

The two protons occupy the $[514]9/2^-$ and $[402]5/2^+$ Nilsson orbitals, respectively. Let us denote the $[514]9/2^-$ level as state $|1\rangle$ and the $[402]5/2^+$ as state $|2\rangle$. The proton occupying state $|1\rangle$ (or $|2\rangle$) carries total, orbital, and spin angular momentum $\vec{j}(1)$, $\vec{\ell}(1)$, and $\vec{s}(1)$ (or $\vec{j}(2)$, $\vec{\ell}(2)$, and $\vec{s}(2)$), respectively. The quantities are related by

$$\vec{j}(i) = \vec{\ell}(i) + \vec{s}(i) \quad (i = 1 \text{ or } 2). \tag{1A}$$

The total angular momentum of the nuclear state is given by

$$\vec{I} = \vec{j}(1) + \vec{j}(2) + \vec{R}, \tag{2A}$$

where $\vec{R}$ is the angular momentum associated with the collective rotation of the nucleus. For an axially symmetric nuclear shape, the vector $\vec{R}$ is perpendicular to the nuclear symmetry axis (the 3-axis in the body-fixed coordinate system), and the projection of total angular momentum (called K in Chapter IV) is given by the algebraic sum of the projections of $\vec{j}(1)$ and $\vec{j}(2)$. In order to obtain the observed value of K = 2, we must assume that $j_3(1)|1\rangle = \Omega_1 = 9/2$ and $j_3(2)|\bar{2}\rangle = -\Omega_2 = -5/2$. The state $|\bar{2}\rangle$ is that obtained from the state $|2\rangle$ after reversal of the signs of the projection of orbital and spin angular momentum on the 3-axis. In the strong-coupling approximation one assumes the total two particle state wavefunction can be written as the simple product $|1\bar{2}\rangle = |1\rangle|\bar{2}\rangle$.

Now the magnetic moment of a state is defined by the relation

$$\mu_I = \langle \vec{\mu}_{op} \cdot \vec{I} \rangle / (I + 1) \tag{3A}$$

where the brackets $\langle\ \rangle$ indicate the expectation value in the state $|1\bar{2}\rangle$ with the projection M_I of $\vec{I}$ on the space-fixed z-axis equal to its maximum value, I. The operator $\vec{\mu}_{op}$ can be written, for our case, as

$$\begin{aligned}\vec{\mu}_{op} &= g_{s1}\vec{s}(1) + g_{\ell 1}\vec{\ell}(1) + g_{s2}\vec{s}(2) + g_{\ell 2}\vec{\ell}(2) + g_R\vec{R} \\ &= g_{s1}\vec{s}(1) + g_{\ell 1}(\vec{j}(1) - \vec{s}(1)) + g_{s2}\vec{s}(2) + g_{\ell 2}(\vec{j}(2) - \vec{s}(2)) + \\ &\qquad g_R(\vec{I} - \vec{j}(1) - \vec{j}(2)).\end{aligned} \tag{4A}$$

Inserting this expression into Eq. (3A) yields

$$\begin{aligned}\mu_I = \frac{1}{I+1}\Big\{&(g_{s1} - g_{\ell 1})\langle \vec{s}(1)\cdot\vec{I}\rangle + (g_{\ell 1} - g_R)\langle \vec{j}(1)\cdot\vec{I}\rangle + \\ &(g_{s2} - g_{\ell 2})\langle \vec{s}(2)\cdot\vec{I}\rangle + (g_{\ell 2} - g_R)\langle \vec{j}(2)\cdot\vec{I}\rangle \\ &+ g_R\langle I^2\rangle\Big\}\ .\end{aligned} \tag{5A}$$

In order to further evaluate the above expression, we note that in the diagonal matrix elements of $\vec{s}\cdot\vec{I}$ (or $\vec{j}\cdot\vec{I}$) only the s_3I_3 (or j_3I_3) terms contribute and that the product state $|1\bar{2}\rangle$ is an eigenstate of the operators $j_3(1)$, $j_3(2)$, I_3 and I^2 with eigenvalues Ω_1, $-\Omega_2$, K, and I(I + 1), respectively. Accounting for this, Eq. (5A) becomes

$$\begin{aligned}\mu_I = \frac{1}{I+1}\Big\{&(g_{s1} - g_{\ell 1})K\langle s_3(1)\rangle + (g_{\ell 1} - g_R)\Omega_1 K - (g_{s2} - g_{\ell 2})K\langle s_3(2)\rangle \\ &- (g_{\ell 2} - g_R)\Omega_2 K + g_R I(I+1)\Big\}\ ,\end{aligned} \tag{6A}$$

where now the notation $\langle s_3(i) \rangle$ signifies the single particle expectation value $\langle i | s_3(i) | i \rangle$.

By defining the quantities g_{Ω_1} and g_{Ω_2} as

$$g_{\Omega_i} \equiv (g_{si} - g_{\ell i}) \frac{\langle s_3(i) \rangle}{\Omega_i} + g_{\ell i} \text{ for } i = 1,2 \ , \qquad (7A)$$

Eq. (6A) is simplified to

$$\mu_I = \frac{K}{I+1} \left[\Omega_1 (g_{\Omega_1} - g_R) - \Omega_2 (g_{\Omega_2} - g_R) \right] + g_R I$$

$$= \frac{K^2}{I+1} \left[\frac{\Omega_1 g_{\Omega_1} - \Omega_2 g_{\Omega_2}}{K} - g_R \right] + g_R I \ . \qquad (8A)$$

The second line above is found after setting $\Omega_1 - \Omega_2$ equal to K. Comparison of Eq. (8A) with Eq. (18) in the text shows that the quantity g_K, for the two-particle state, is given by

$$K g_K = \Omega_1 g_{\Omega_1} - \Omega_2 g_{\Omega_2} \ . \qquad (9A)$$

The quantities, g_{Ω_1} and g_{Ω_2}, have been tabulated by Nilsson[55] for various values of the nuclear deformation parameter. The deformation parameter, ϵ, is related to the intrinsic electric quadrupole moment, Q_0, by[95]

$$Q_0 = \frac{4}{5} Z R_0^2 \epsilon (1 + \frac{1}{2} \epsilon) \ , \qquad (10A)$$

where Z is the atomic number and $R_0 = 1.2 \times 10^{-13} A^{1/3}$ cm (A = atomic mass) is the approximate nuclear radius. Stokstad and Persson[56] have deduced the value $Q_0 = 6.57 \pm 0.06$ b for the intrinsic quadrupole moment of the ground state K = 0 rotational band in ^{182}W. If we assign the same value to the K = 2 band considered above, then Eq. (10A)

yields a deformation parameter of $\epsilon = 0.216$. By interpolation from the tables of Nilsson[55], we find, for this deformation, the values

$$g_{\Omega_1} = 1.454 \text{ and } g_{\Omega_2} = 1.892 \text{ for } g_s = g_s^{free} = 5.58$$

and

$$g_{\Omega_1} = 1.233 \text{ and } g_{\Omega_2} = 1.457 \text{ for } g_s = 0.6\ g_s^{free} .$$

These values, in conjunction with Eq. (9A), yield values for g_K of

$$g_K = 0.906 \text{ for } g_s = g_s^{free} \text{ and } g_K = 0.953 \text{ for } g_s = 0.6\ g_s^{free}.$$

It is seen that the strong-coupling prediction of g_K is relatively insensitive to the assumed value of g_s. Thus, a comparison of the predicted g_K value with experiment will test the strong-coupling rule without great interference from effects of spin polarization.

APPENDIX B

Calculation of Corrections for Source Decay in ^{171}Tm Measurements

1. Exponential Decay

When the effects of electronic dead time can be neglected, the coincidence counting rate will decay exponentially in time with the mean life τ of the source. Let us assume that the experimental configuration is periodically changed between state A and state B as shown in Fig. B.1a. The experiment is in a given state for a time '$t_c - t_d$' before the configuration is changed. The time t_d is the pause needed to change states, during which no data are collected. The experiment continues for a total time Nt_c (including pauses), and the coincidence counts corresponding to states A and B are accumulated separately. At any given time, the counting rate in state A (or B) is given by $1/\tau\ N_A e^{-t/\tau}$ (or $1/\tau\ N_B\ e^{-t/\tau}$). The ratio, N_A/N_B, is the quantity to be measured.

The total counts collected in state A can be calculated as

$$C_A = \frac{N_A}{\tau} \sum_{\substack{m=1 \\ \text{odd}}}^{N} \int_{(m-1)t_c}^{mt_c - t_d} e^{-t/\tau} dt = N_A [1 - e^{-(t_c - t_d)/\tau}] \sum_{n=0}^{[\frac{N-1}{2}, \frac{N-2}{2}]} e^{-2nt_c/\tau} . \tag{1B}$$

For N even, this yields

$$C_A = N_A [1 - e^{-(t_c - t_d)/\tau}] \cdot \frac{1 - e^{-Nt_c\tau}}{1 - e^{-2t_c/\tau}} . \tag{2B}$$

Similarly, the total counts collected in state B is given by

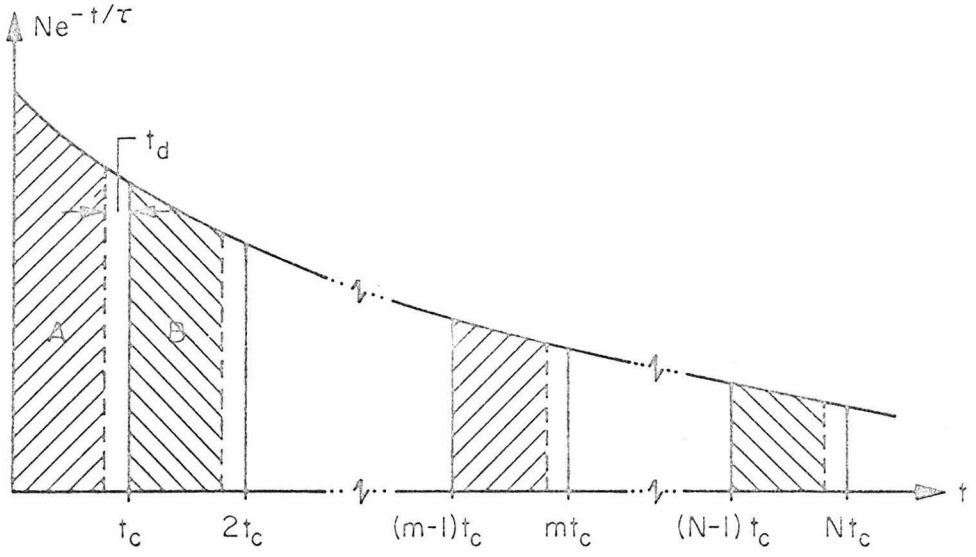

Figure B.1a

Exponential decay of coincidence counting rate and normal switching pattern.

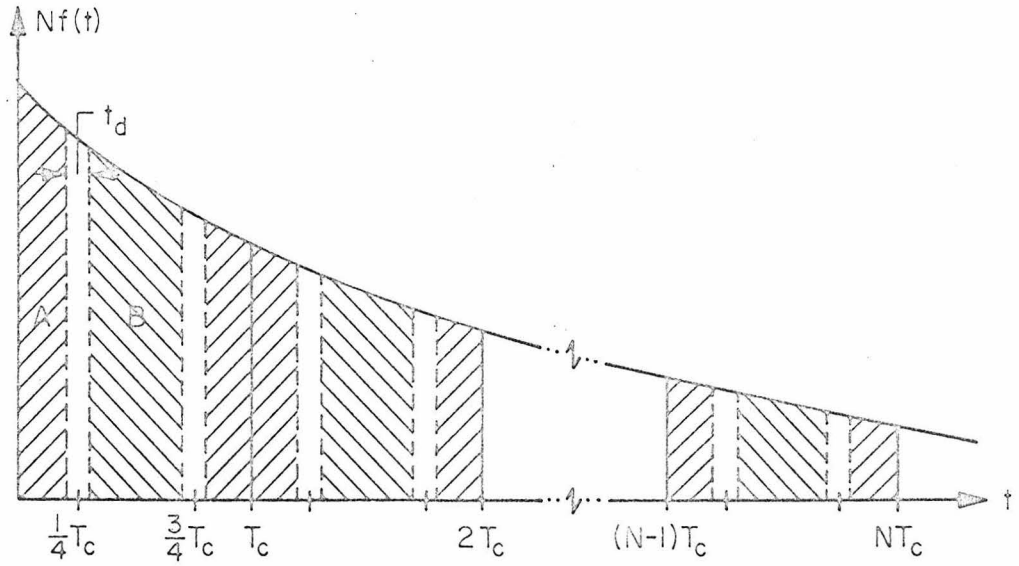

Figure B.2a

General decay of coincidence counting rate and improved switching pattern.

$$C_B = \frac{N_B}{\tau} \sum_{\substack{m=2 \\ \text{even}}}^{N} \int_{(m-1)t_c}^{mt_c - t_d} e^{-t/\tau} dt = N_B e^{-t_c/\tau} [1 - e^{-(t_c - t_d)/\tau}] \sum_{n=0}^{[\frac{N-3}{2}, \frac{N-2}{2}]} e^{-2nt_c/\tau} , \tag{3B}$$

which, for N even, reduces to

$$C_B = N_B e^{-t_c/\tau} [1 - e^{-(t_c - t_d)/\tau}] \cdot \frac{1 - e^{-Nt_c\tau}}{1 - e^{-2t_c/\tau}} . \tag{4B}$$

Thus, we see immediately from Eqs. (2B) and (4B) that the quantity of interest, N_A/N_B, can be written in terms of the experimentally observed total counts C_A and C_B as

$$N_A/N_B = e^{t_c/\tau} C_A/C_B . \tag{5B}$$

The factor, $e^{t_c/\tau}$, can be used to correct the data collected in experiments on ^{171}Tm, where its value is approximately 1.005.

2. Experimental Compensation for Time-Dependent Counting Rates

Figure B.1b displays, in more detail, the alternate configuration switching pattern mentioned in the text and shown in Fig. 31. This pattern differs from the one described above only in that the experimental states at the beginning and end of the experiment are the same and the duration of the first and last time intervals is half that of all the others. We show below that the use of this pattern compensates for the effects of source decay through first order in T_c/τ. The notation used in Fig. B.1b has the same meaning as that employed in Fig. B.1a with the exception that the time interval T_c now refers to

the repetition period of a complete cycle through both configurations A and B. In the following,we do not restrict the calculation to the case of exponential time-dependence of the coincidence counting rate. The counting rate is assumed to follow the functions $N_A f(t)$ and $N_B f(t)$ in states A and B, respectively. The only restrictions on f(t) is that it be a monotonically decreasing function of time and that an exponential approximation to f(t) in any small time interval have a time constant of the order of τ, the mean life of the source. These restrictions are satisfied in practice, since f(t) originates from the source decay directly and from time dependent electronic dead time which also arises from source decay.

The total coincidence counts can be expressed as

$$C_A = N_A \sum_{m=0}^{N-1} \left[\int_{mT_c}^{(m+1/4)T_c - \frac{1}{2}t_d} f(t)dt + \int_{(m+3/2)T_c + \frac{1}{2}t_d}^{(m+1)T_c} f(t)\, dt \right] \qquad (6B)$$

and

$$C_B = N_B \sum_{m=0}^{N-1} \int_{(m+1/4)T_c + \frac{1}{2}t_d}^{(m+3/4)T_c - \frac{1}{2}t_d} f(t)\, dt \quad . \qquad (7B)$$

The function f(t) can be expanded in a Taylor series about the midpoint of each time interval T_c in the following form:

$$f(t) = f[(m + \tfrac{1}{2})T_c] + f'[(m + \tfrac{1}{2})T_c][t - (m + \tfrac{1}{2})T_c] + \frac{1}{2} f''[(m + \tfrac{1}{2})T_c][t - (m + \tfrac{1}{2})T_c]^2 + \ldots . \qquad (8B)$$

Inserting Eq. (8B), keeping terms through second order, into Eqs. (6B) and (7B) and performing the indicated integration yields

$$C_A = N_A \sum_{m=0}^{N-1} \left\{ f[(m+\tfrac{1}{2})T_c](\tfrac{1}{2}T_c - t_d) + \tfrac{1}{4} f''[(m+\tfrac{1}{2})T_c] \cdot \left(\frac{7T_c^3}{48} - \frac{T_c^2 t_d}{8} - \frac{T_c t_d^2}{4} - \frac{t_d^3}{6} \right) \right\} \qquad (9B)$$

and

$$C_B = N_B \sum_{m=0}^{N-1} \left\{ f[(m+\tfrac{1}{2})T_c](\tfrac{1}{2}T_c - t_d) + \tfrac{1}{24} f''[(m+\tfrac{1}{2})T_c](\tfrac{1}{2}T_c - t_d)^3 \right\}. \qquad (10B)$$

The above-mentioned restrictions on the function $f(t)$ require that $f''/f \approx 1/\tau^2$. Thus the ratio of the second to the first term in the brackets of both Eq. (9B) and (10B) is of the order of $(T_c/\tau)^2$. The ratio N_A/N_B can then be written as

$$N_A/N_B = C_A/C_B \times (1 + O[(T_c/\tau)^2]) , \qquad (11B)$$

which confirms that a first order correction to the experimental rates is not present when the switching pattern of Fig. B.1b is used.

APPENDIX C

Demonstration that the Value of the Matrix Element, $\langle K = \frac{1}{2}|\mathcal{M}(E2,1)|K = -\frac{1}{2}\rangle$, is Identically Zero

The intrinsic states of a particle in an axially symmetric deformed potential, such as that used in the Nilsson model[46], can be indexed by the two good quantum numbers, N and K. The number N designates the major oscillator shell in question and is related to the energy eigenvalues of a harmonic oscillator Hamiltonian. The number K is the projection of intrinsic angular momentum on the symmetry axis of the potential well. Although the total intrinsic angular momentum, $\vec{j}$, is not a constant of the motion, the state vectors can be expanded in terms of eigenstates of $\vec{j}$ as follows:[46]

$$|NK\rangle = \sum_j C_j |NjK\rangle \quad . \tag{1C}$$

The wavefunction, χ_K, in Eq. (22) in the text, is just the coordinate representation of the state vector $|NK\rangle$. The symmetric wavefunction, χ_{-K}, in Eq. (22), is degenerate with χ_K and can be obtained from χ_K by a rotation of coordinates of 180° about an axis perpendicular to the symmetry axis. For the appropriate choice of phase for the vectors $|NjK\rangle$, it has been shown by Bohr and Mottelson[96] that the state vector corresponding to χ_{-K} can be written as

$$|\overline{NK}\rangle = \sum_j C_j (-1)^{j+K} |Nj-K\rangle \, . \tag{2C}$$

Using Eqs. (1C) and (2C), the matrix element in question appears as

$$\langle NK|\mathcal{M}(E2,1)|\overline{NK}\rangle = \sum_{j,j'} C_j^* C_{j'} (-1)^{j' + K} \langle NjK|\mathcal{M}(E2,1)|Nj'-K\rangle$$

$$= \sum_{j,j'} C_j^* C_{j'} (-1)^{j'+K} (-1)^{j - K} \begin{pmatrix} j & 2 & j' \\ -K & 1 & -K \end{pmatrix} \langle Nj||\mathcal{M}(E2)||Nj'\rangle, \tag{3C}$$

where the Wigner-Eckart theorem[97] has been used to obtain the second expression. We now note the symmetry relation,

$$\begin{pmatrix} j & 2 & j' \\ -K & 1 & -K \end{pmatrix} = (-1)^{j + 2 + j'} \begin{pmatrix} j' & 2 & j \\ -K & 1 & -K \end{pmatrix}, \tag{4C}$$

for the vector addition coefficient (3-j symbol) and the relation,

$$\langle Nj||\mathcal{M}(E2)||Nj'\rangle = (-1)^{j - j'} \langle Nj'||\mathcal{M}(E2)||Nj\rangle, \tag{5C}$$

for the reduced (double-bar) matrix element. Equation (5C) depends on the Hermiticity of the $\mathcal{M}(E2)$ operator and reality of the reduced matrix element which follows from time-reversal invariance[97]. Inserting Eqs. (4C) and (5C) in Eq. (3C) yields

$$\langle NK|\mathcal{M}(E2,1)|\overline{NK}\rangle = \sum_{j,j'} C_j^* C_{j'} (-1)^{3j + j'} \begin{pmatrix} j' & 2 & j \\ -K & 1 & -K \end{pmatrix} \langle Nj'||\mathcal{M}(E2)||Nj\rangle. \tag{6C}$$

The phase $(-1)^{2j}$ can be factored from the sum in the above expression since j, for the case of an odd-mass nucleus, is always a half-odd integer and $(-1)^{2j} = -1$. Also, since the C_j coefficients are either purely imaginary (for N odd) or purely real (for N even) numbers

because of the choice of phase for the $|NjK\rangle$ vectors and parity conservation, the identity

$$C_j^* C_{j'} \equiv C_j C_{j'}^* \tag{7C}$$

holds. Thus, Eq. (6C) takes the form

$$\langle NK|\mathcal{M}(E2,1)|\overline{NK}\rangle = -\sum_{j,j'} C_j C_{j'}^* (-1)^{j+j'} \begin{pmatrix} j' & 2 & j \\ -K & 1 & -K \end{pmatrix} \langle Nj'||\mathcal{M}(E2)||Nj\rangle. \tag{8C}$$

One can now see that the sums in Eq. (8C) and (3C) are identical since one can be obtained one from the other by the interchange of the dummy indices, j and j'. Therefore, the desired result of

$$\langle NK|\mathcal{M}(E2,1)|\overline{NK}\rangle = -\langle NK|\mathcal{M}(E2,1)|\overline{NK}\rangle \equiv 0 \tag{9C}$$

is obtained.

References

1. J.D. Bowman, E.N. Kaufmann, S.K. Bhattacherjee and M. Levanoni, Phys. Rev. Letters 20 (1968) 1176.

2. S.K. Bhattacherjee, J.D. Bowman and E.N. Kaufmann, Physics Letters 26B (1968) 583.

3. E.N. Kaufmann, J.D. Bowman and S.K. Bhattacherjee, to be published in Nuclear Physics.

4. E.L. Brady and M. Deutsch, Phys. Rev. 78 (1950) 558.

5. H. Aeppli, H. Albers-Schönberg, A.S. Bishop, H. Frauenfelder and E. Heer, Phys. Rev. 84 (1951) 370.

6. K. Alder, Helv. Phys. Acta 25 (1952) 235 and Phys. Rev. 84 (1951) 369;
   A. Abragam and R.V. Pound, Phys. Rev. 92 (1953) 943; and
   H. Frauenfelder and R.M. Steffen in Alpha-, Beta-, and Gamma-Ray Spectroscopy, ed. K. Siegbahn (North-Holland Publ. Co., Amsterdam, 1965) vol. 2, Ch. 19, p. 997.

7. H. Frauenfelder and R.M. Steffen in Alpha-, Beta-, and Gamma-Ray Spectroscopy (North-Holland Publ. Co., Amsterdam, 1965) p.1031.

8. H. Ferentz and N. Rosenzweig, Argonne National Laboratory Report 5324 (1954); and
   A.H. Wapstra, G.J. Nijgh and R. van Lieshout, Nuclear Spectroscopy Tables (North-Holland Publ. Co., Amsterdam, 1959).

9. H. Frauenfelder and R.M. Steffen in Alpha-, Beta-, and Gamma-Ray Spectroscopy (North-Holland Publ. Co., Amsterdam, 1965) p.1160.

10. A. Abragam and R.V. Pound, Phys. Rev. 92 (1953) 943.

11. D. Dillenburg and Th. A.J. Maris, Nuclear Phys. 33 (1962) 208; Physics Letters 5 (1963) 357.

12. E. Bodenstedt and J.D. Rogers in Perturbed Angular Correlations, ed. E. Karlsson, E. Mattias and K. Siegbahn (North-Holland Publ. Co., Amsterdam, 1964) pp 95-96.

13. G. Racah, Phys. Rev. 62 (1942) 438; and 63 (1943) 367.

14. H.J. Körner, J. Radeloff and E. Bodenstedt, Z. Physik 172 (1963) 279.

15. H. Frauenfelder and R.M. Steffen in Alpha-, Beta-, and Gamma-Ray Spectroscopy (North-Holland Publ. Co. Amsterdam, 1965)p.1144.

16. P. Debye, Polar Molecules (Dover Publications, New York, 1945).

17. N. Bloembergen, E.M. Purcell and R.V. Pound, Phys. Rev. 73 (1948) 679.

18. C.M. Lederer, J.M. Hollander and I. Perlman, Table of Isotopes, 6th ed. (John Wiley & Sons, Inc., New York, 1967).

19. A. Bohr, Mat. Fys. Medd. Dan. Vid. Selsk. 26, No. 14 (1952); and A. Bohr and B.R. Mottelson, Mat. Fys. Medd. Dan. Vid. Selsk. 27, No. 16 (1953).

20. O. Nathan and S.G. Nilsson in Alpha-, Beta-, and Gamma-Ray Spectroscopy, ed. K. Siegbahn (North-Holland Publ. Co., Amsterdam, 1965).

21. S.T. Belyaev, Mat. Fys. Medd. Dan. Vid. Selsk. 31, No. 11 (1959).

22. T. Marumori, Prog. Theo. Phys. 24 (1960) 331.

23. M.G. Mayer, Phys. Rev. 75 (1949) 1969; 78 (1950) 16.

24. O. Haxel, J.H.D. Jensen and H.E. Suess, Phys. Rev. 75 (1949) 1766 and Z. Physik 128 (1950) 295.

25. L.S. Kisslinger and R.A. Sorensen, Rev. Mod. Phys. 35 (1963) 853, and Mat. Fys. Medd. Dan. Vid. Selsk. 32, No. 7 (1960).

26. S. Yoshida, Nuclear Phys. 38 (1962) 380.

27. T. Tamura and T. Udagawa, Prog. Theo. Phys. 26 (1961) 947.

28. R.J. Lombard, Nuclear Phys. A114 (1968) 449.

29. K. Auerbach et al., Physics Letters 23 (1967) 367.

30. V.S. Shirley, Table of Nuclear Moments in Hyperfine Interactions and Nuclear Radiation (North-Holland Publ. Co., Amsterdam, 1968).

31. P.H. Stelson and F.K. McGowan, Phys. Rev. 121 (1961) 209.

32. R.G. Stokstad et al., Nuclear Phys. A92 (1967) 319;
P.H. Stelson et al., Bull. Am. Phys. Soc. 10 (1965) 427; and
J.J. Simpson et al., Nuclear Phys. A94 (1967) 177; and
J. de Boer and J. Eichler, data tabulated in Hyperfine Structure and Nuclear Radiations, ed. E. Mattias and D.A. Shirley (North-Holland Publ. Co., Amsterdam, 1968).

33. T. Tamura and T. Udagawa, Phys. Rev. 150 (1966) 783.

34. T. Marumori, M. Yamamura and A. Tokunaga, Prog. Theo. Phys. 31 (1964) 1009;
T. Marumori, M. Yamamura, A. Tokunaga and K. Takada, Prog. Theo. Phys. 32 (1964) 726; and
S.T. Belyaev and V.G. Zelevinsky, Nuclear Phys. 39 (1962) 582.

35. H. Ikegami and M. Hirata in Contributions to the International Conference on Nuclear Structure, Tokyo 1967.

36. M. Yamamura, A. Tokunaga and T. Marumori, Prog. Theo. Phys. 37 (1967) 336.

37. Nuclear Data Sheets (Academic Press, New York, 1965).

38. Yu. P. Gangrksii et al., Sov. Phys. JETP 15 (1962) 711.

39. J.D. Bowman, Thesis, California Institute of Technology (1968).

40. D.A. Shirley, S.S. Rosenblum and E. Matthias, Phys. Rev. 170 (1968) 363.

41. M. Kontani and J. Itoh, J. Phys. Soc. Japan 22 (1967) 345.

42. M. Hansen, Constitution of Binary Alloys (McGraw-Hill, New York, 1958) p. 704; and
R.P. Elliot, Constitution of Binary Alloys, First Supplement (McGraw-Hill, New York, 1965) p. 431.

43. S.K. Bhattacherjee, J.D. Bowman, and E.N. Kaufmann, Phys. Rev. Letters 18 (1967) 223.

44. K. Johansson, E. Karlsson, L.O. Norlin, P.N. Tanden and H.C. Jain in Hyperfine Structure and Nuclear Radiations, ed. E. Mattias and D.A. Shirley (North-Holland Publ. Co., Amsterdam, 1968).

45. A.K. Kerman, Nuclear Reactions 1, ed. P.M. Endt and M. Demeur, (North-Holland Publ. Co., Amsterdam, 1959) p. 427.

46. S.G. Nilsson, Mat. Fys. Medd. Dan. Vid. Selsk. 29, No. 16 (1955).

47. A.J. Rassey, Phys. Rev. 109 (1958) 949.

48. E.P. Grigor'ev et al., Yadernaya Fiz. 4 (1967) 5.

49. C.J. Gallagher, Jr., and V.G. Soloviev, Mat. Fys. Skr. Dan. Vid. Selsk. 2, No. 2 (1962).

50. N.J. Pyatov, Acta Phys. Polonica 25 (1964) 21.

51. V.G. Soloviev, JETP SSSR 35 (1958) 823; 36 (1959) 1869; Nuclear Phys. 9 (1958/59) 655; Doklady Akad. Nauk SSSR 133 (1960) 325; and

S.T. Belyaev, Mat. Fys. Medd. Dan. Vid. Selsk, 31, No. 11 (1959).

52. W.M. Hooke, Phys. Rev. 115 (1959) 453.

53. E. Bashandy, M.S. El-Nesr and S.C. Pancholi, Nuclear Phys. 41 (1963) 346;
R. Manquenouille, Ann. Phys. (Paris) (1961) 1121;
E.E. Berlovich et al., Izo. Akad. Nauk. Ser. Fiz. 28 (1964) 80; and
W. Meiling and F. Stary, Nuclear Phys. 84 (1966) 534.

54. M. Ferenz and N. Rosenzweig in Alpha-, Beta-, and Gamma-Ray Spectroscopy, ed. K. Siegbahn (North-Holland Publ. Co., Amsterdam, 1965) Vol. 2, App. 8.

55. S.G. Nilsson, Mat. Fys. Medd. Dan. Vid. Selsk. 29, No. 16 (1955) and private communication to Prof. F. Boehm.

56. R.G. Stokstad and B. Persson, Phys. Rev. 170 (1968) 1072.

57. J. de Boer and J.D. Rogers, Physics Letters 3 (1963) 304; and
E.M. Bernstein and J. de Boer, Nuclear Phys. 18 (1960) 40.

58. B.R. Mottelson, Selected Topics on the Theory of Collective Phenomena in Nuclei (Int. School of Physics, Varenna 1960, Nordita Publ. No. 78); and
S.G. Nilsson and O. Prior, Mat. Fys. Medd Dan. Vid. Selsk. 32, No. 16 (1961).

59. E. Bodenstedt and J.D. Rogers in Perturbed Angular Correlations ed. E. Karlsson, E. Mattias and K. Siegbahn (North-Holland Publ. Co., Amsterdam, 1964) p. 140.

60. P. Gilad, G. Goldring, R. Herber and R. Kalish, Nuclear Phys. A91 (1967) 85; and
E. Bodenstedt et al., Z. Physik 165 (1961) 57.

61. O. Prior, F. Boehm and S.G. Nilsson, Nuclear Phys. A110 (1968) 257.

62. C. Günther et al., Nuclear Phys. 61 (1965) 65.

63. C. Günther and I. Lindgren in Perturbed Angular Correlations (Amsterdam, 1964) p. 357.

64. T. Sundström, P. Sparrman, J.O. Lindström, and J. Lindskog, Ark. Fysik 26 (1964) 377.

65. A.E. Blaugrund, Phys. Rev. Letters 3 (1959) 226.

66. R.E. McAdams, G.W. Eakins, and E.N. Hatch, Nuclear Phys. 82 (1966) 449.

67. J.D. Bowman, J. de Boer and F. Boehm, Nuclear Phys. 61 (1965) 682.

68. A.E. Blaugrund, V. Dar and G. Goldring, Phys. Rev. 120 (1960) 1328.

69. G. Manning and J. Rogers, Nuclear Phys. 19 (1960) 675.

70. H. Frauenfelder and R.M. Steffen in Alpha-, Beta-, and Gamma-Ray Spectroscopy (North-Holland Publ. Co., Amsterdam, 1965) p. 1192.

71. V.M. Kel'man, R. Ya. Matskhvarishvili, B.K. Preobrazhenskii, V.A. Romanov and V.V. Tuchkevich, Sov. Phys. JETP 10 (1960) 456;
J.W. Michelich, Phys. Rev. 103 (1956) 1285;
Z. Grabowski, J.E. Thun and B. Lindström, Z. Physik 169 (1962) 303;
M. Martin, P. Marmier and J. de Boer, Helv. Phys. Acta 31 (1958) 435;
D. Ashery, A.E. Blaugrund, R. Kalish, J.S. Sokolowski and Z. Vager, Nuclear Phys. 67 (1965) 385.

72. T. Sundström, J.O. Lindström, P. Sparrman, and J. Lindskog, Ark. Fysik 26 (1964) 397.

73. H.E. Leming, BAPS 11, No. 3 (1966) 369.

74. Y.K. Agarwal, C.V.K. Baba and S.K. Bhattacherjee, Physics Letters 14 (1965) 214.

75. L. Varnell, to be published.

76. R.S. Hager and E.C. Seltzer, Internal Conversion Tables, Nuclear Data A4 (1968).

77. D.G. Megli, G.P. Agin, V.R. Potnis and C.E. Mandeville, Nuclear Phys. A107 (1968) 217.

78. J.S. Geiger, R.L. Graham and M.W. Johns, BAPS 13, No. 4 (1968) 672; and private communication.

79. B.R. Mottelson, Selected Topics in the Theory of Collective Phenomena in Nuclei, International School of Physics, Varenna, 1960 (Nordita Publ. No. 78, Copenhagen, 1960).

80. S.G. Nilsson and O. Prior, Mat. Fys. Medd. Dan. Vid. Selsk. 32, No. 16 (1961).

81. Z. Bochnacki and S. Ogaza, Nuclear Phys. 69 (1965) 186.

82. Z. Bochnacki and S. Ogaza, Nuclear Phys. 83 (1966) 619.

83. Z. Bochnacki and S. Ogaza, Inst. of Nuclear Phys. Cracow, Report No. 482/PL (1966); and

Z. Bochnacki and S. Ogaza in Hyperfine Structure and Nuclear Radiations ed. E. Mattias and D.A. Shirley (North-Holland Publ. Co., Amsterdam, 1968).

84. A. Bohr and B.R. Mottelson, Sov. Atom. Energy 14 (1963) 36, (Trans. from Atomnaya Energiya).

85. T. Sundström, J. Lindskog, J.O. Lindström and P. Sparrman, Ark. Fysik 26 (1964) 361; and
P. Sparrman, T. Sundström, and J. Lindskog, Ark. Fysik 31 (1966) 409.

86. B.S. Dzhelepov and G.F. Dranitsyna, Izv. AN SSSR, Ser. Fiz. 32 (1967), (Trans. Bull. 32 (1967) 169).

87. D.W. Marquardt, J. Soc. Indust. and Appl. Math. 11, No. 2 (1963) 431.

88. J.P. Bocquet, J. de Phys. 26 (1965) 795.

89. E. Münch, D. Quitmann and S. Hüfner, Z. Naturforsch. 21a (1966) 847.

90. J.D. Kurfess and R.P. Scharenberg, Phys. Rev. 161 (1967) 1185.

91. B.S. Dzhelepov and G.F. Dranitsyna, Izv. AN SSSR, Ser. Fiz. 31 (1967), (Trans. Bull. 31 (1967) 146).

92. V. Feifrlik, Izv. AN SSSR. Ser. Fiz. 30, No. 3 (1966) 501 (Trans. Bull. 30 (1966) 510).

93. S.G. Nilsson, in Lectures in Theoretical Physics, ed. P.D. Kunz, D.A. Lind, and W.E. Brittin (University of Colorado Press, Boulder, Colorado, 1966) Vol. VIIIC-- Nuclear Structure Physics.

94. V.G. Soloviev and P. Vogel, Nuclear Phys. A92 (1967) 449.

95. B.R. Mottelson and S.G. Nilsson, Mat. Fys. Skr. Dan. Vid. Selsk. 1, No. 8 (1959).

96. A. Bohr and B.R. Mottelson, Lecture Notes, Nordita 1962. (Revised 1965), unpublished.

97. A.E. Edmunds, Angular Momentum in Quantum Mechanics, (Princeton University Press, Princeton, New Jersey, 1960).